



Influence of various boundary conditions on local buckling of steel tubular piles

Effects of restraints, imperfections and residual stresses

S.J.M. de Jong

Influence of various boundary conditions on local buckling of steel tubular piles

Effects of restraints, imperfections and residual stresses

by

S.J.M. de Jong

Thesis committee: Prof. dr. ir S.N. (Bas) Jonkman TU Delft
Ir. C.M.P. (Marcel) 't Hart RoyalHaskoningDHV
Dr. ir. D.J. (Dirk Jan) Peters TU Delft
Dr. ir. P.C.J. (Pierre) Hoogenboom TU Delft

Abstract

The main focus of this thesis is the influence of different real boundary conditions on the failure mechanism of local buckling of steel tubular piles. The research was started with the theoretical method of describing boundary condition by specifying the degrees of freedom per boundary condition. The method makes use of the radial, meridional and rotational degrees of freedom. This method is also used in the current design code for steel shell structures, the NEN-EN 1993-1-6 [1]. By varying the amount and types of constrained degrees of freedom, eight possible boundary conditions can be generated. Looking to the practical applications, a ninth variant with a non-homogeneous boundary completes a list of nine. From the nine boundary conditions, eight conditions are selected to be included in a FEM model study. The current design code describes only five of the nine conditions, what allows for a comparison of the known and unknown conditions with the prescribed rules.

Two types of parameters that influence the local buckling failure mechanism are material and geometrical imperfections. In the study to geometrical imperfections, initial ovalisation, accidental eccentricity and dimples are considered. The effect on the design yield stress of the different imperfections is determined following the calculation methods described by the current design code. The calculated reduction of the design yield stress by specific boundary condition and an increasing imperfection is compared to results of ABAQUS FEM model tests. Residual stresses are investigated on the side of material imperfections. The used residual stresses are validated with a simple FEM ring model test that shows deformations due to the introduced residual stresses. The observed displacements could be compared with measured data of real experiments.

A range of 36 different tubes is selected to investigate the influences of the eight different boundary conditions on the buckling failure behaviour. This test range covers a wide range of tubes with cross-section class 3 and 4 known for their sensitivity for local buckling. A base model is generated for all the 288 model tests, 36 tubes with all 8 boundary conditions per tube. The results from all tests are displayed in normalized moment-curvature diagrams. Because of a lack of test data of real experiments with boundary conditions involved, a validation with an analytical method is used that describes a linear and bi-linear part of the moment-curvature relation.

Finally the results of the FEM model tests are analyzed per parameter but also the overall behaviour is discussed. From the model results could be concluded that residual stresses hardly influence the moment capacity but causes an increase in the curvature of most boundary condition. Geometrical imperfections cause a decreasing moment capacity and an increasing critical curvature whit an increasing imperfection. The trend of the influence of dimple imperfections is decreasing slightly faster compared to the trend observed from the code calculations. A safety of approximately 20% is observed between the failure stresses of the test results and the design stresses from the code. With an increasing diameter over thickness (D/t) ratio or yield stress, the moment capacity decreases and the critical curvature increases. The relative influence of the D/t ratio within the tested range is larger compared to the yield stress.

To investigate the influence of the different boundary conditions, the effect of all parameters is investigated per boundary condition. Following the test results, all boundary conditions except BC4F show the same influence on the maximum moment and corresponding curvature. Boundary condition BC4F shows a moment resistance reduction of 14% and a critical curvature reduction of 26% compared to the other conditions. Small observed differences in the post buckling behaviour between the other different boundary conditions are reported to complete this study.

Preface

This report represents the work that has been performed for my Master thesis. The master thesis is the final part of my study at the Delft University of Technology to obtain the Master of Science degree in Civil Engineering. After a Bachelor of Applied Science in the field of building engineering, a civil master with the specialisation 'Hydraulic structures and flood risk' is carried out. This master is the last phase of my time as a student, as from now on I am looking forward to develop myself in the professional work field.

The subject of this research is, 'Influence of various boundary conditions on local buckling of steel tubular piles'. In previous internships, during the bachelor and master, I was already involved in research projects to the behavior of steel tubular piles. These experiences triggered my interest in this topic and are the main reason I chose to do this research.

RoyalHaskoningDHV gave me the opportunity to execute the research within their company, using their facilities and expertise. During the process of this master thesis I received a lot of great help from my daily supervisors from RoyalHaskoningDHV and the TU Delft, Marcel 't Hart and Dirk Jan Peters which I appreciate a lot. I am also grateful to prof. Bas Jonkman and Pierre Hoogenboom for joining my committee.

Besides all the professional help, I should not forget the support I received from my family and friends, and especially from my girlfriend Michelle during my whole study period.

*S.J.M. de Jong
Bergen op Zoom, September 2019*

Nomenclature

List of symbols

D	-	Diameter	[mm]
D_{max}	-	Maximum diameter	[mm]
D_{min}	-	Minimum diameter	[mm]
D_{nom}	-	Nominal diameter	[mm]
D_m	-	Diameter from material center(D-t)	[mm]
t	-	Thickness	[mm]
U	-	Meridional displacement	[mm]
W	-	Radial displacement	[mm]
Φ	-	Rotational displacement	[rad]
r	-	Radius	[mm]
L	-	Length	[mm]
L_1	-	Pendel length	[mm]
L_2	-	System length	[mm]
L_{inf}	-	Influence length	[mm]
e_a	-	Accidental eccentricity	[mm]
Δ_w	-	Imperfection height	[mm]
δ	-	Imperfection amplitude	[mm]
U_r	-	Out of roundness parameter	[-]
U_e	-	Accidental eccentricity parameter	[-]
U_0	-	Dimple imperfection parameter	[-]
C_x	-	Boundary condition parameter	[-]
f_{yk}	-	Yield stress	[N/mm ²]
σ_{xRk}	-	Characteristic resistance stress	[N/mm ²]
χ_x	-	Buckling reduction factor	[-]
σ	-	stress	[N/mm ²]
E	-	E-modulus	[MPa]
ϵ	-	Extension coefficient	[-]
[F]	-	Force vector	[-]
[K]	-	Stiffness matrix	[-]
[U]	-	Displacement vector	[-]
M	-	Moment	[kNm]
M_{pl}	-	Plastic moment	[kNm]
M_p	-	Plastic moment	[kNm]
RF_2	-	Vertical reaction force	[kN]
K	-	Curvature	[1/mm]
K_{cr}	-	Critical curvature	[1/mm]
K_i	-	Curvature like	[1/mm]
K_e	-	Elastic curvature	[1/mm]
I	-	Moment of inertia	[kg * m ²]
ν	-	Poisson ratio	[-]
U_1	-	Horizontal radial displacement ABAQUS	[mm]
U_2	-	Vertical radial displacement ABAQUS	[mm]
U_3	-	Axial displacement ABAQUS	[mm]
UR_1	-	Rotation around U_1 ABAQUS	[rad]
UR_2	-	Rotation around U_2 ABAQUS	[rad]
UR_3	-	Rotation around U_3 ABAQUS	[rad]

Abbreviations

FEM	-	Finite element method
BC	-	Boundary condition
BC1F	-	Boundary condition type 1 rotational free
BC1R	-	Boundary condition type 1 rotational restrained
BC2F	-	Boundary condition type 2 rotational free
BC2R	-	Boundary condition type 2 rotational restrained
BC3F	-	Boundary condition type 3 rotational free
BC3R	-	Boundary condition type 3 rotational restrained
BC4F	-	Boundary condition type 4 rotational free
BC4R	-	Boundary condition type 4 rotational restrained
BC11	-	Boundary condition 1 at both tube ends
BC22	-	Boundary condition 2 at both tube ends
BC12	-	Boundary condition 1 and 2 at a tube end
BC-UCF	-	Boundary condition combination
RP	-	Reference point
CS	-	Cross-section
S4	-	Element with 4 nodes
SR4	-	Element with 4 nodes and reduced integration

Contents

Abstract	iii
Preface	v
Nomenclature	vii
1 Introduction	1
1.1 Background	1
1.2 Intended results.	1
1.3 Research objectives	2
1.3.1 Main research question	2
1.3.2 Sub questions / Topics to be included	2
1.4 Methodology	2
2 Boundary condition analyses	5
2.1 Introduction	5
2.2 Theoretical boundary conditions.	5
2.3 Boundary conditions in practical situations	7
2.3.1 BC1	7
2.3.2 BC2	7
2.3.3 BC3	8
2.3.4 BC4	9
2.3.5 BC-UCF.	9
2.4 Discussion	10
3 Geometrical and material Imperfections	11
3.1 Introduction	11

3.2	Geometrical imperfections	11
3.2.1	Initial ovalisation	13
3.2.2	Accidental eccentricity	14
3.2.3	Dimples	15
3.3	Residual stresses.	16
3.3.1	Cold bending	16
3.3.2	Residual stress ring model.	18
3.4	Discussion	19
4	FEM model tests	21
4.1	Model test approach	21
4.2	Finite element method	21
4.3	Theoretical model	22
4.3.1	Mechanical model	22
4.3.2	Data generation.	24
4.4	Geometrical and material properties.	25
4.5	FEM model	26
4.5.1	Base model	26
4.5.2	Local and global boundary conditions (constraints).	28
4.5.3	Mesh and element configuration.	30
4.5.4	Eigenmode analyses	32
4.5.5	Model results	33
4.6	Model validation	35
4.6.1	Analytical model	35
4.6.2	Validation by analytical model	37
4.6.3	Discussion	38
5	Parametric study	39
5.1	Introduction	39
5.2	Residual stresses.	39

5.3	Geometrical imperfections	41
5.3.1	Influence of imperfections in the model study.	43
5.3.2	Comparison with the design code	45
5.4	D/t ratio	46
5.4.1	Influence of the D/t ratio in the model study.	48
5.5	Yield stress	50
5.5.1	Influence of yield stress in the model study	52
5.6	Influence length.	53
5.6.1	Buckling location	55
5.7	Boundary conditions	55
5.7.1	Overall trend over the boundary conditions	56
5.7.2	Failure behaviour per boundary condition.	57
6	Conclusions and recommendations	59
6.1	Conclusions.	59
6.2	Recommendations	61
	Bibliography	63
A	Literature study	65
A.1	Buckling of steel tubular piles	65
A.1.1	Types of analysis	66
A.1.2	Class 4 cross-sections	67
A.2	Geometrical tolerances.	68
A.2.1	Out of roundness	68
A.2.2	Accidental eccentricity	70
A.2.3	Dimples	71
A.2.4	Interface flatness	71
A.3	Boundary conditions	72
A.4	Residual stress	73

A.5	Design codes	74
A.5.1	NEN-EN 1993-1-6	74
A.5.2	NEN-EN 1993-4-3	75
A.5.3	DNV-RP-C202 (classification Notes – No. 30.1)	75
A.6	Thesis scope	77
B	Design code calculations	79
B.1	NEN-EN 1993-1-6	80
C	ABAQUS modeling and post-processing	85
C.1	Modeling resources	85
C.2	Post-processing python script	86
D	Eigenmode analyses	89
E	Moment curvature diagrams from FEM models	97

Introduction

Safety against failure is an important benchmark in engineering, this while engineers are nowadays more triggered to design on the limits of the materials. More specific knowledge of the behaviour of materials has resulted in a reduction of the safety factors over the years. Steel tubular piles are used in civil engineering for a lot of purposes, as bearing piles in the soil, as a part of soil retaining walls and also as structural elements in all type of structures. Steel tubular piles are the main focus for this thesis. The steel piles are available in a variety of diameters and thicknesses (the so called D/t ratio). In previous studies it is shown that slender piles with a D/t ratio larger than 90 are more sensitive for the failure mechanism of local buckling.

1.1. Background

The risk of local buckling of thin-walled tubular piles has up to now been investigated for various shapes, sizes, idealized load cases and support conditions. As at this moment, design code NEN-1993-1-6 [1] specifies requirements for different boundary conditions like clamped, pinned and free edge boundary condition. These boundary conditions for shells are mainly based on large diameter ($\gg 2\text{m}$) cylindrical tanks and silo's. The tubular piles used for civil engineering purposes have commonly a diameter within the range of 0.5 to approximately 2 meters. The application of piles in design has increased over time both in amount as well as in possibilities. These applications come with boundary conditions that do not match the prescribed conditions from the design codes. Because of the different influences of the boundary conditions on the local buckling failure mechanisms of the piles, further research is needed. The study of the different, frequently used applications of tubular piles and their specific boundary conditions will be the subject of this thesis.

The use of tubular piles in final design requires a correct understanding of the failure mechanisms and their conditions of influence. The aim of this thesis is to research the influence of different boundary (support) conditions and load patterns on the risk of local buckling. Different partial factors derived from NEN-EN-1993-1-6 [1] will be compared to the results of this study.

1.2. Intended results

The intended result of this study is to find the gaps in the current design code for the application of steel tubular piles with specific boundary conditions. A comparison is made between FEM model tests and the prescribed partial factors for known boundary conditions as they are described in the current design code. As completion, FEM model tests of non-described boundary conditions are performed to

enlarge the knowledge of the behaviour of steel tubular piles in more specific situations. An overview will be presented of the results of the FEM model tests. This overview includes model tests of the, in the current design code described and non-described boundary conditions and their influence on the failure mechanism of local buckling.

1.3. Research objectives

1.3.1. Main research question

What is the influence of a full or semi-clamped or encastered boundary condition on the failure mechanism of local buckling of tubular piles?

1.3.2. Sub questions / Topics to be included

Questions that will help answering the main question, and subdivide the study in more manageable parts are:

1. How are the results from the FEM model related to the prescribed idealized boundary conditions from the current design code like pinned, sliding and clamped?
2. Which boundary conditions, corresponding to practical applications, are not covered in the current design code?
3. What is the influence of residual stresses on the failure mechanism of local buckling?
4. Which realistic and theoretical imperfections (production imperfections, dimples and damages) related to the calculations, are common for tubular piles and how to model them?

1.4. Methodology

To complete the thesis, this method of approach is made with different studies and activities. These activities in this order cause a structured way of working, and deliver the wanted results from this model test research. The outline of these processes is shown in figure 1.1.

- Literature study;
- Boundary condition analyses;
- Parameter study;
- Familiarizing with FEM software (ABAQUS), using Eigenvalue analysis and elastoplastic, geometrical non-linearity;
- Making FEM model calculations and compare with known outcomes of literature studies and/or known outcomes of experiments for validation;
- Making FEM models of the geometries and load cases of interest;
- Compare the outcomes with the design codes, and make recommendations for analysis of the structures with the geometries and load cases of interest.

A study to the available literature and codes is performed as introduction to the subject. For better understanding of the influences of boundary conditions that are already included in the design code, the prescribed calculations method is studied. The results of the literature study and the study to the calculation method are shown in respectively appendix A and B.

Chapter 2 shows the study of theoretical and real boundary conditions. In this chapter the range of boundary condition included in the FEM model studies is selected. The boundary conditions together with imperfections form the input data for the model study, an analyses to the different imperfections can be seen in chapter 3.

The modelling process from a theoretical basic mechanical model to a 3D materially and geometrically non-linear FEM model is described in chapter 4. This process included studies to buckling eigenmodes, plastic-stain, mesh sizes and the basic principals of the finite element method.

After running 288 FEM models the result of these models for different parameters are discussed in the parametric study of chapter 5. In this chapter also the influences of the parameters per boundary condition are discussed.

The observations and results of the parametric study per parameter and per boundary condition are combined to a general conclusion in chapter 6. By answering the sub-questions a final answer to the main research question is derived. The report is completed with some observed recommendations as also is shown in figure 1.1.

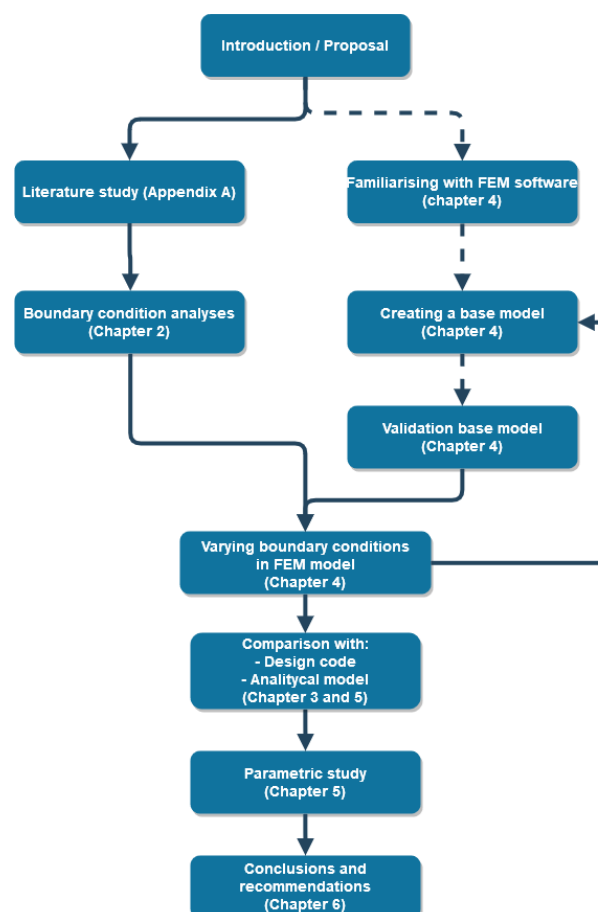


Figure 1.1: Research outline

2

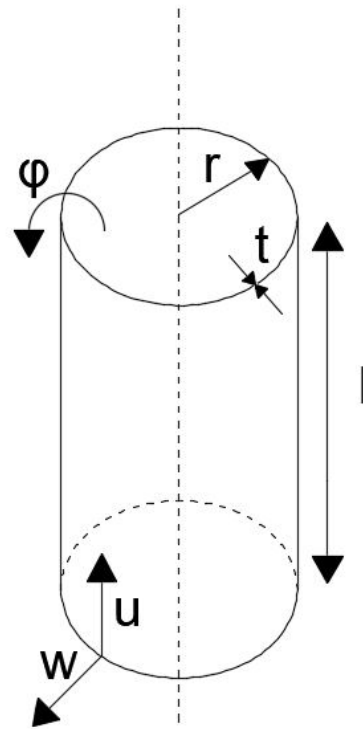
Boundary condition analyses

2.1. Introduction

The aim of this thesis is to find the gap between the boundary conditions used in practice and the ones that are covered in the current design code. The NEN-EN 1993-1-6 [1], used to design and test steel tubular piles is the code that is representing the strength and stability of steel shell structures. The steel shell structures known from the past are mostly steel tanks and silo's. In the part about boundary conditions this origin is well represented. The boundary conditions are formulated and supported with sketches of several tank and silo visualizations. Tank and silo structures are mostly designed to store bulk materials or liquids. The steel shell elements that are represented by this study, have most of the time a different function. Tubular piles with a diameter varying from approximately 0.5 to 2 meters with in most cases a structural function. The application of steel tubular piles has increased over time, both in amount as well as in possibilities. This wide spectrum of applications comes with more specific boundary conditions which are not fully covered by the current design code.

2.2. Theoretical boundary conditions

The current design code (NEN-EN 1993-1-6 [1]) make use of three degrees of freedom to describe a boundary condition theoretically. The three displacement directions are: meridional (u), radial (w) and rotational (ϕ). The code describes radial as a displacement in perpendicular direction to the tubes surface, meridional as a displacement in the length direction of the tube and rotational as a rotation around an axis parallel to the tubes surface. In figure 2.1 the geometrical degrees of freedom are presented in a schematic representation of a tubular pile. Varying the degrees of freedom and assuming a homogeneous boundary condition, a set of eighth conditions is found. Adding a situation with a non-homogeneous condition, a set of nine boundaries as shown in the overview of figure 2.1 are derived from the theoretical perspective. For clarity the system of numbering the conditions is chosen in line with the system used in the design code.



(a) Geometrical degrees of freedom

Boundary conditions	Degrees of freedom	Visualisation
BC1F	$w = 0$ $u = 0$ $\phi \neq 0$	
BC1R	$w = 0$ $u = 0$ $\phi = 0$	
BC2F	$w = 0$ $u \neq 0$ $\phi \neq 0$	
BC2R	$w = 0$ $u \neq 0$ $\phi = 0$	
BC3F	$w \neq 0$ $u \neq 0$ $\phi \neq 0$	
BC3R	$w \neq 0$ $u \neq 0$ $\phi = 0$	
BC4F	$w \neq 0$ $u = 0$ $\phi \neq 0$	
BC4R	$w \neq 0$ $u = 0$ $\phi = 0$	
BC_UCF	$w \neq / = 0$ $u = 0$ $\phi \neq / = 0$	

(b) Boundary conditions with corresponding visualizations

Figure 2.1: Theoretical local boundary conditions at shell end

2.3. Boundary conditions in practical situations

The scope of this research is mainly determined by the types of boundary conditions that are used in practical situations. The practical examples in combination with the known boundary conditions from the design code is included in this study. In this paragraph, pictures from practical applications are showed to visualize the types of boundary conditions that are later be analyzed. In section 2.2, nine types of boundary conditions are distinguished that are subdivided in five groups. Per subdivision there are two types, a rotational free (F) and a rotational restrained (R) variant.

2.3.1. BC1

Type one boundary conditions are fully restrained in the radial as well in the meridional direction. The difference between BC1F and BC1R is the possibility of rotation of the tube wall. On the pictures of figure 2.2, two examples of practical applications with type 1 boundary conditions are shown. The first picture (a) shows a situation where the upper ends of the tubular piles are fully encastered in the concrete cope beam. The second picture (b) shows a building pit with steel tubular struts connected by steel plates in the middle as well as on the tube ends. In both examples the tubes are radial and meridional restrained at the boundary condition. A boundary condition is rotational restrained when the material of the steel tubular pile reaches the maximum capacity by bending, before the boundary conditions allows any displacements. For the two situations in figure 2.2, the anchoring depth and concrete quality or the stiffness of the mid/end plates determine the distinction between BC1F and BC1R.



(a) Concrete cope beam on a Quay wall (picture from: Dawson Wam piling)

(b) Plate mid or end connection (Picture from: CalSTA High speed rail)

Figure 2.2: Typical examples of type 1 boundary conditions

2.3.2. BC2

Boundary conditions from type two are restrained in radial but free in meridional directions. The possibility of rotation distinguishes the differences between the conditions BC2F and BC2R. Boundary conditions of type two are not very common, figure 2.3 shows a tubular pile that functions as a support for a floating structure. The anchoring of the floating structure around the tubular pile works as a constraint against ovalisation (radial displacement), but allows meridional displacement. The height, stiffness and fitting of the anchoring ring determining the degree of rotation stiffness. A tube supported in radial direction with a welded ring or flange at the tube end represent the BC2R boundary condition.



Figure 2.3: Sliding boundary condition type 2 (Picture from: Kooiman marine group)

2.3.3. BC3

Type three boundary conditions are free of displacement in radial as well as meridional direction. they are often used in temporarily constructions tubular piles with open end are used as shown in figure 2.4. Tubular piles with an open end are most of the time also free for rotational displacement. These piles are known as piles with a BC3F boundary condition. Piles with an open end boundary in combination with closely spaced rotation stiffeners are distinguished as the BC3R type.



Figure 2.4: Free-end boundary condition type 3 (Picture from: Wikipedia bouwkuip)

2.3.4. BC4

Boundary condition type four consists mostly of practical applications in temporarily structures. Type four boundary conditions are restrained in meridional and free in radial direction. Because temporarily constructions must have the possibility to be reassembled within a relative short period, the connections between elements are not always bolted or welded. Figure 2.5 shows struts with open end that are placed between girders functioning as a part of a soil retaining structure. The tubular piles without stiffening against rotation are categorized as BC4F boundary conditions, while with severe stiffening it is a BC4R condition.



(a) Struts with support plates (Picture from: Folker staal en funderingen)

(b) Struts meridional supported (Picture from: Kandt b.v.)

Figure 2.5: Typical examples of type 4 boundary conditions

2.3.5. BC-UCF

Until now, the current design code only describes homogeneous boundary conditions. In many projects, situations as schematized in figure 2.6 (b) are present during the building phase but also more and more in finalized projects (a). At the position of the concrete floor the tubular pile does have two different types of boundary conditions at both sides of the retaining wall. At the side of the concrete floor the tubular pile is fully restrained and corresponds to a BC1R boundary condition. At the sand side of the pile only soil is present what does not function as a constrain. In almost all cases the retaining wall continues deeper into the ground under the concrete floor. To investigate this situation, a boundary condition is assumed at the location of the concrete floor. Because the steel tubular pile continues deeper into the ground a boundary condition corresponding to BC4F is chosen for the soil side of the pile.

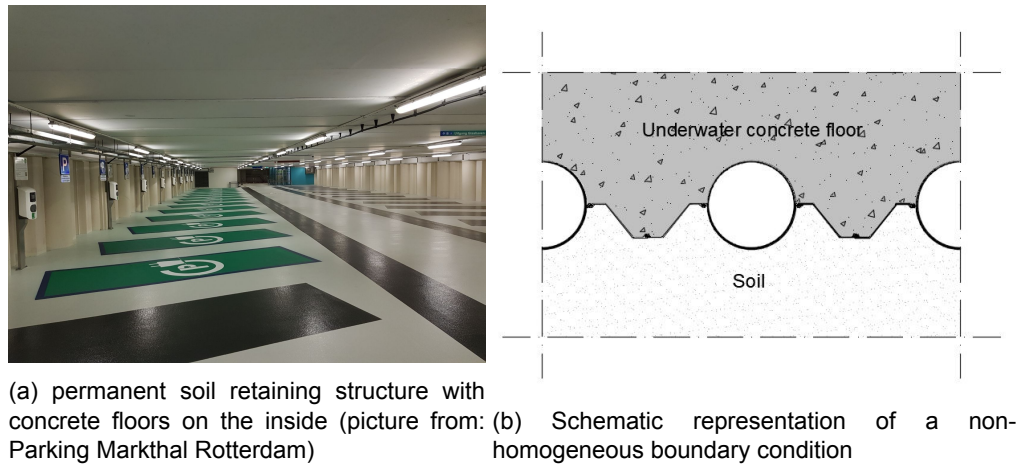


Figure 2.6: Example of a Underwater concrete floor (UCF) boundary conditions

2.4. Discussion

In this chapter boundary conditions for steel tubular piles are discussed. Started with the theoretical method of describing boundary condition by specifying certain degrees of freedom per boundary condition. This method is also used in the current design code for steel shell structures, the NEN-EN 1993-1-6 [1]. The code describes five types of boundary conditions: BC1F, BC1R, BC2F, BC2R and BC3F. By varying the amount and types of constrained directions eight possible boundary conditions can be generated. Looking to the practical applications, a ninth variant with a non-homogeneous boundary completes the list as described in the table of figure 2.1.

From the nine boundary conditions of figure 2.1 eight conditions are selected to be included in the FEM model study. BC3F (free end) is not included in the model because it is not able to generate any stiffness while the model is based on the influence of a boundary condition on a imposed bending moment. Boundary conditions BC2R and BC4R are both not very common in civil engineering practise, for completeness these conditions are included in the model study.

Geometrical and material Imperfections

3.1. Introduction

In the literature study is shown that different types of parameters influence the failure mechanism of local buckling. The parameters that are discussed are geometrical imperfections and residual stresses. The influence of those two parameters in combination with the boundary conditions of interest are investigated in this chapter.

3.2. Geometrical imperfections

Geometrical imperfections are initiators of local peak stresses and mark often the location of possible failure. The imperfection types that are discussed in this chapter are: out of roundness, accidental eccentricity, and dimples as shown in figure 3.1.

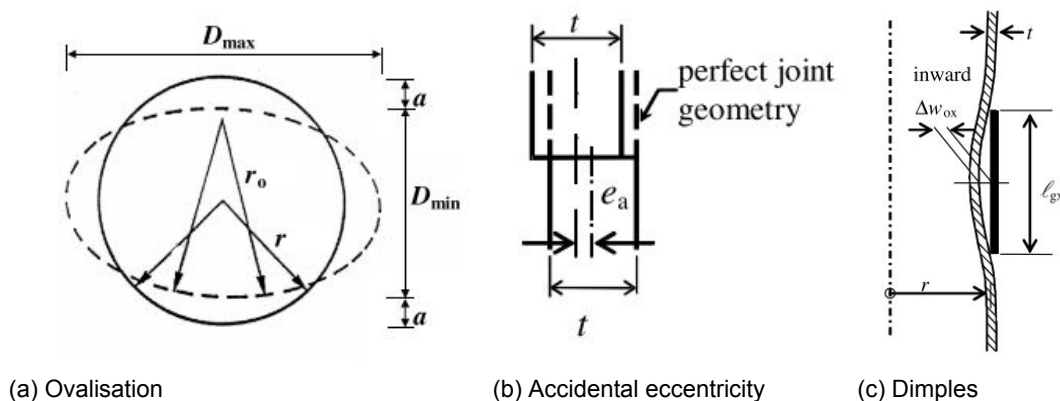


Figure 3.1: Geometrical imperfections following the NEN-en 1993-1-6 [1]

The imperfections are investigated in combination with the influence of different boundary conditions. The purpose of this part is to create an overview of the influence factors known from the current design code. These factors can be compared with FEM model tests with varying imperfections in combination with different imposed boundary conditions. An influence factor for imperfections following the current

design code (NEN-EN 1993-1-6[1]) can be calculated by varying the Quality class parameter Q over the imperfection. The corresponding Q -values from an excellent, high or normal tube quality are included in the resistance calculation as shown in appendix B. The quality classes and there corresponding imperfection parameters are shown in table 3.1. The imperfection with the lowest quality class per tube is normative for the whole tube. The Imperfections are indicated with specific U parameters that are determined as shown in equations 3.1, 3.2 and 3.3.

$$U_r = \frac{D_{max} - D_{min}}{D_{nom}} \quad (3.1)$$

$$U_e = \frac{e_a}{t} \quad (3.2)$$

$$U_0 = \frac{\Delta_{w0x}}{l_{gx}} \quad (3.3)$$

In figure 3.1, the parameters used for the calculation of the U values per imperfection are indicated. The maximum imperfections values per quality class are shown in table 3.1.

Quality class:	Description:	Q:	U _{r,max} :	U _{e,max} :	U _{0,max} :
Class A	Excellent	40	0,007	0,14	0,006
Class B	High	25	0,01	0,2	0,01
Class C	Normal	16	0,015	0,3	0,016

Table 3.1: Prescribed quality classes with there maximum imperfection parameters following the NEN-EN-1993-1-6 [1].

The influence line of the different imperfections is, besides from a quality class, dependent on the type of boundary condition at pile end and the D/t ratio. In the design code the conditions of both pile ends determine the value of the parameter C_x . In the figures 3.2, 3.3 and 3.4 the resistance reduction for even a perfect pile without imperfections is smaller than one. This is caused by the use of ranges per quality class, where the highest class starts by a zero value imperfection but represent imperfections until the limit value of that quality class. The reduced value of the characteristic stress resistance (σ_{xRk}) is normalized by the yield stress (f_{yk}). The ratio is represented by the buckling reduction factor χ_x as shown in equation 3.4.

$$\chi_x = \frac{\sigma_{xRk}}{f_{yk}} \quad (3.4)$$

This ratio (Buckling reduction factor χ_x) shows the influence of an imperfection on the final bearing capacity following the calculation method of the NEN-EN 1993-1-6 [1]. In the graphs the imperfections are represented by their U value, a dimensionless quantity. These values are in all cases dependent on the ratio of the imperfection to the diameter and/or thickness. The effect of the imperfections is shown for the range of D/t ratios used in this study.

3.2.1. Initial ovalisation

The initial ovalisation of steel tubular piles does influence the maximum bearing capacity by influencing the local radius of curvature. The NEN-EN 1993-4-3 [3] shows how the local radius of curvature (r_0) influence the critical compressive strain. Out of roundness consists of initial ovalisation and ovalisation due to bending. The influence of initial out of roundness is included in the current design code, the NEN-EN 1993-1-6 [1]. The amount of initial out of roundness divides piles in one of three quality classes with corresponding reduction in resistance against local buckling. The cases that are distinguished are shown in figure 3.2 below. From the figure a decreasing reduction factor is observed with an increasing D/t ratio. Also, a lower value is observed by piles with one or two BC2 pile ends. These reductions come over an increasing out of roundness parameter U_r described in the literature review in appendix B.

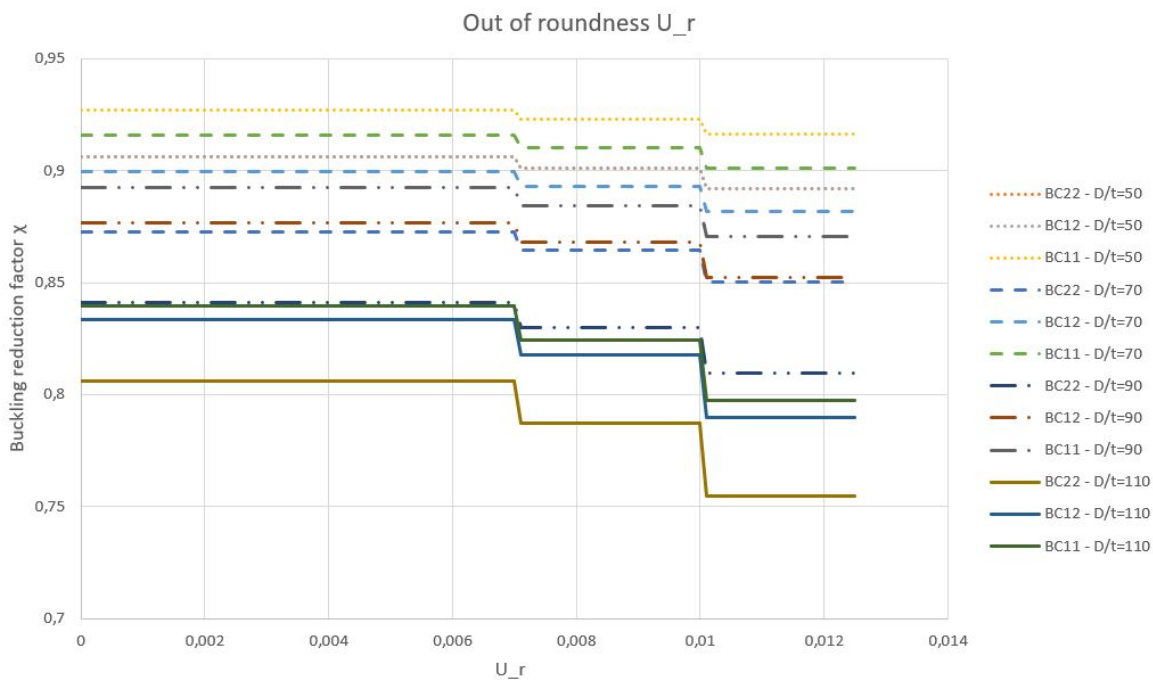


Figure 3.2: Calculated buckling reduction factor on the tube resistance in bending, based on NEN-EN 1993-1-6 for initial ovalisation

The effect of this initial imperfection is included in the finite element models by adding an initial discontinuity with the help of an eigen mode. The eigen mode causes initial out of roundness's. Ovalisation caused by bending is not manually included in the model, this effect is difficult to predict when rigid influences of boundary conditions take part. The effect of boundary conditions that counteract ovalisation have an estimated influence length given by equation 3.5. This parameter represents an estimated length where the ovalisation, and so the buckling resistance is influenced.

$$L_{influence} = r/t * \text{sqrt}(r * t) \quad (3.5)$$

3.2.2. Accidental eccentricity

Eccentricity of two joined pile pieces is the second imperfection discussed in this chapter. As discussed in the literature review from appendix A the U_e parameter represents a ratio between the eccentricity and thickness (shown in figure 3.1). For this imperfection the same analyses is made and the same trend can be seen in figure 3.3.

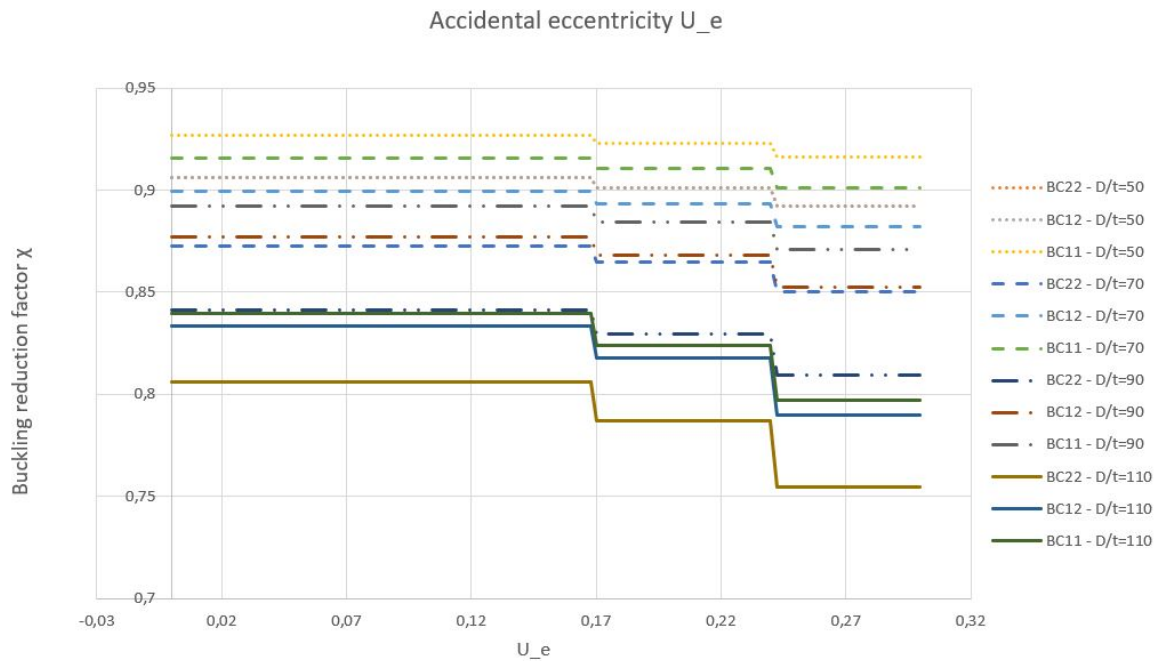


Figure 3.3: Calculated buckling reduction factor on the tube resistance in bending, based on NEN-EN 1993-1-6 for accidental eccentricity

Accidental eccentricity will not be included in the FEM models, This imperfection only exists when two or more segments are connected. The imperfection is more controllable and therefore not leading in this study.

3.2.3. Dimples

Dimple imperfections are deviations in the shell surface that reduce the radius locally. The dimple amplitude is dependent on the specific gauge length for that direction as described in appendix B. For the analyses on the reduction of the local buckling resistance, dimples in the tube length direction are used. The reduction of the resistance is described for the parameter U_0 . Figure 3.4 shows also for this imperfection the same prescribed trend as is seen by the other imperfections.

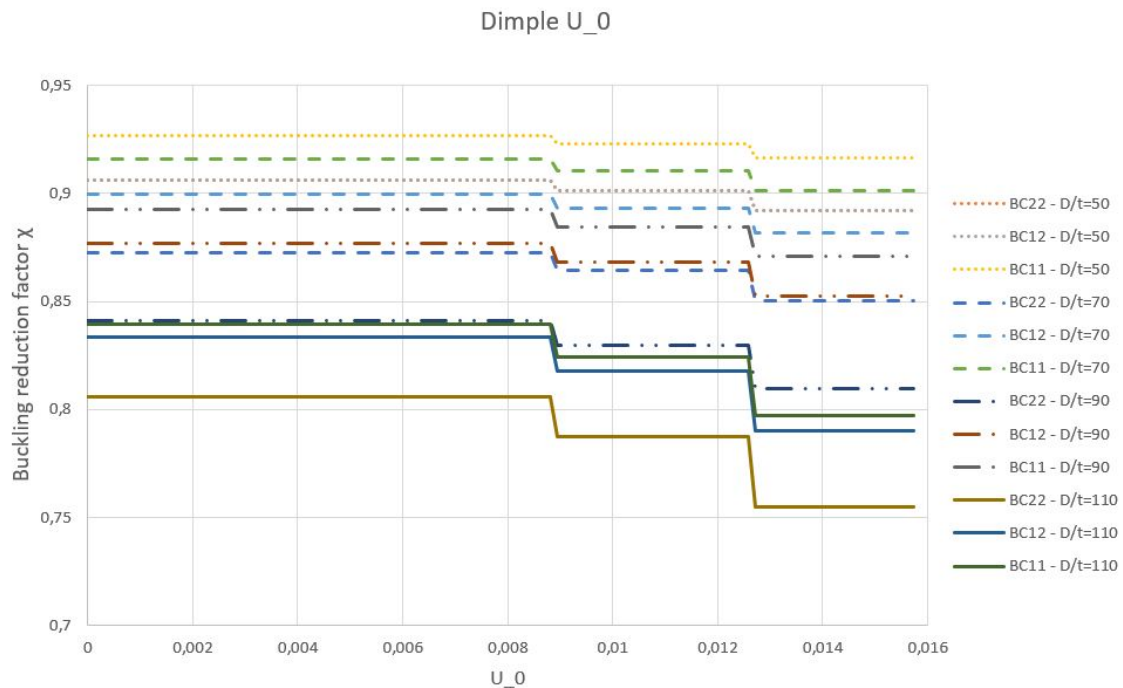


Figure 3.4: Calculated buckling reduction factor on the tube resistance in bending, based on NEN-EN 1993-1-6 for dimple imperfections

Dimple depths, corresponding to the limit values of the quality classes, are used to compare the behaviour of tubes with specific boundary conditions to the prescribed situations in the NEN-EN 1993-1-6 [1]. The amplitude of an eigen mode is used to represent the dimple in the initial state of the finite element models.

3.3. Residual stresses

Residual stresses in steel tubular piles are mostly generated during the production process of the piles. During this production process, long steel plates are made and stored on a coil. These coils are used to feed the machine that spiral bend and weld the plates into tubular piles. The process of cold uncoiling, straightening and spiral bending cause stresses in the material that are present after finishing the production process. Not only plastic deformation by cold bending, but also the welding and the cooling processes after manufacturing of the plates are known as influence factors for residual stresses. The entire production process of a spiral welded tubular pile is shown in figure 3.5. In this thesis only the residual stresses from the cold bending process are investigated. The interest of this study is to research the influence of residual stresses on tubular piles with boundary conditions that allow or counteract ovalisation.

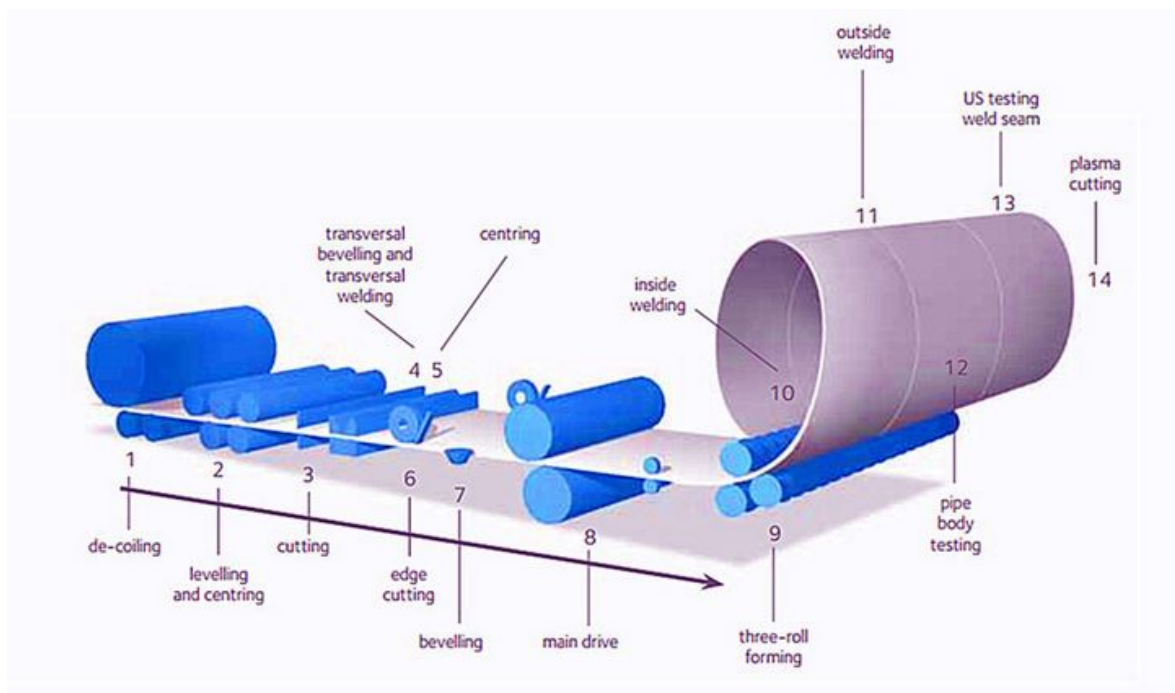


Figure 3.5: Production process of steel tubular piles, Picture from: www.primesteeltube.com

3.3.1. Cold bending

During the production process of steel tubular piles, steel plates from a coil are uncoiled, straightened and spiral bended. The process of spiral bending is analyzed by Vasilikis et al.[4], modeling this process in ABAQUS [12]. From the FEM model they derived residual stresses that are present in the model after spiral bending. Figure 3.6 gives a graphical representation of the normalized hoop and axial stresses found over the thickness of the material. These stresses are normalized over the yield stress f_y , and specified from the inside to the outside of the material. For the three steel qualities used in this study the actual residual stresses are presented in table 5.1.

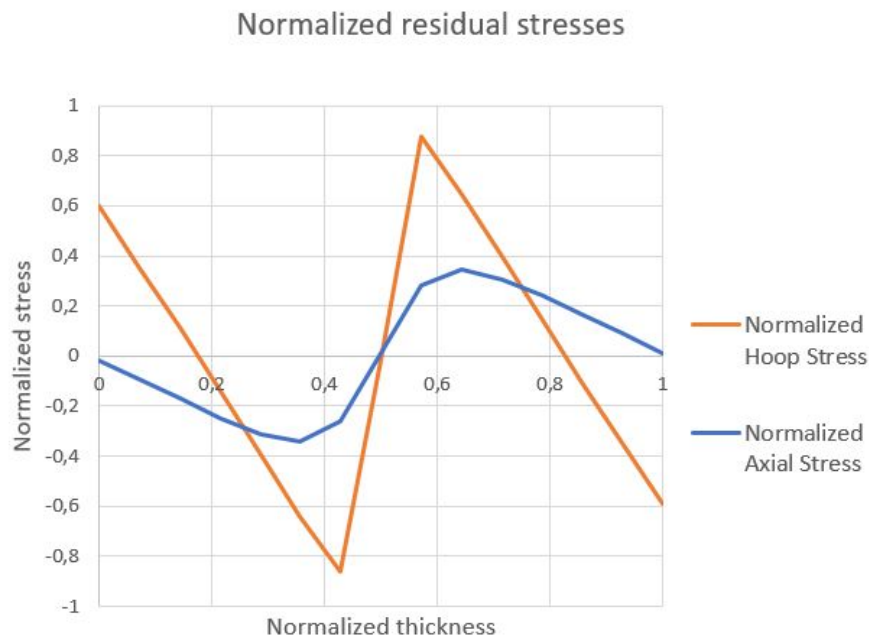


Figure 3.6: Residual stress distribution over the thickness, derived by Vasilikis et al.[4]

Steps:	Normalized values:			S355:		S420:		S460:	
Intergration points	Normalized thickness	Normalized Axial Stress	Normalized Hoop Stress	Axial Stress	Hoop stress	Axial Stress	Hoop stress	Axial Stress	Hoop stress
#	[-]	[-]	[-]	[N/mm ²]	[N/mm ²]	[N/mm ²]	[N/mm ²]	[N/mm ²]	[N/mm ²]
1	0,00	-0,018	0,598	-6,4	212,3	-7,6	251,2	-8,3	275,1
2	0,07	-0,096	0,354	-34,1	125,7	-40,3	148,7	-44,2	162,8
3	0,14	-0,171	0,114	-60,7	40,5	-71,8	47,9	-78,7	52,4
4	0,21	-0,248	-0,139	-88,0	-49,3	-104,2	-58,4	-114,1	-63,9
5	0,29	-0,312	-0,392	-110,8	-139,2	-131,0	-164,6	-143,5	-180,3
6	0,36	-0,342	-0,641	-121,4	-227,6	-143,6	-269,2	-157,3	-294,9
7	0,43	-0,262	-0,862	-93,0	-306,0	-110,0	-362,0	-120,5	-396,5
8	0,50	0,010	-0,017	3,6	-6,0	4,2	-7,1	4,6	-7,8
9	0,57	0,284	0,875	100,8	310,6	119,3	367,5	130,6	402,5
10	0,64	0,343	0,646	121,8	229,3	144,1	271,3	157,8	297,2
11	0,71	0,307	0,398	109,0	141,3	128,9	167,2	141,2	183,1
12	0,79	0,241	0,146	85,6	51,8	101,2	61,3	110,9	67,2
13	0,86	0,165	-0,106	58,6	-37,6	69,3	-44,5	75,9	-48,8
14	0,93	0,089	-0,345	31,6	-122,5	37,4	-144,9	40,9	-158,7
15	1,00	0,010	-0,59	3,6	-209,5	4,2	-247,8	4,6	-271,4

Table 3.2: Normalized residual stresses over the thickness, following Vasilikis et al. [4]

3.3.2. Residual stress ring model

From the research of S. van Es [13], a method is known to indicate residual stresses in tubular piles. From the tubular piles used in his research experiments, ring segments were made and cutted. Residual stress in the material causes opening or closing of the ring segment as shown in figure 3.7.



Figure 3.7: cutted ring segments from residual stress estimation S. van Es [13]

The stresses found by Vasilikis et al. [4] represent the cold bending process from a straight plate to a tubular shape. The residual stresses in this case should show an opening ring segment with some eccentricity. In the results of the experiments of S. van Es, not only opening ring segments were found but also closing segments. In case of a closing segment, the trend in the residual stresses defined in table 3.2 should change of sign. The actual residual stresses in a tubular pile is a summation of the position on the coil, the straitening process and the spiral bending process. To validate the residual stresses of table 3.2, a ring model with these stresses is created in ABAQUS. Since the found residual stresses are obtained from a coordinate system parallel and perpendicular to the spiral weld and applied in cylindrical one, only opening or closing displacements are expect. The used ABAQUS [12] model from figure 3.8 is already cutted and restrained at one of the cutted sides.

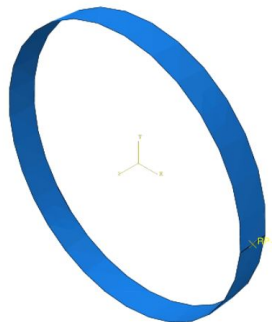


Figure 3.8: Ring model (ABAQUS [12]) used for validation residual stresses. Tested tube: $D = 1422\text{mm}$, $t = 16\text{mm}$, $f_y = 355\text{N/mm}^2$, $D/t = 89$

Two separate FEM models are created to check the influence of the found residual stresses. One model with the stresses as showed in table 3.2, and one with these stresses with a changed sign. The base model from figure 3.8 is loaded by the residual stresses in 15 thickness integration points. To run the model, a dummy load is placed on the restrained boundary of the cutting edge. The model runs in 100 steps (increments) and produces the by residual stress displaced ring segments of figure 3.9. The displacements are in line with the expectations of only opening and closing movement. No eccentric movement is observed because the coordinate system is cylindrical and not spiral as in the model of Vasilikis et al. [4].

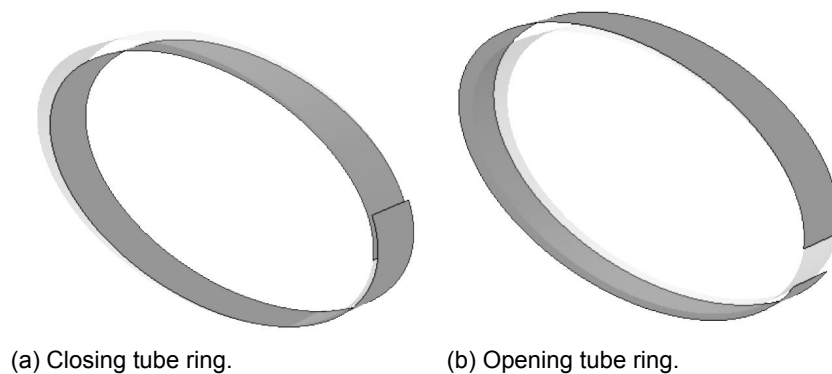


Figure 3.9: Effect of residual stress on a ring segment modeled in ABAQUS [12]. Tested tube: $D = 1422\text{mm}$, $t = 16\text{mm}$, $f_y = 355\text{N/mm}^2$, $D/t = 89$

The vertical displacements that are observed in the ABAQUS ring model tests, for the opening and closing segments are shown in figure 3.10. The opening and closing displacements in the tests of S. van Es [13] are in a range of -156mm to $+865\text{mm}$. The displacements of the model tests are within this range (-70mm and $+79\text{mm}$) but are quite small in comparison to the real measurements. A possible reason for these differences is the fact that in the FEM model only the residual stress by spiral bending is included.

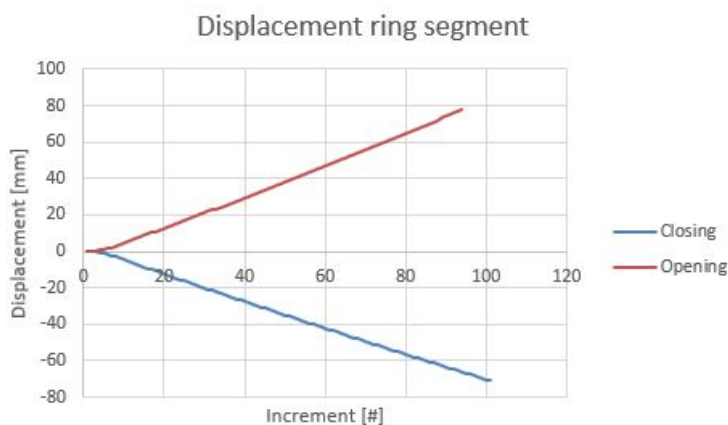


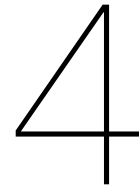
Figure 3.10: Opening or closing displacements of the cutting edge by residual stresses. Tested tube: $D = 1422\text{mm}$, $t = 16\text{mm}$, $f_y = 355\text{N/mm}^2$, $D/t = 89$

3.4. Discussion

In the study into geometrical imperfections, initial ovalisation, accidental eccentricity and dimples are treated. These imperfections are included in the current design code and are represented by three quality classes. The quality classes impact the calculated maximum resistance. This resistance reduction is shown per imperfection type in the figures 3.2, 3.3 and 3.4. For this study it is chosen to investigate the influence of dimple imperfections in combination with boundary conditions on the resistance of the tubular pile. The limit values of each quality class in combination with, one boundary condition that can ovalize (BC4) and one that counteract ovalisation (BC1) are compared with the resistance reduction curves of figure 3.4. The imperfections are generated by the buckling eigenmodes. In chapter 5 the results of this study are shown and discussed.

Accidental eccentricities are not included in the model study because these imperfections can most easily be provided by inspection before using a tubular pile. Dimple imperfections are often caused when the tube is already in use and not easy to replace. Initial ovalisation is included in the model because the initial discontinuities are introduced for the dimple imperfection analyses. Nevertheless there is no further study to the impact of this imperfection in combination with different boundary conditions. Because of the choice to use a fixed tube length in the model, a varying influence length as described in equation 3.5, makes the results incomparable.

Residual stresses in tubular piles can have different reasons, as described in this chapter. One of these reasons is cold spiral bending of the steel plate into a tubular pile. The residual stresses introduced by this bending process are studied by Vasilikis et al. [4]. From experiments by S. van Es [13], a method is known to check residual stresses by cutting a ring segment open and analyze the displacements. From The preformed ABAQUS model tests with such a ring segment, is known that the residual stresses of the cold spiral bending process found by Vasilikis et al. are in the range of the observed residual stresses by S. van Es. The effect of residual stresses in combination with one boundary condition that can ovalize (BC4) and one that counteract ovalisation (BC1) is included in the FEM model study. The results of this study are also discussed in chapter 5.



FEM model tests

4.1. Model test approach

In the previous two chapters the input parameters for the FEM model research are studied. The influence of these parameters on the local buckling failure mechanism is studied by varying the parameters in a model and compare the results. To create a model that fits this study sufficiently and produces the needed information, the following steps are taken:

- Familiarise with the finite element method and the corresponding software.
- Create a theoretical base model capable of testing all boundary conditions under the same circumstance, loaded by bending only.
- Specify the needed data, and the process of gaining this data from the FEM models.
- Define the geometrical and material properties of the test range as input for the FEM software.
- Transfer the theoretical model and boundary conditions into a volumetric shell model with the correct boundary conditions in the ABAQUS FEM software.
- Determine the needed element type and size for accurate model test results.
- Generate different eigenmodes to gain information about the failure shape and introduce imperfections in the model.
- Run the models and produce the needed data with the post processing script (see appendix C).

In the upcoming paragraphs these steps are each discussed in detail. With the information of chapter 2, a model is created to determine the influence of various boundary conditions on the failure mechanism of local buckling of steel tubular piles. Chapter 3 describes the geometrical imperfections and the residual stresses that need to be included in the FEM models. The results of the FEM model tests are presented in the parametric study of chapter 5.

4.2. Finite element method

The study to the influence of different boundary conditions on the failure mechanism of local buckling initiated the use of the finite element method (FEM). This numerical method solves partial differential equation of finite connected elements of a subdivided structure. The system of partial differential

equations is reduced to algebraic equations that can be solved using linear algebra techniques. By subdividing a structure in finite elements with all their own degrees of freedom, it can be used to predict the behaviour of a real structure. The precision of the method can be enlarged by increasing the number of elements. A logical consequence is large numbers of equations with possible complex geometries that asks computers to solve them. Figure 4.1 shows the algebraic base relation that couples the forces with the use of the stiffness matrix to the displacements. Plasticity is not included in this explanation, but it is in the models used in this thesis.

$$[F] = [K] * [U] \quad (4.1)$$

Figure 4.1 shows the relations used in FEM software, which in combination with the algebraic method from equation 4.1 makes it possible to solve the equations and generate the information that is necessary. As stated above, computers are used to solve the equations and speed up the process. For this thesis the ABAQUS [12] software is used for the finite element analyses.

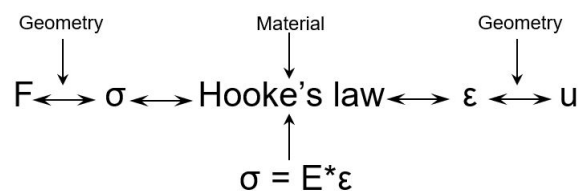


Figure 4.1: Basic principles of the finite element method

The proposal to use the ABAQUS software is based on the previous work (S. van Es [13], J. Winkel [14], N. Kostis [9] and Vasilikis et al. [4]) that is done in the field of local buckling analyses over the past years. In all these projects, the ABAQUS software is used because it fits sufficient for a geometrically and materially nonlinear analyses. For this study, material and geometric non-linearity are also included so the ABAQUS software is chosen.

4.3. Theoretical model

To investigate the influences of the boundary conditions described in chapter 2 on the failure mechanism of local buckling, a model needs to be constructed. In a parametrical study, a base model is chosen, and by varying just one parameter, the influence of that parameter is observed. To test the influence of imperfections and residual stresses, this method is sufficient and also used in this study. For a study to the effect of boundary conditions not just one parameter varies, but the base model itself is varying with every support condition. To make it still possible to compare the different boundary conditions, the starting points for each model need to be the same. When a support condition is not able to resist normal and shear actions, only bending remains. The setup of the models is explained in paragraphs 4.3.1 and 4.3.2.

4.3.1. Mechanical model

To meet the main starting point of the model, pure bending only, the mechanical base model of figure 4.2 shows a half "4 point bending test" model. This setup provides the possibility of modeling a boundary condition at point C in combination with pure bending only. The standard length of the system is set on 10 meters, $L_1 = \frac{1}{3} * L$ and $L_2 = \frac{2}{3} * L$. The bar between point A and B (L_1), functions as a pendel bar to introduce rotation at point B. The rotation is created by an imposed displacement of the support at point A. The beam model as it is showed in figure 4.2 is not capable of generating any bending moment

in the bar between point B and C. Replacing the line in the model by a volumetric element (figure 4.3), makes it capable to generate a uniform moment over L_2 . The sliding support conditions at point A and B prevent the model from introducing normal forces.

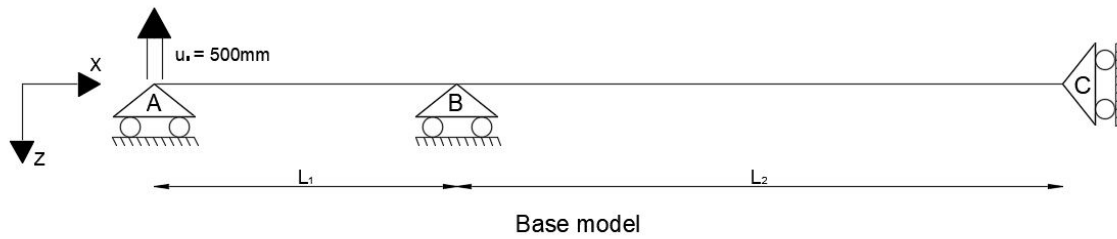


Figure 4.2: Basic mechanical model (pure bending only)

The boundary conditions (BC) in the volumetric model from figure 4.3 are situated in line with the center of the tubular pile at reference points (RP). Later in the modeling process the RP's are coupled to a tube cross-section (CS). In this way, imposed displacements, constraints and boundary conditions can be given and later varied.

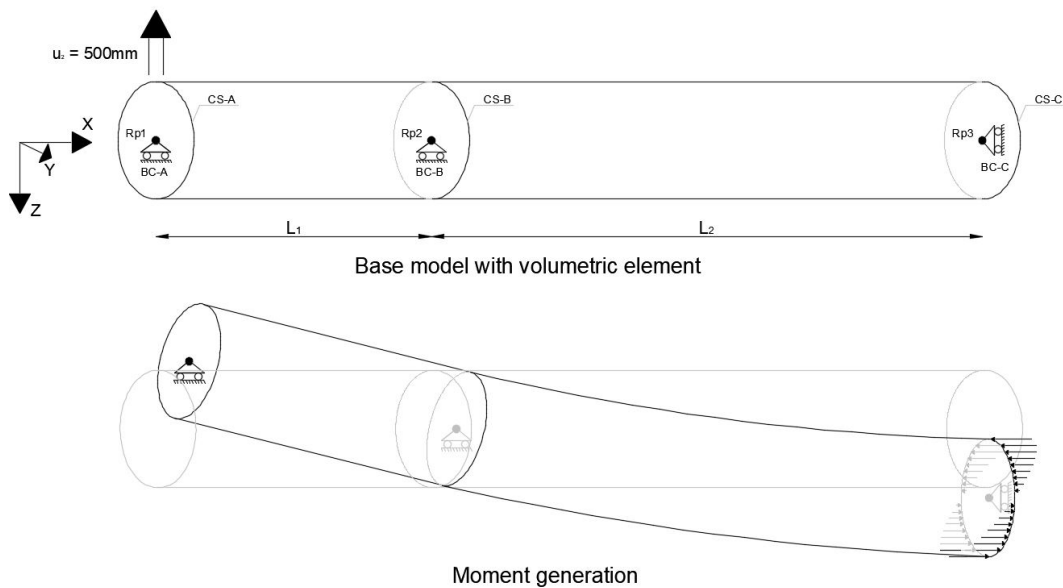


Figure 4.3: Volumetric base model and moment generation model

4.3.2. Data generation

By creating a model to investigate the influence of certain parameters, the way of collecting the correct data for analyses is important. In the model used for this study not only comparison to the own generated data is important, also the fit within other researches in the field is taken into a count. For the tubular piles in this study a moment-curvature diagram needs to be created. The test setup as shown in figure 4.2 and 4.3 represents a half four point bending test. In this setup the moment in the tested area (B-C) of the tubular pile is calculated with use of the vertical reaction force (RF_2) in A and is given by equation 4.2. The curvature of the tested area (B-C) is calculated with use of the rotation at B and the length of the tested area as shown by equation 4.3.

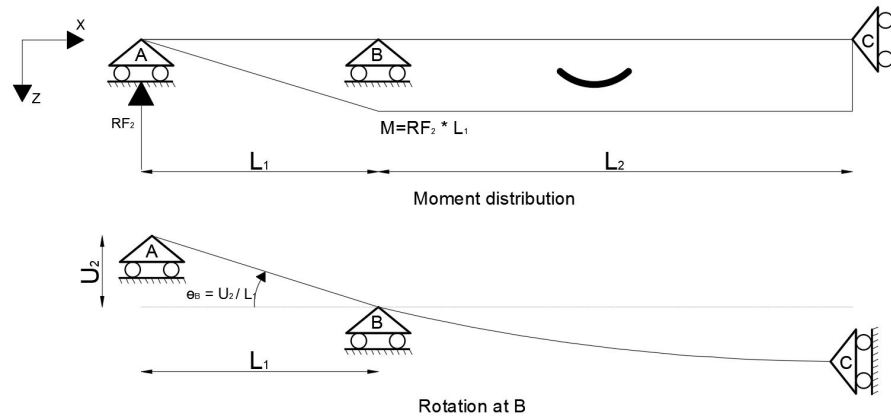


Figure 4.4: Moment distribution and rotation at point B of the base model

$$M = RF_2 * L_1 \quad (4.2)$$

$$K = \frac{\theta_B}{L_2} = \frac{U_2/L_1}{L_2} \quad (4.3)$$

A schematic overview of the determination of the moment and curvature quantities is given in figure 4.4. Because the range of tested tubular piles consists of different steel qualities and D/t ratios, there is chosen to normalize the observed moment and curvature. The observed moment is normalized by the full plastic moment (as in Rotter 2016 [11]). The plastic moment is chosen because, the test range consists only of cross-section class 3 and 4 tubes. These tubes are known for their buckling sensitivity and therefore buckle before reaching the plastic moment, what results in normalized values all smaller than one. The calculation used for $M_p l$ is shown in equation 4.4. The curvature observed from the tests will be normalized by the curvature-like quantity (K_i as in equation 4.5) as in Vasilikis et al. [4] for analyses where the tested tube is constant, only a imperfection is varying. In studies where the model test results of different geometries and steel qualities are compared, Kappa elastic (K_e as in equation 4.6) is used to normalize the curvature.

$$M_p l = \frac{4}{3} D^3 \left(\frac{3}{4} \left(\frac{t}{D} \right) - \frac{3}{2} \left(\frac{t}{D} \right)^2 + \left(\frac{t}{D} \right)^3 \right) f_y = \frac{1}{6} * (D^3 - (D - 2t)^3) * f_y \quad (4.4)$$

$$K_i = t/(D - t)^2 \quad (4.5)$$

$$K_e = \frac{f_y/E}{(D - t)/2} \quad (4.6)$$

4.4. Geometrical and material properties

For the model tests that are preformed, a specific range of samples is selected to create a solid representation of the piles used in practise. For the range of samples, the D/t ratio and the steel quality are the important parameters. The D/t ratio is varied within four groups represented by a D/t ratio of 50, 70, 90 and 110. Per subgroup three geometries with a D/t ratio close to the one of the subgroup are selected of the real dimensions used by the manufacturer [7]. Every tubular pile that is selected, is tested in three different steel qualities, S355, S420 and S460. The combination of these two parameter variations gives an test range of 36 different tubular piles as shown in table 4.1. The parameter (with $\epsilon = \sqrt{235/f_y}$) in the last column is used to determine the cross-section class of each tube. When this parameter is larger than 90, it is a class 4 tube.

$\approx D/t$	D/t	t	D	D	L _{invoed}	Steel quality	$(D/t)/\epsilon^2$
-	-	[mm]	[inch]	[mm]	[mm]	-	-
50	50,80	25	50	1270	3200,299	S355	76,97
						S420	90,71
						S460	99,61
	53,35	20	42	1067	2755,413	S355	80,83
						S420	95,27
						S460	104,61
	54,00	16	34	864	2244,738	S355	81,82
						S420	96,43
						S460	105,88
70	69,08	25	68	1727	5074,853	S355	104,67
						S420	123,36
						S460	135,45
	71,10	20	56	1422	4239,254	S355	107,73
						S420	126,96
						S460	139,41
	69,88	16	44	1118	3304,135	S355	105,88
						S420	124,79
						S460	137,02
90	89,40	25	88	2235	7471,388	S355	135,45
						S420	159,64
						S460	175,29
	91,45	20	72	1829	6183,873	S355	138,56
						S420	163,30
						S460	179,31
	88,88	16	56	1422	4739,63	S355	134,67
						S420	158,71
						S460	174,27
110	109,70	25	108	2743	10158,36	S355	166,21
						S420	195,89
						S460	215,10
	111,75	20	86	2235	8353,266	S355	169,32
						S420	199,55
						S460	219,12
	107,94	16	70	1727	6343,567	S355	163,54
						S420	192,75
						S460	211,64

Table 4.1: Range of tubular piles used in model tests

In this model test study no material tests are performed that can be used to define the material properties as they are in practise. An engineering stress-strain diagram is made from the three materials that are used in the test range. An assumed E-modules for the plastic behavior of 0.001 times the elastic E-modulus due to strain hardening is used to determine the plastic strain. This simplification is made because the non-linear part of a sigma epsilon diagram is not reached in the model tests. The Poisson ratio for steel is assumed as $\nu = 0.3$. The graphs that represent the material properties of the engineering sigma-epsilon diagrams for S355, S420 and S460 are presented in figure 4.5.

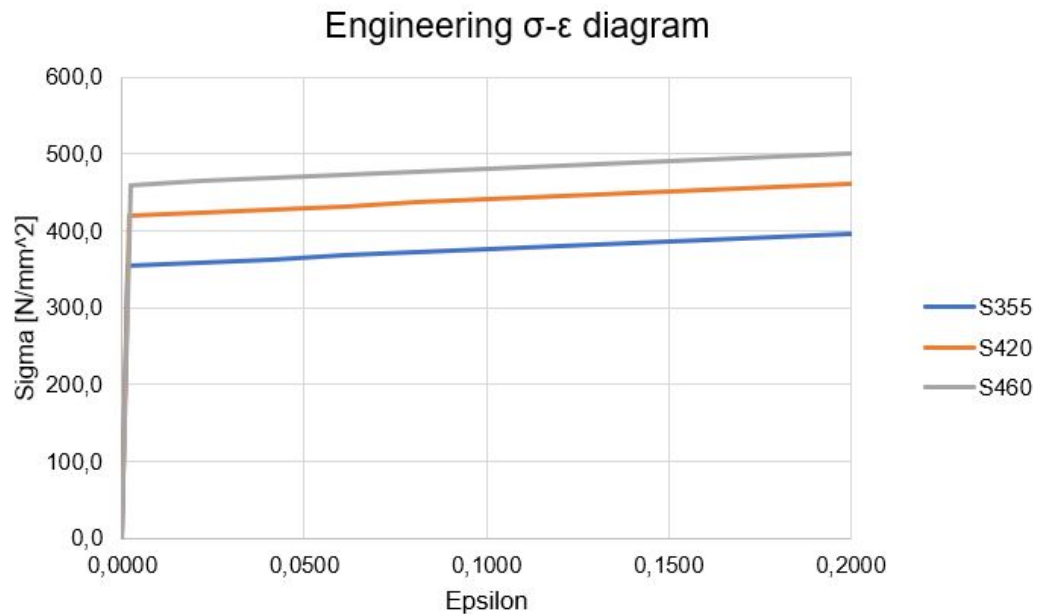


Figure 4.5: Engineering sigma-epsilon diagrams for the steel qualities S355, S420 and S460

4.5. FEM model

The theoretical model from paragraph 4.3 is transformed to a FEM base model with the help of the ABAQUS software. For each tube size a new geometrical model is made with the same outline to have a consistent base, so only the variables of interest will influence the outcomes. The base model consists of a geometry, reference points and partitions/cross-sections.

4.5.1. Base model

The base model is created with the help of the ABAQUS software interface. A step by step guideline of the modeling process is added in appendix C. Within the software a geometry of the 3D plate element is designed and within the sub menus the material and the thickness are assigned. To be able to assign boundary conditions and constraints later on in the process, reference points and partitions are made. In figure 4.6 the model with the reference points and partitions at position A, B and C (as in figure 4.2) is shown.

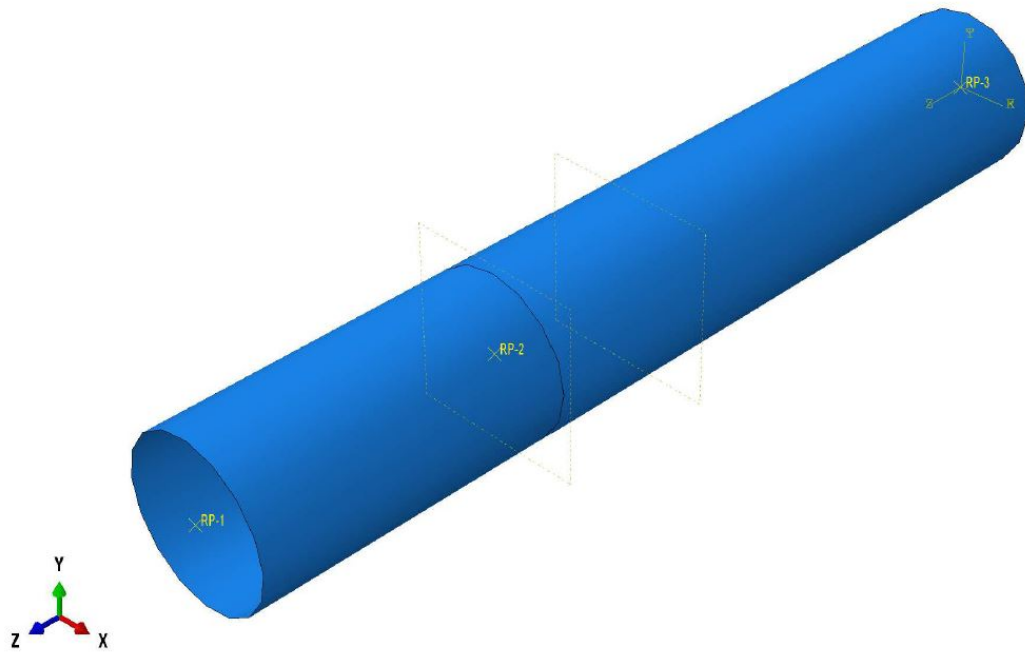


Figure 4.6: ABAQUS base model

4.5.2. Local and global boundary conditions (constraints)

To be able to test the influence of the different boundary conditions on the failure mechanism of local buckling, these boundaries need to be modeled in the ABAQUS software. Following the mechanical base model, the changing boundary condition must be modeled at the tube end on position C. Position A and B have a constant boundary conditions over all tests. The figures 4.7 and 4.8 show the positions of boundary conditions and the constraints in the model.

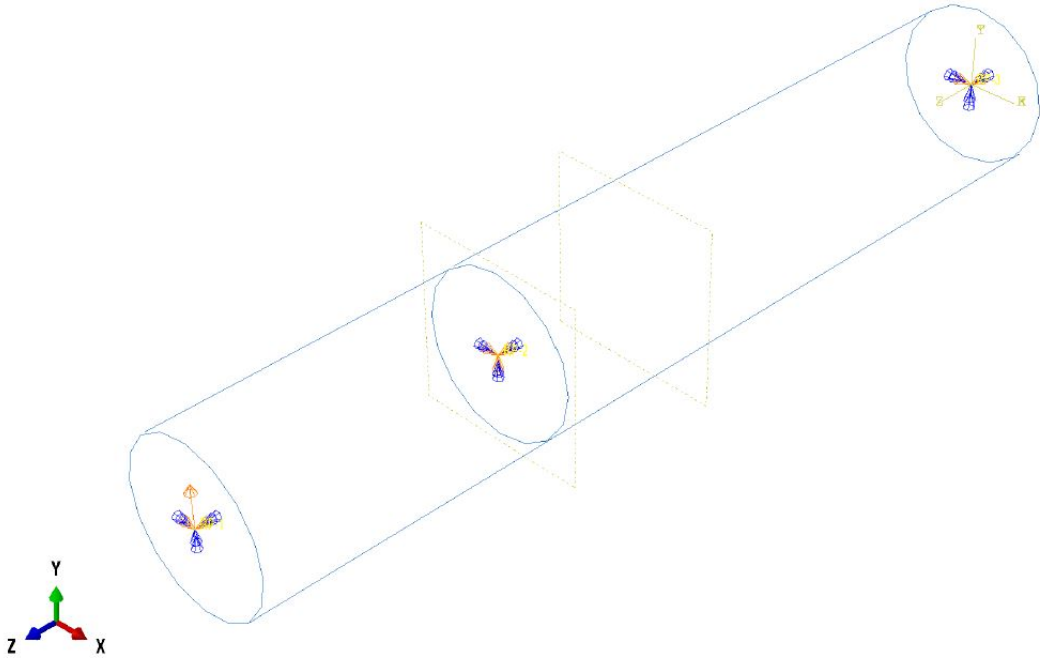


Figure 4.7: Placement of the boundary conditions in the ABAQUS FEM model

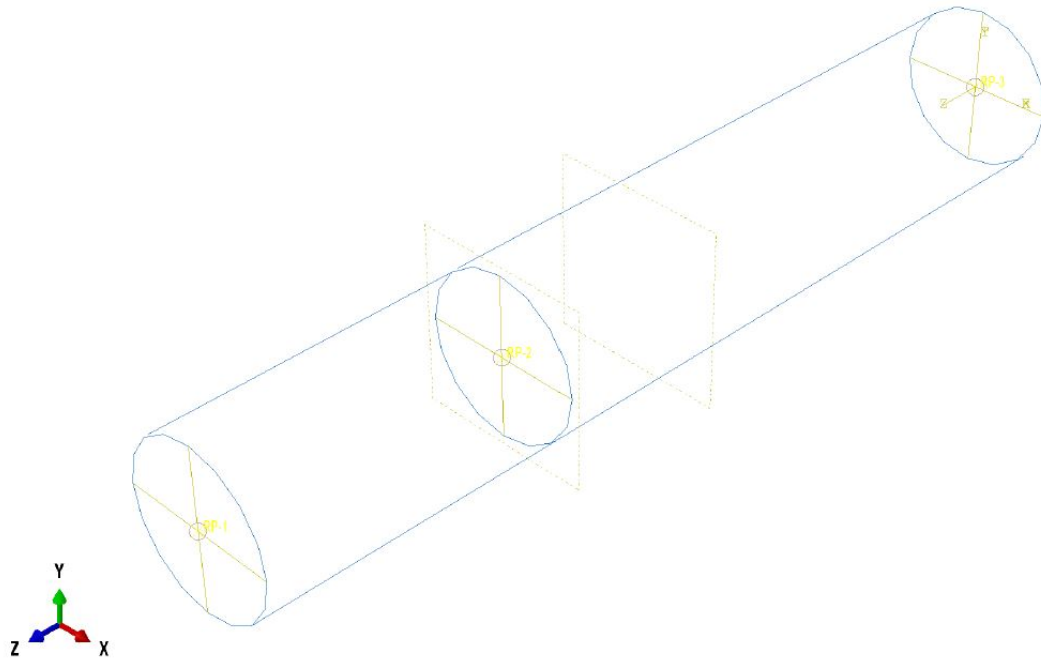


Figure 4.8: Placement of the constraints (CS) in the ABAQUS FEM model

Important to know is the difference between the local and global conditions. All boundary conditions are tested with the same mechanical base model of figure 4.2. The support at position C can displace free in vertical direction. Not all boundary conditions that are tested have a degree of freedom in the vertical direction. A distinction between a local system and a global system will provide the possibility to run all boundaries with the same base model. The boundary conditions as they are distinguished in chapter 2, are the local conditions at the tube end. These conditions specify the behaviour of the tube end or cross-section with respect to the reference point. A kinematic coupling between the cross-section (CS) and the reference point (RP) is made as shown in figure 4.9. The conditions (local constraints) that are given to the kinematic coupling, represent the boundary conditions of chapter 2. In figure 4.9 only 15 coupling lines are showed for visualization, in practise the whole cross-section is coupled under the prescribed conditions. The global system is used to describe the degree of freedom of the reference points (RP) itself. The combination of the global and local system makes it possible to generate a vertical (U_2) displacement of RP-3 while the displacements, horizontal and vertical in the plane of the cross-section with respect to RP-3 remain zero.

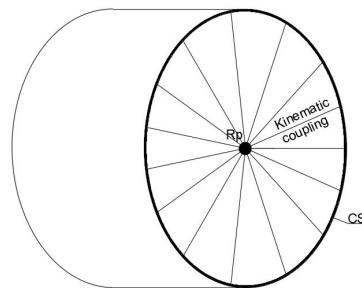


Figure 4.9: Schematization of the kinematic coupling between CS and RP

BC	Local constraints at CS Constraint displacement = X							Global boundary condition at RP Constraint displacement = X							Imposed displacement
	Location	U1	U2	U3	UR1	UR2	UR3	Location	U1	U2	U3	UR1	UR2	UR3	Displacement in mm
BC1F	CS-A	X	X			X	X	RP-1	X	X	X	X	X	X	500
	CS-B		X					RP-2	X	X	X	X	X	X	0
	CS-C	X	X	X				RP-3	X		X	X	X	X	0
BC1R	CS-A	X	X			X	X	RP-1	X	X	X	X	X	X	500
	CS-B		X					RP-2	X	X	X	X	X	X	0
	CS-C	X	X	X	X	X	X	RP-3	X		X	X	X	X	0
BC2F	CS-A	X	X			X	X	RP-1	X	X	X	X	X	X	500
	CS-B1		X					RP-2	X	X	X	X	X	X	0
	CS-C	X	X	X				RP-3	X			X	X	X	0
BC2R	CS-A	X	X			X	X	RP-1	X	X	X	X	X	X	500
	CS-B1		X					RP-2	X	X	X	X	X	X	0
	CS-C	X	X	X	X	X	X	RP-3	X			X	X	X	0
BC3R	CS-A	X	X			X	X	RP-1	X	X	X	X	X	X	500
	CS-B1		X					RP-2	X	X	X	X	X	X	0
	CS-B2			X				RP-3	X	X		X	X	X	0
BC4F	CS-A	X	X			X	X	RP-1	X	X	X	X	X	X	500
	CS-B		X					RP-2	X	X	X	X	X	X	0
	CS-C			X				RP-3	X	X	X	X	X	X	0
BC4R	CS-A	X	X			X	X	RP-1	X	X	X	X	X	X	500
	CS-B		X					RP-2	X	X	X	X	X	X	0
	CS-C			X	X	X	X	RP-3	X	X	X	X	X	X	0
BC-UCF	CS-A	X	X			X	X	RP-1	X	X	X	X	X	X	500
	CS-B		X					RP-2	X	X	X	X	X	X	0
	CS-C1	X	X	X	X	X	X	RP-3	X		X	X	X	X	0
	CS-C2			X											

Table 4.2: Restrained degrees of freedom for Constraints and BC's in ABAQUS models

The boundary conditions as described in table 4.2 are schematized in figure 4.3. The coupling between the local and the global system is represented by the rigid RP block.

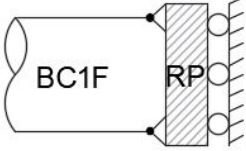

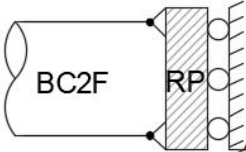

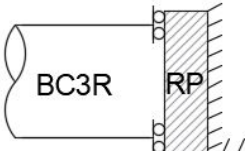
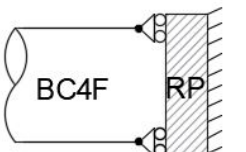

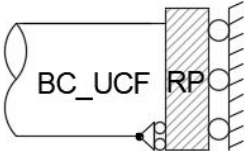
BC	Rotational Free	Rotational Restrained
1		
2		
3		
4		
UCF		

Table 4.3: Schematic representation of the boundary conditions of table 4.2

4.5.3. Mesh and element configuration

Related studies (N.kostis [9], J.Liu [10]) into the improvement of the accuracy by decreasing the mesh size are performed in the field of local buckling analyses. From these studies is known that an accurate mesh size for a steel shell element is in the range of 0.02 to 0.05 times the diameter. Tests that are performed for the tubes of this research show results that are in line and therefore not reported in this research. Because this study involves 12 different tube sizes, the smallest diameter (864mm) is chosen as reference to determine the mesh size. The mesh size in this situation must be chosen between 17.3mm ($0.02 \cdot 864$) and 43mm ($0.05 \cdot 864$). Since this tube is the smallest one in the test range, a mesh size of 40mm is chosen. The part of the model that only is used as a pendel to introduce rotation, is meshed with a larger mesh to decrease the amount of elements. The reason for decreasing the amount of elements is the time a model needs to run the computations. Parts of the structure where realistic deformations are less important are therefore having a coarser mesh. The final mesh configuration is show in figure 4.10.

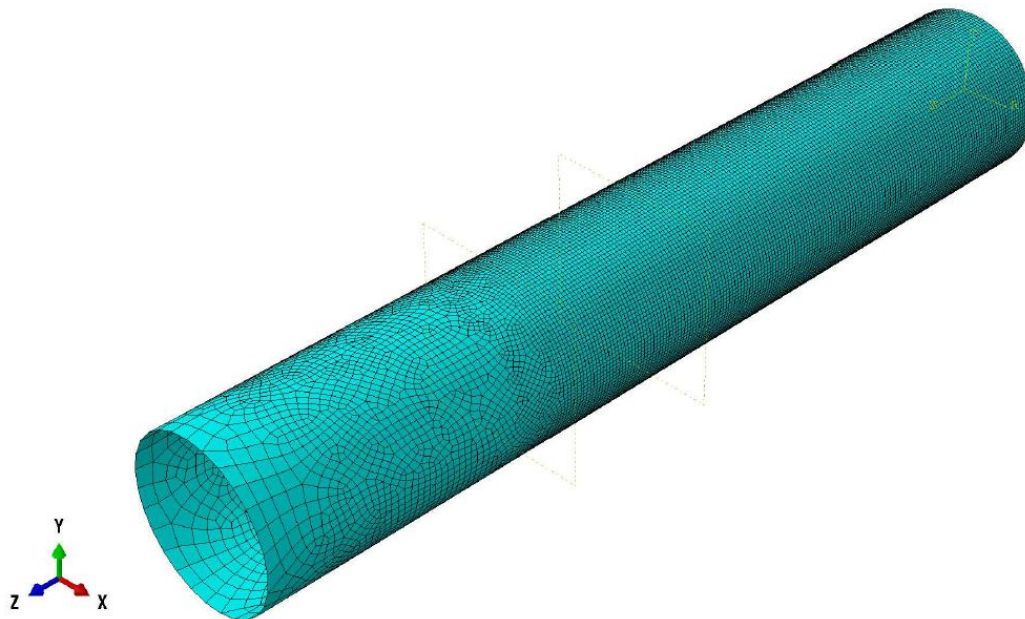


Figure 4.10: Final mesh configuration.

An important part of this research is to investigate the influence of imperfections on different types of boundary conditions. The dimple imperfections are modeled with the help of an eigenmode and a scaling factor. These eigenmodes, that further will be discussed in paragraph 4.5.4, have a geometric shape. To model the initial imperfections accurate and smooth, a minimum of 10 mesh elements must be present in one period / wave length. Figure 4.11 shows a close-up of eigenmode 1, where one period / wave length is formed by 10 to 11 mesh elements.

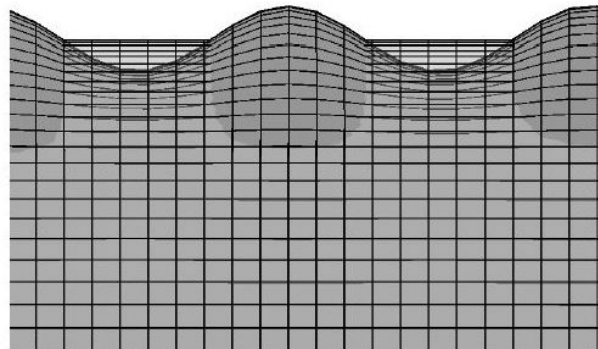


Figure 4.11: Ratio between the mesh size and the period of a eigen mode.

For the shell element choice a reference is made to the study of N.Kostis [9], that describes an influence study to three types of elements. A SR4, S4 and a 2^e -order element are compared for a steel shell structure analyses. No significant differences in the results are found, so the SR4 (reduced integration) element type is used because of the computational advantages.

The amount of integration points in thickness is for this study determined by the format of the residual stresses described in paragraph 3.3.1. This format consists of 15 thickness integration points what is considered as very accurate.

4.5.4. Eigenmode analyses

Eigenmode analyses, or eigen value buckling analyses are used for structures with nonlinear behavior before collapse. thin walled tubular piles with a high D/t ratio are known for their nonlinear failure mechanism. For this type of structures an eigenmode analyses gives information about the failure shape. For this study the eigenmode analyses are mainly used to determine the most likely buckling location to ad imperfections.

Eigenmode analyses are preformed for all tubes and boundary conditions. In the figures 4.12 and 4.13 the first two eigenmodes of a tube with the boundary condition BC1R are shown. A wave pattern of sinusoidal or co-sinusoidal waves with a maximum amplitude of 1mm in the middle can be observed. This pattern is common for the first two eigenmodes. Looking to eigenmodes 3 till 12 in appendix D, the same wave patterns with two or three local maximum values are observed.

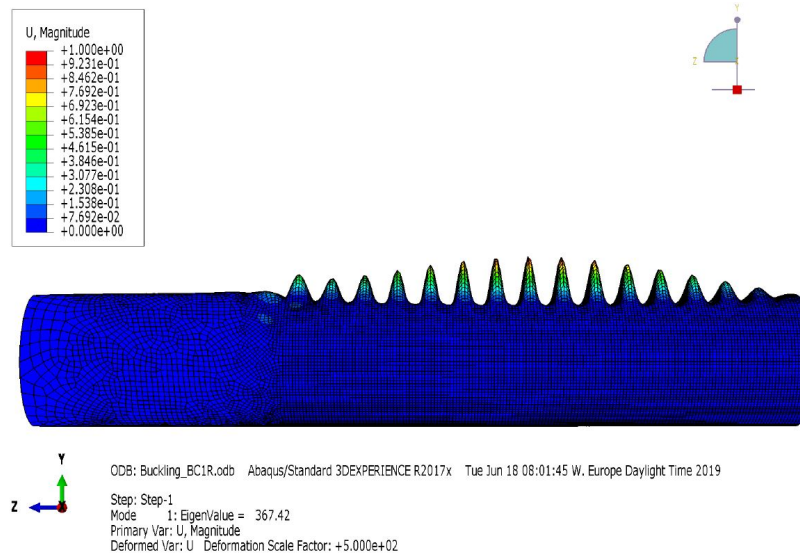


Figure 4.12: Eigenmode 1

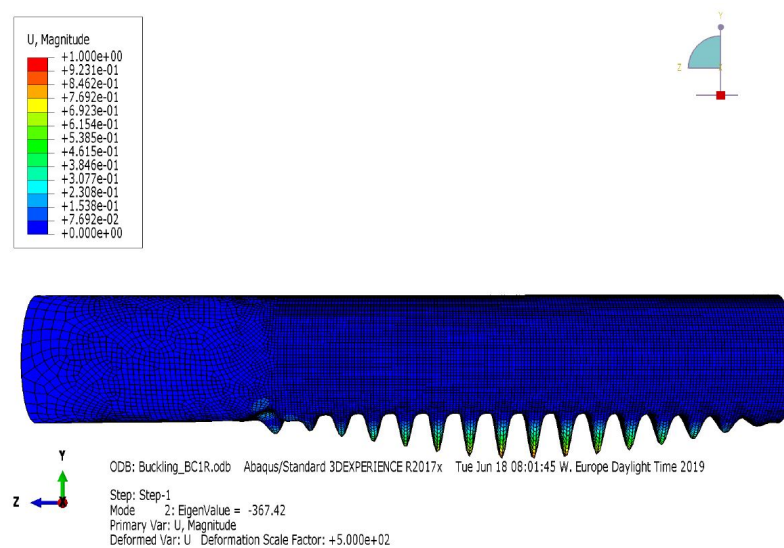


Figure 4.13: Eigenmode 2

As already mentioned in chapter 3, the eigenmodes are used to study the influence of imperfections on different boundary conditions. For this process an eigenmode is loaded into the model (by the keyword) in the initial step, before loading. a scaling factor is used to set different imperfection heights by multiplying the amplitude δ with it. The imperfection height ΔW is defined as two times the amplitude as shown in figure 4.14. Per tube and boundary condition a qualitative choice is made for the use of a specific eigenmode. This was needed because in the buckling analyses of the ABAQUS software no fixed order is obtained. For accurate results, all tested tubes need to be modeled with the eigenmode imperfection at the compressive top side of the tube. In figure 4.14 The implementation of imperfections by eigenmodes is described.

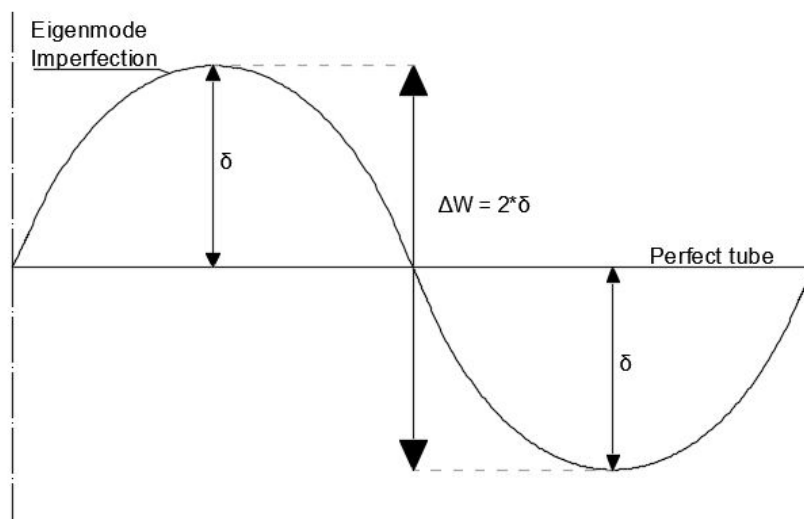


Figure 4.14: Eigenmode Imperfection to dimple imperfection

4.5.5. Model results

All input variables discussed in the previous sections of this paragraph are required to run the model and generate results. For this study the results consists of reaction forces and displacements to do the post-processing as described in paragraph 4.3.2, and visual representations of the buckling failure. The visual representations are used to observe the failure behaviour of the tubes. The combination of the failure behaviour and the measured data of the tubular piles is used in the parametric study of chapter 5. In the figures 4.15 and 4.16 a visual representation of a tube failure is showed for two different boundary conditions BC1R and BC4F.

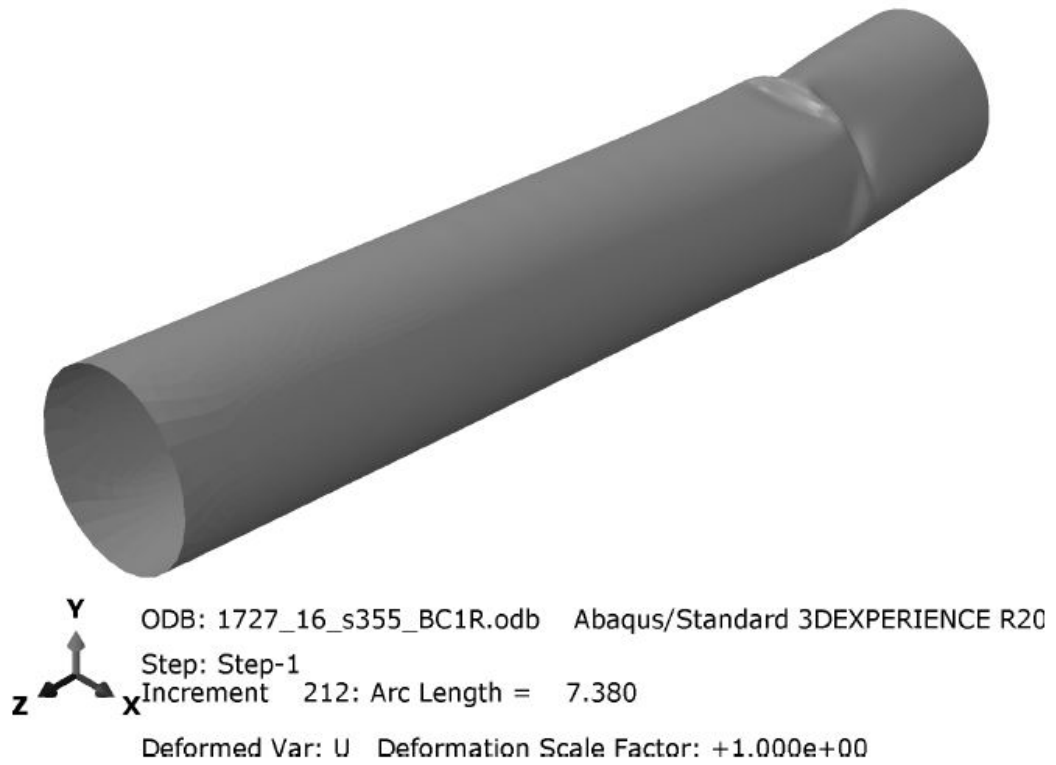


Figure 4.15: Illustrative visualisation of buckling failure for BC1R.

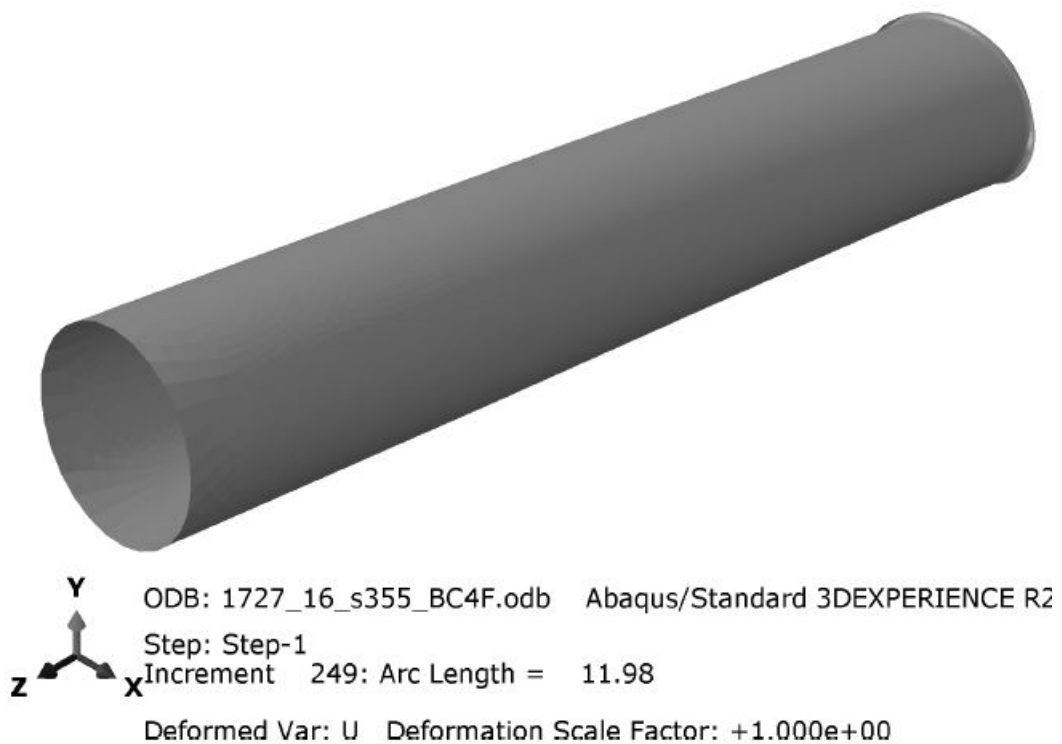


Figure 4.16: Illustrative visualisation of buckling failure for BC4F.

4.6. Model validation

Checking the quality and rightness of a computer model is an important step before results of that model can be used. In many cases a FEM model is validated with a real full scale or model test. In that case FEM software models are used to execute more tests with varying parameters without the costly and time consuming full scale tests. For this study no specific test-results of full scale tests are available. FEM software models in this study are used to check the behaviour of possible missing or outdated boundary conditions in the design code. To validate the created models analytical methods or test results of similar conditions can be used.

4.6.1. Analytical model

To validate models by an analytical method, results of both the analytical and the FEM model need to be presented in the same format. Because all the results of this study are presented in moment curvature diagrams there is chosen to do also for this validation. For both methods the same parameters are used for normalization. these parameters are given by equations 4.4 and 4.5. Paragraph 4.3.2 gives the further information of how the results from the FEM models are processed to a moment-curvature diagram.

For the analytical method, the approach of Gresnigt 1986 [8] is used to determine the moment-curvature relation for the elastic and the elastic-plastic part separately. In the analytical method no strain hardening or nonlinear effects are included.

Elastic behaviour:

$$M = K * EI \quad (4.7)$$

with:

$$I = \pi * r^3 * t \quad (4.8)$$

$$K = \frac{\sigma}{E * r} = \frac{\epsilon}{r} \quad (4.9)$$

By varying sigma (σ), kappa is determined with equation 4.9 and with equation 4.7 the corresponding moment is calculated. At the end of the elastic range is reached and by increasing bending yielding starts from the extreme outer fibers. A bi-linear $\sigma - \epsilon$ diagram as in figure 4.17 is present in the cross-section.

Elastic - plastic behaviour:

$$M = M_p * 0.5 * \left(\frac{\theta}{\sin(\theta)} + \cos(\theta) \right) \quad (4.10)$$

with:

$$M_p = \frac{1}{6} * (D^3 - (D - 2t)^3) * f_y \quad (4.11)$$

$$\theta = \arcsin\left(\frac{\epsilon_y}{\epsilon}\right) \quad \text{for } \epsilon \geq \epsilon_y \quad (4.12)$$

$$K = \frac{\sigma_y}{E * r * \sin(\theta)} \quad (4.13)$$

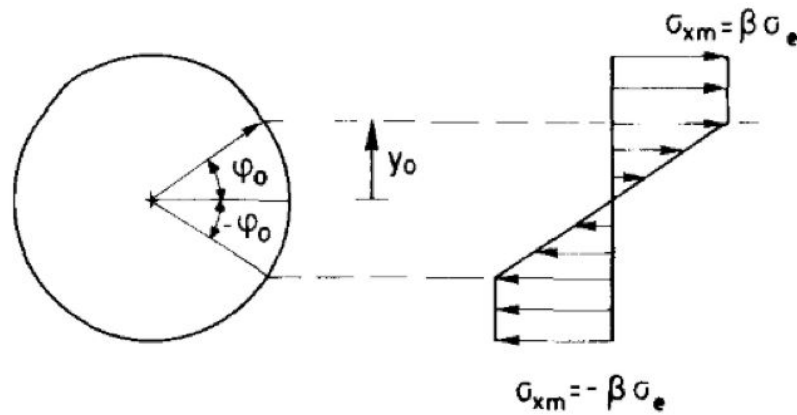


Figure 4.17: Bi-linear stress distribution in the cross-section, from Gresnigt 1986 [8]

Following this analytical method and normalize the determined moment and curvature by the plastic moment of equation 4.4 and the curvature like parameter of equation 4.5, the analytical moment-curvature diagram of figure 4.18 is formed.

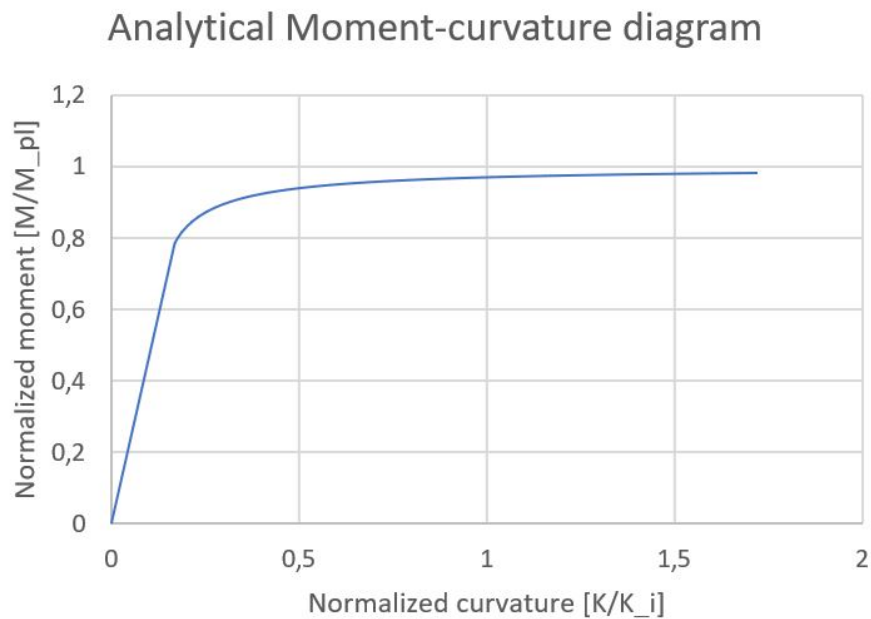


Figure 4.18: Analytical, normalized moment-curvature diagram following the method of Gresnigt [8]. Tube: $D=1270\text{mm}$, $t=25\text{mm}$, $f_y = 355\text{N/mm}^2$, $D/t=51$

4.6.2. Validation by analytical model

To validate the ABAQUS FEM models made for this study, a comparison is made between the analytical model and a FEM model with the corresponding properties. Three models are chosen that represent each another D/t ratio and steel quality. With a D/t ratio of 51 and a S355 steel quality figure 4.19 shows the first validation.

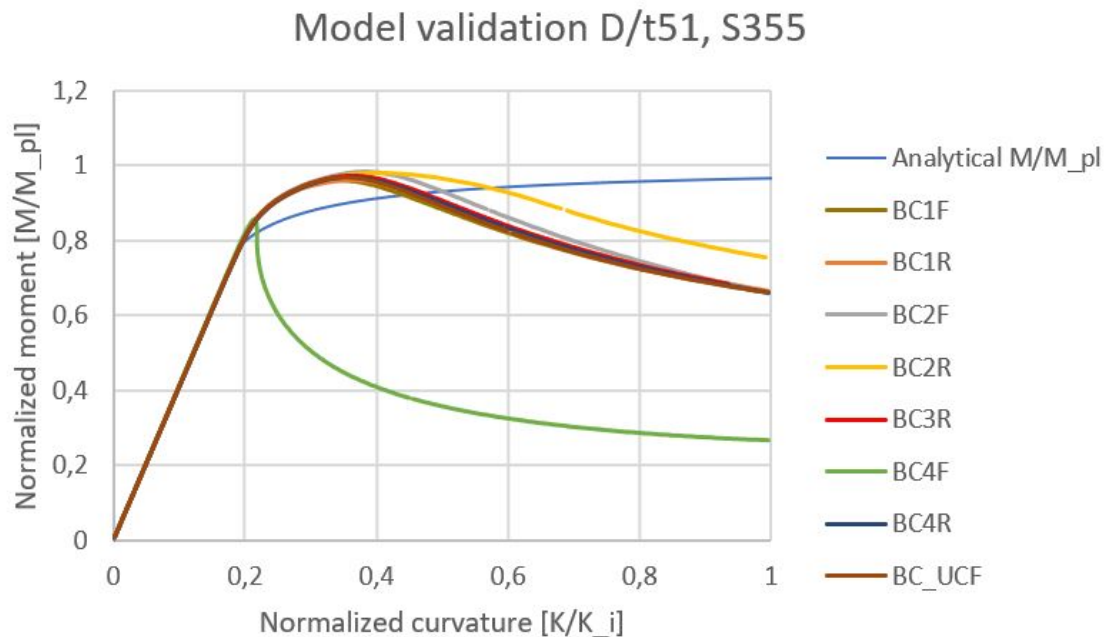


Figure 4.19: Model validation of Tube: D=1270mm, t=25mm, $f_y = 355\text{N/mm}^2$, D/t=51

The ABAQUS model tests from the figure, show a corresponding elastic behaviour to the analytical validation curve. At the point where the analytical model reaches the maximum of the elastic behaviour, the model test curves starts to deviate from the validation curve. This deviation can be explained by the fact that in the analytical method no strain hardening is included. The used model test for this validation is of a class 3 tube very close to the lower boundary with class 2. The plastic moment is almost reached for most of the tests what also explains the deviation of the analytical model. The normalized maximum values of both the analytical and the ABAQUS FEM models are about 0.95 within the range of the graph. For a tube with a D/t ratio of 51 and a steel quality of S355 these results are in line with the expectations. The used model test for this validation is of a class 3 tube very close to the lower boundary with class 2. The plastic moment is almost reached for most of the tests what also explains the

In the figures 4.20 and 4.21 the same kind of validations are made for tubes with a higher D/t ratio and steel quality. These tubes are typical class 4 tubular piles following the guidelines of the NEN-EN 1993-1-1 [2] design code. These tubular piles are known for there sensitivity for local buckling. Looking to the linear elastic part of both set of curves, no deviations from the analytical curve are visible. With an increasing D/t ratio and steel quality, the maximum normalized moment decreases and the non-linear behaviour after failing increases. These effects are well known for cross-section class 4 tubular piles.

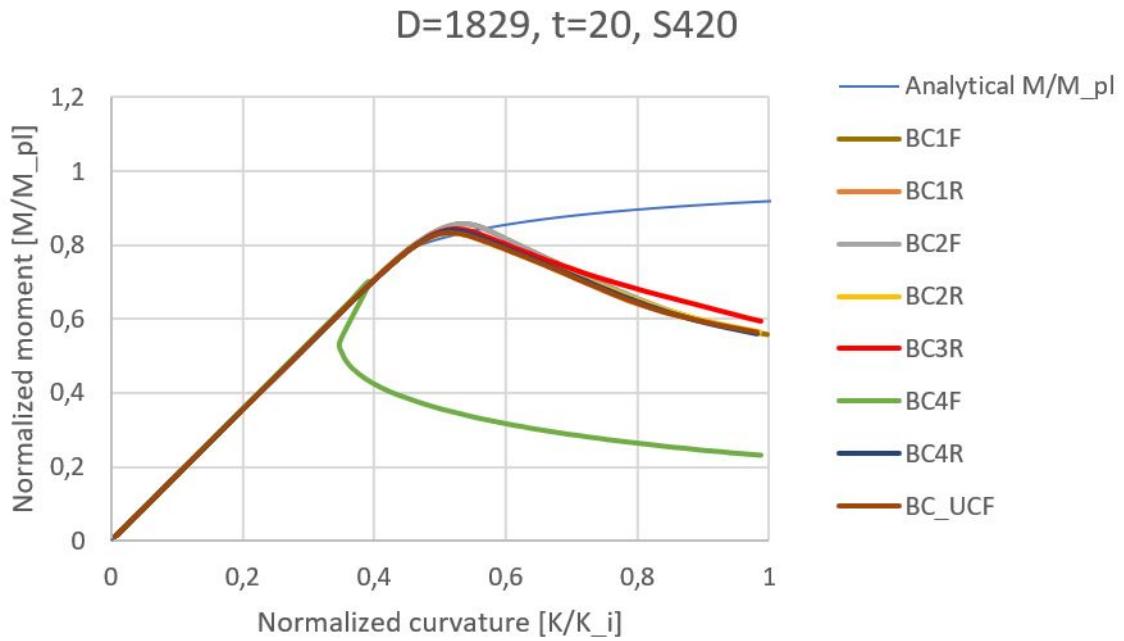


Figure 4.20: Model validation of Tube: D=1829mm, t=20mm, $f_y = 420\text{N/mm}^2$, D/t=91

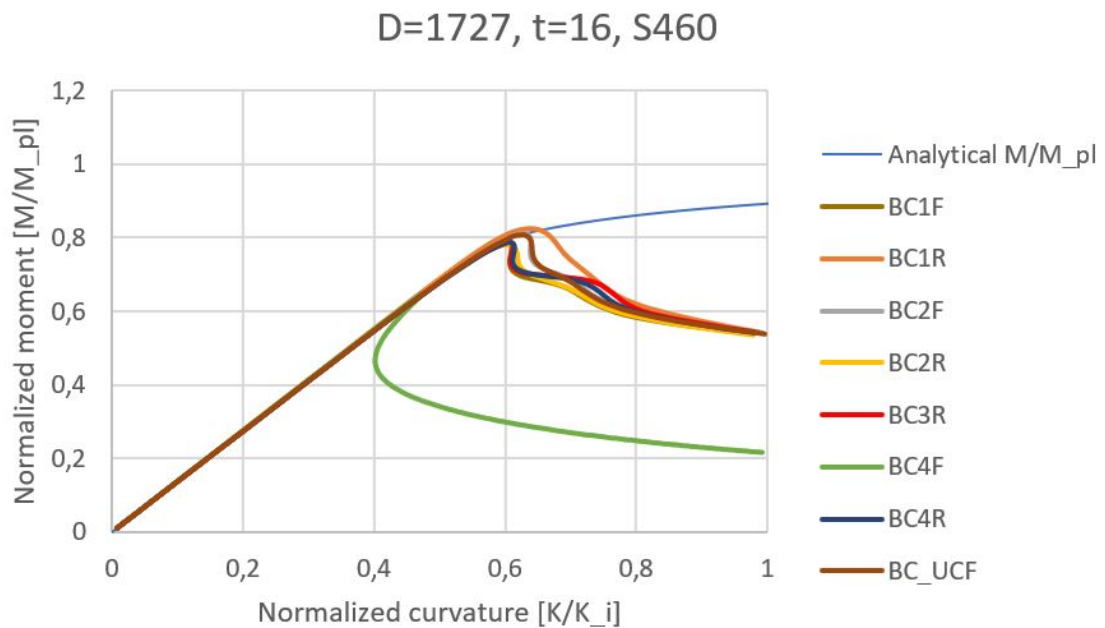


Figure 4.21: Model validation of Tube: D=1727mm, t=16mm, $f_y = 460\text{N/mm}^2$, D/t=108

4.6.3. Discussion

The validation shows a corresponding behaviour with the analytical model for all D/t ratios and steel qualities in the elastic part of the curve. The varying behaviour between the different D/t ratios in the post-elastic part of the model test curves is conform the expectations. This validation do not give a good view on the accuracy of the nonlinear part of the ABAQUS model tests. To increase the effect of the validation, results of full scale test could be included to check the post-linear behaviour.

5

Parametric study

5.1. Introduction

In this study to the influence of boundary conditions on the failure behaviour of local buckling, more parameters than only boundary conditions play a role. In this chapter these parameters are handled and their influence on the local buckling failure mechanism is investigated. For residual stresses and geometric imperfections, a study is preformed to check the influence on the failure resistance before the parameters are included in the final models.

Parameters included in the test range such as the D/t ratio, yield stress and the influence length are treated by specific examples. To generate an overview of the influence of al different parameters on the different boundary conditions, an average value of M_{max}/M_{pl} and K_{cr}/K_e per boundary and in total are determined. In the end, the failure patterns of the different parameters and boundary conditions are compared and an overall overview is created.

5.2. Residual stresses

In chapter 3 residual stresses, generated by the cold spiral bending process are described. The axial and hoop stresses that are determined by Vasilikis et al. [4] and shown in table 3.2 are added in the FEM models by introducing an initial condition (see appendix C). Because the study of S.van Es [13] shows residual stresses resulting in an opening and closing behaviour of cutted ring segments, in this parametric study both directions are investigated.

As described in the discussion of chapter 3, The effect of residual stresses are investigated for two types of boundary conditions. The boundary conditions chosen for this analyses are selected on their behaviour with respect to ovalization. Boundary condition BC1 counter acts ovalization while BC4 allows displacements perpendicular to the shell wall at the tube end. Figure 5.1 shows the moment-curvature diagrams of four boundary conditions BC1F, BC1R, BC4F and BC4R with residual stresses in both directions and without any residual stresses. The labels of the graphs show the signs in and out, the sign in refers to the closing ring segment and the sign out to the opening one of paragraph 3.3.2. The tests are preformed for a tube with the specifications: $D = 1422\text{mm}$, $t = 16\text{mm}$, $f_y = 355\text{N/mm}^2$ (S355) and $D/t = 89$.

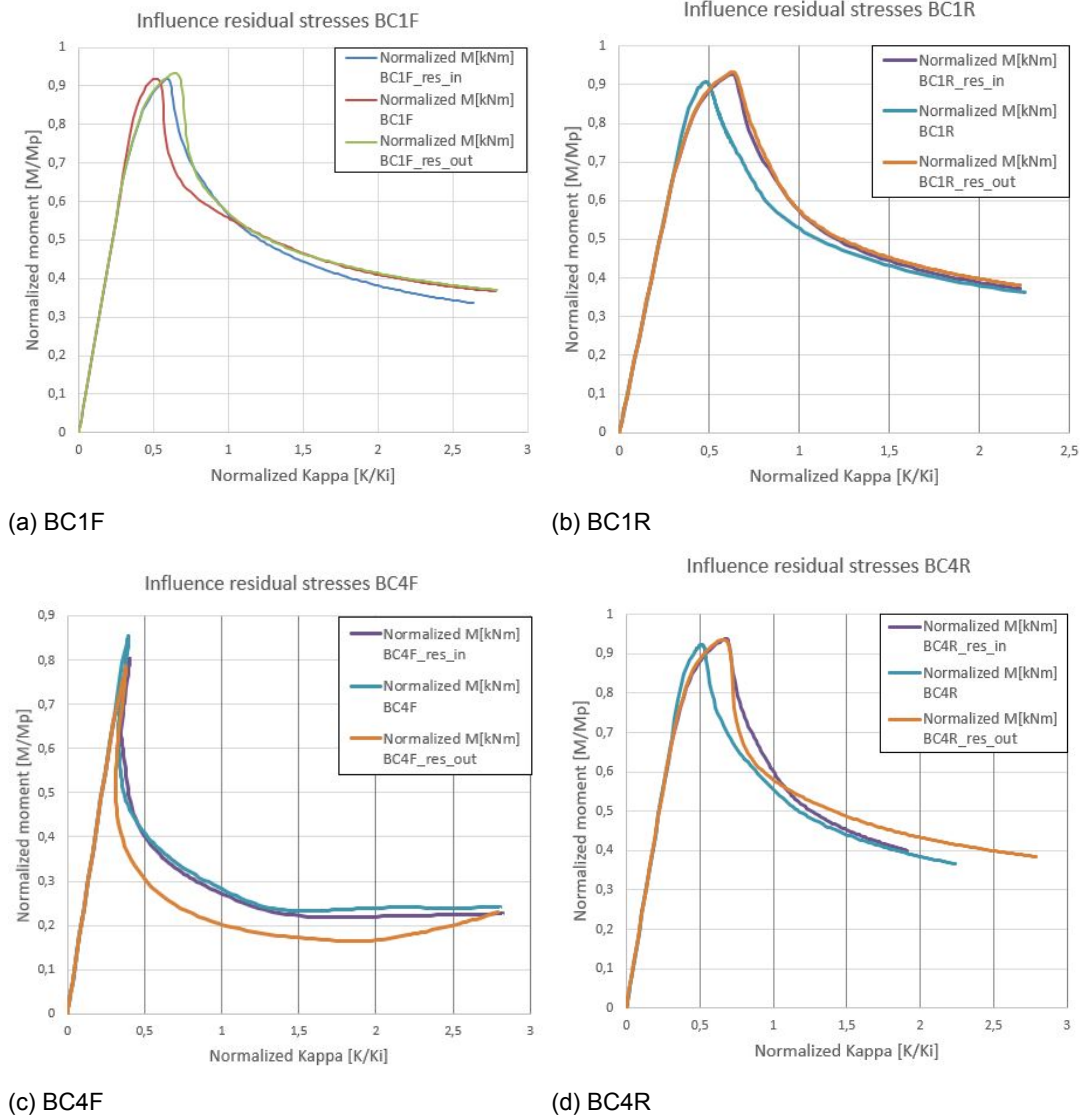


Figure 5.1: Influence of closing (in) and opening (out) residual stresses on different boundary conditions. Tested tube: $D = 1422\text{mm}$, $t = 16\text{mm}$, $f_y = 355\text{N/mm}^2$, $D/t = 89$

In the graphs of figure 5.1 the normalized moment-curvature diagrams as result of the ABAQUS FEM models are shown. Observing the diagrams a divergent behaviour can be seen for boundary condition BC4F. The different behaviour of this boundary condition is assumed to be not caused by residual stresses. Looking to the normalized M-K diagrams, an increased curvature is observed at the maximum moment when residual stresses are present. The variation in maximum moment is small for all boundary condition except for BC4F, here a reduced M_{max} is shown for the tests with residual stresses. Table 5.1 gives the values of the normalized maximum moments and the corresponding normalized critical curvature.

Residual stress	BC1F		BC1R		BC4F		BC4R	
	M_{max}/M_p	K_{cr}/K_i	M_{max}/M_p	K_{cr}/K_i	M_{max}/M_p	K_{cr}/K_i	M_{max}/M_p	K_{cr}/K_i
No stress	0,919	0,519	0,907	0,483	0,854	0,396	0,924	0,514
Res-stress in	0,919	0,596	0,929	0,625	0,804	0,401	0,938	0,681
Res-stress out	0,932	0,644	0,933	0,632	0,785	0,381	0,936	0,647

Table 5.1: Effect residual stress per boundary condition. Tested tube: $D = 1422\text{mm}$, $t = 16\text{mm}$, $f_y = 355\text{N/mm}^2$, $D/t = 89$

For the boundary conditions BC1F, BC1R and BC4R a small increase in maximum moment of 1 – 3% and a increase in curvature of approximately 20% is observed for the models with residual stresses. For boundary condition BC4F a quite constant curvature by a decreasing maximum moment of 6 – 8% is observed for the models with compared to the models without residual stresses. Residual stresses have almost no influences on the maximum moment capacity, and there are hardly differences observed between the boundary conditions (except from BC4F). Therefore residual stresses are not included in the models to investigate the effect of different boundary conditions.

5.3. Geometrical imperfections

The effect of geometrical imperfections on the buckling behaviour of cross-section class 4 tubular piles is well studied in the past years. The influence of these imperfections in combination with different types of boundary conditions are investigated in this study. As described in paragraph 4.5.4, the dimple imperfections are modeled with the help of a buckling eigenmode with a scaling factor to adjust the imperfection height. Because ABAQUS FEM models with a small imperfection run much smoother and faster, there is chosen to ad a fixed imperfection to all models.

In the range of test tubes, three different thicknesses are used for tubes with different diameters and steel qualities. This varying thickness in combination with a fixed imperfection height causes a discontinuity in the imperfection over thickness height ($\delta W/t$). The range of thicknesses varying of 16mm, 20mm and 25mm with a constant imperfection height of 4mm gives imperfection over thickness ratios of 0.16, 0,2 and 0,25. From the models in the test range three tubes are selected with the same steel quality and D/t ratio, but with a varying wall thickness. The normalized moment-curvature diagrams are shown in figure 5.2.

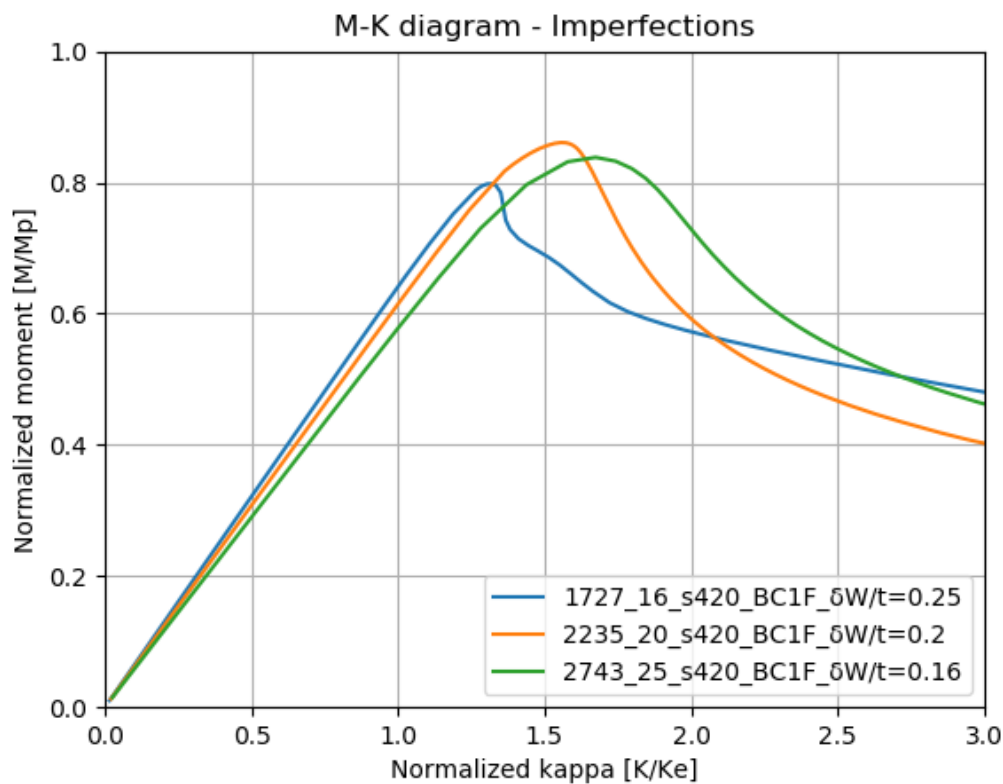


Figure 5.2: Normalized moment-curvature diagram for imperfection over thickness ratios: 0.16, 0.20 and 0.25 (tube description legend: Diameter, thickness, steel quality. boundary condition, imperfection)

A significant scatter in the shape and maximum values of the moment-curvature diagram are observed from the graph. The development of the normalized maximum moment and corresponding critical curvature are displayed in the figures 5.3 and 5.4.

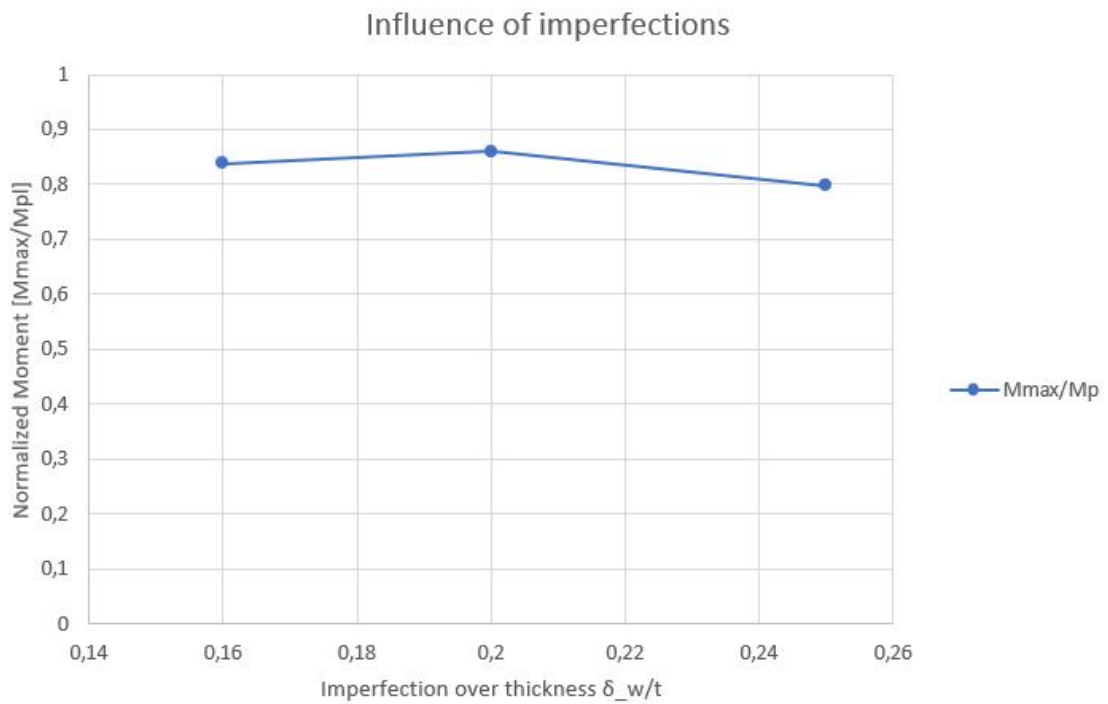


Figure 5.3: Influence of imperfections on the Normalized moment for $\delta W/t$ ratios: 0.16, 0.20 and 0.25

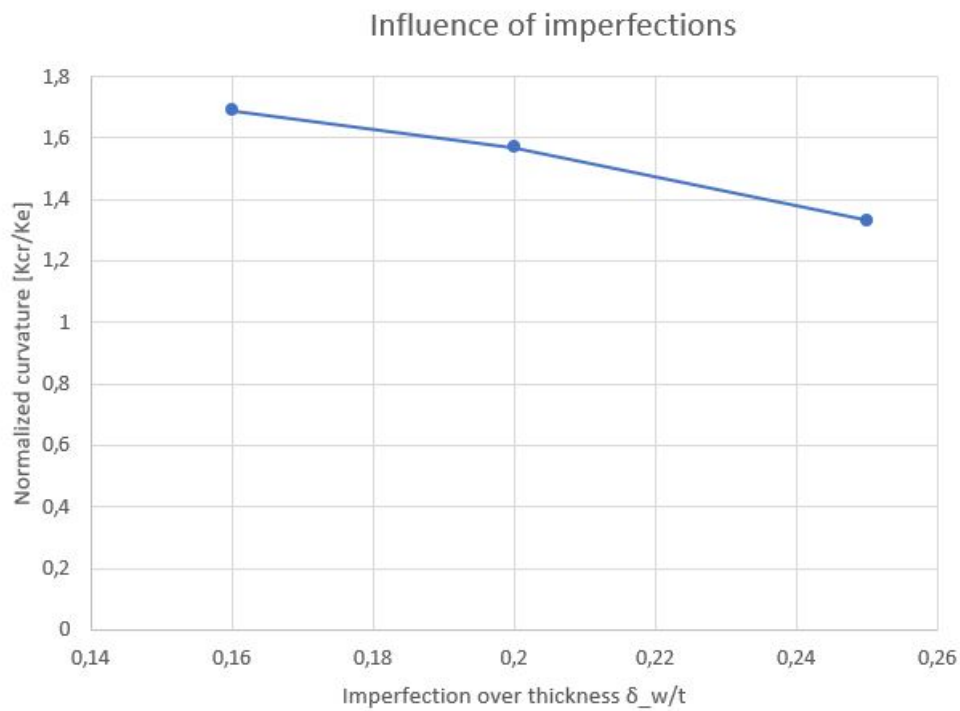


Figure 5.4: Influence of imperfections on the Normalized curvature for $\delta W/t$ ratios: 0.16, 0.20 and 0.25

In the graph of figure 5.3, no clear trend can be observed for the development of the maximum moment over an increasing $\delta W/t$ ratio. Following model and test results of other studies, a decreasing M_{max} was expected by an increasing $\delta W/t$ ratio. Since the tested tubes from this example have the same steel quality and D/t ratio, a reason for the discontinuity is searched by the model length to diameter ratio or influence length. The influence length as described in paragraph 3.2.1, represents a stiffening effect over a certain distance. Increasing maximum moments are expected by an increasing influence length, what not declares the decreasing maximum moment for the largest tube diameter in figure 5.3. However, paragraph 5.6 shows an opposite behaviour for the results of this study, the trends of the model data confirm a decreasing maximum moment by an increasing influence length.

Figure 5.4 shows a decreasing critical curvature with an increasing imperfection over thickness ratio. Looking to the moment-curvature diagram not only the critical curvature is changing with an increasing wall thickness. The post buckling behaviour shows a less rapid decrease with a smaller wall thickness.

5.3.1. Influence of imperfections in the model study

As discussed in paragraph 5.3, all FEM model tests are performed with a geometrical imperfection of 4mm. This imperfection in combination with three varying wall thicknesses generated three imperfection over wall thickness ratios of 0.16, 0.20 and 0.25. In total, 288 ABAQUS FEM model tests are performed for this study. Each thickness over imperfection ratio represents 96 models divided over a total of 8 different boundary conditions. The effect of the imperfections on different types of boundary conditions is shown in table 5.2 by an average of the normalized maximum moment and corresponding critical curvature per boundary condition per $\delta W/t$ ratio.

Average per parameter		δ_w/t		
BC		0,16	0,2	0,25
BC1F	M_{max}/M_p	0,90	0,90	0,88
	K_{cr}/K_e	1,77	1,66	1,62
BC1R	M_{max}/M_p	0,90	0,90	0,88
	K_{cr}/K_e	1,82	1,70	1,66
BC2F	M_{max}/M_p	0,91	0,91	0,89
	K_{cr}/K_e	1,83	1,68	1,67
BC2R	M_{max}/M_p	0,89	0,90	0,87
	K_{cr}/K_e	1,80	1,67	1,62
BC3R	M_{max}/M_p	0,90	0,90	0,88
	K_{cr}/K_e	1,81	1,66	1,66
BC4F	M_{max}/M_p	0,82	0,78	0,73
	K_{cr}/K_e	1,39	1,25	1,15
BC4R	M_{max}/M_p	0,89	0,90	0,88
	K_{cr}/K_e	1,78	1,66	1,64
BC_UCF	M_{max}/M_p	0,91	0,91	0,89
	K_{cr}/K_e	1,71	1,73	1,66

Table 5.2: Average normalized maximum moment and critical curvature per boundary condition per $\delta W/t$ ratio.

The trend of the normalized maximum moment and critical curvature over the $\delta W/t$ ratio of all the tests is shown in the figures 5.5 and 5.6. Corresponding to other studies these trends show a decreasing maximum moment and critical curvature for an increasing imperfection over thickness ($\delta W/t$) ratio. For all boundary conditions the decreasing trend as pictured in the figures 5.5 and 5.6 also can be seen in table 5.2. Boundary condition BC4F shows 10-20% lower values for as well the normalized maximum moment as the critical curvature in comparison to the other boundaries who react all within a range of 1 – 2%.

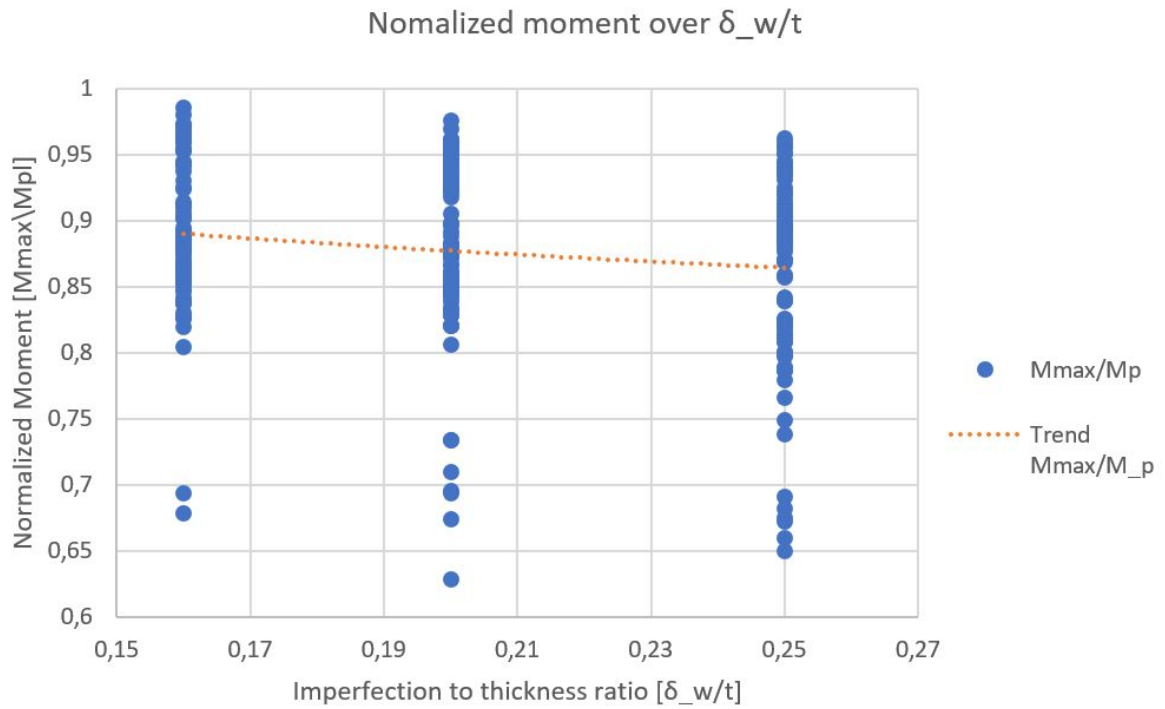


Figure 5.5: Trend of the influence of imperfections on the Normalized moment for $\delta W/t$ ratios: 0.16, 0.20 and 0.25

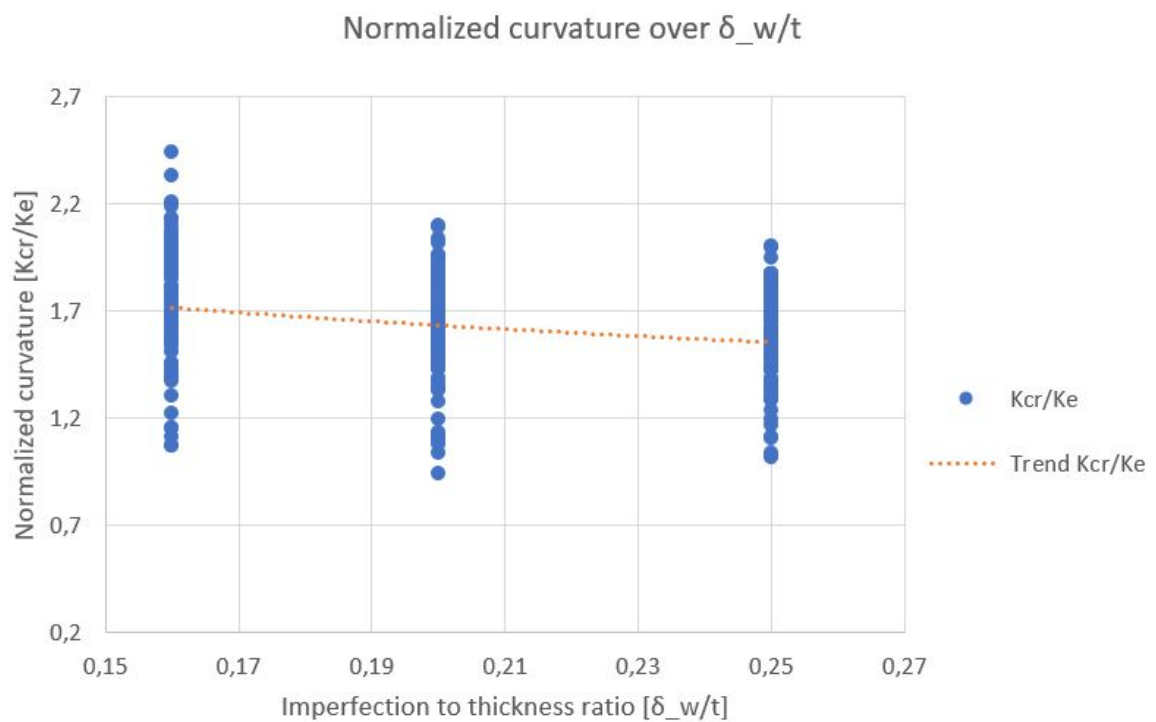
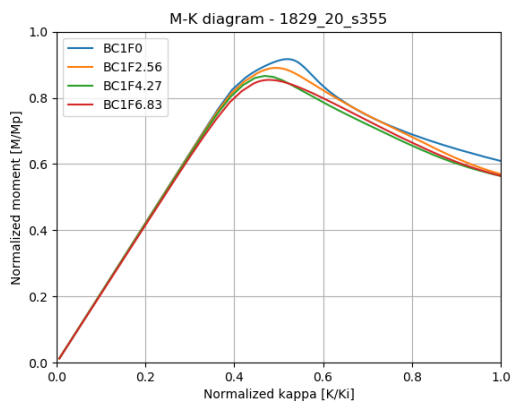


Figure 5.6: Trend of the influence of imperfections on the Normalized curvature for $\delta W/t$ ratios: 0.16, 0.20 and 0.25

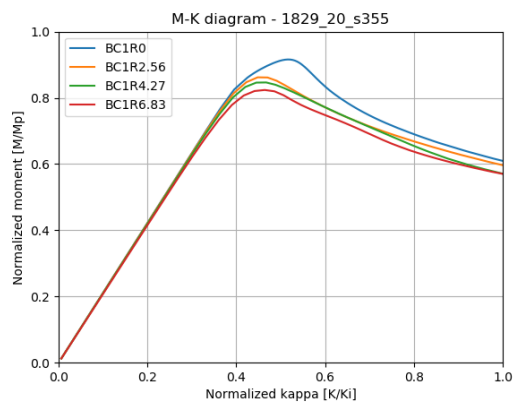
5.3.2. Comparison with the design code

The current design code for shell structures, the NEN-EN 1993-1-6 [1], describes different parameters to use for accounting the influence of imperfections and boundary conditions. For long tubular piles three different options can be selected to represent the boundary conditions. The options are BC1-1, BC1-2 and BC2-2 and represent per option the boundary conditions at both pile ends. In the calculation no difference is made between a rotational free or restrained boundary condition.

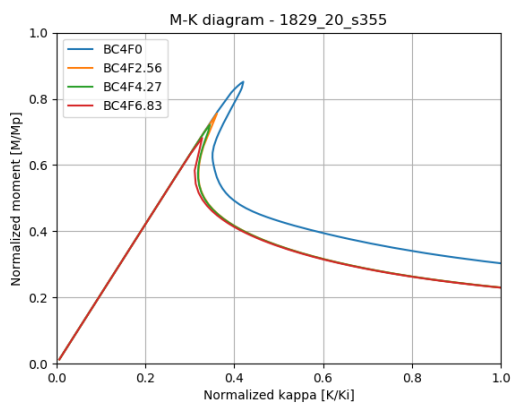
To compare the results of the prescribed calculation methods of the design code with the results of FEM model tests, the same tubular pile with the same imperfections is calculated following the design code (NEN-EN 1993-1-6) and modelled with ABAQUS FEM software. From paragraph 3.2.3 is known that the calculation method of the design code works with quality classes. The limit values for imperfections, of these quality classes are also used in the FEM model tests. For comparison, also in this study is chosen to use the BC4 and BC1 boundary conditions that allow or counteract ovalisation. The tubular pile that is tested is known by the specification: $D = 1422\text{mm}$, $t = 16\text{mm}$, $f_y = 355\text{N/mm}^2$ (S355) and $D/t = 89$. The imperfection heights that are used, corresponding to the limit values are 0mm, 2.56mm, 4.27mm and 6.43mm. Figure 5.7 shows the results of the FEM model tests for different boundary conditions with the different imperfection heights.



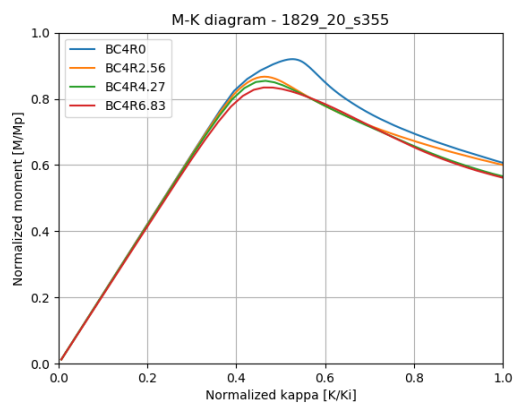
(a) BC1F



(b) BC1R



(c) BC4F



(d) BC4R

Figure 5.7: Influence of dimple imperfections on piles with BC1 (no ovalisation) and BC4 (Ovalisation). Tested tube: $D = 1829\text{mm}$, $t = 20\text{mm}$, $f_y = 355\text{N/mm}^2$, $D/t = 91$

In figure 5.7, the normalized moment-curvature diagrams for different imperfection heights per boundary are shown. A decreasing maximum moment with an increasing imperfection height is observed for all boundary conditions. The moments observed from the FEM models, as well as the moments corresponding to the characteristic steel stresses from the design code calculation are normalized by the plastic moment. This normalization makes it possible to compare the results. Both, the calculated limit values of the design code and the maximum moments from the model tests are displayed in figure 5.8.

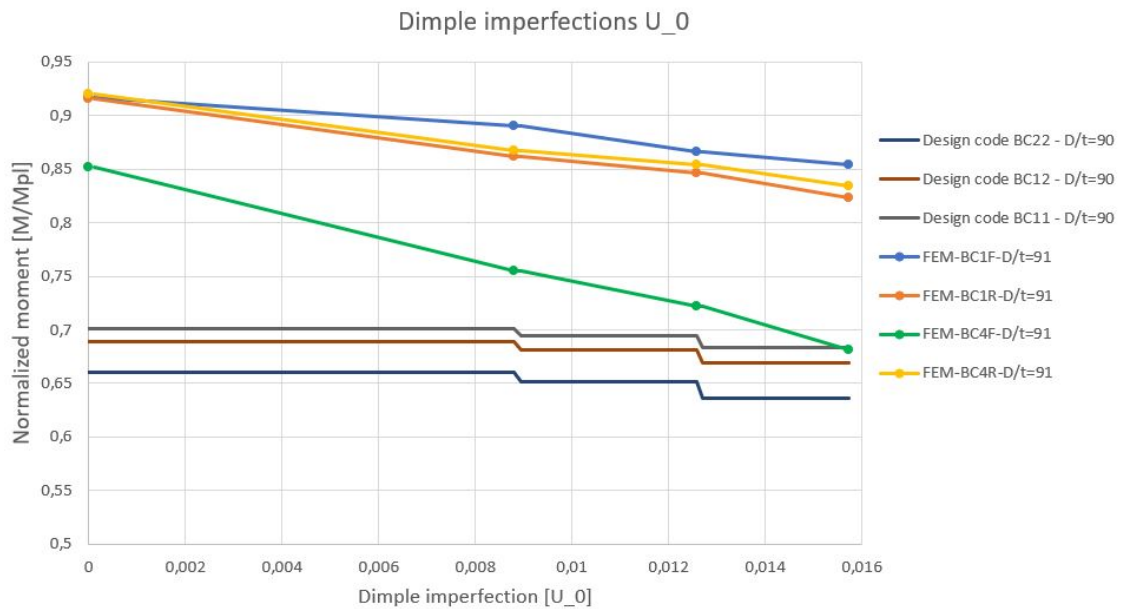


Figure 5.8: Theoretical resistance reduction from the NEN-en 1993-1-6 compared with FEM model tests of BC1 and BC4 for tested tube: $D = 1829\text{mm}$, $t = 20\text{mm}$, $f_y = 355\text{N/mm}^2$, $D/t = 91$

Looking to the results of the comparison between the design code and the FEM model tests as included in figure 5.8, the results of the FEM model tests show a higher moment capacity in almost all cases. The results of the BC4F model tests are deviating from the results of the other boundary conditions. Not only a lower maximum moment value is observed, but also a faster decrease of capacity by an increasing imperfection height. Comparing the decrease in moment capacity between the code and the FEM model tests over the imperfection range, significant differences are indicated. The code shows a decrease in moment capacity of 5%, both BC1 conditions and BC4R show a decrease of 10-12% and BC4F show a decrease of 25%. Boundary condition BC4F reacts more sensitive on the increasing imperfection height than the other ones. This behaviour was also mentioned in table 5.2 of paragraph 5.3.1.

5.4. D/t ratio

The Diameter over thickness ratio is in combination with the yield stress the parameter that subdivides tube cross-sections in different classes. Tubular piles with high D/t ratios are placed in cross-section class 4, this class represents buckling sensitive cross-sections. The tubes used in this study are all class 4 tubular piles but have a varying D/t ratio of approximately 50, 70, 90 and 110.

To investigate the influence of the D/t ratio on the resistance capacity, the results of a FEM model test of each ratio is added to the graph of figure 5.9. This figure shows the normalized moment-curvature diagrams of the tested tubes. To prevent side effects, tubes with the same steel quality and an approximately matching diameter are selected out of the test range.

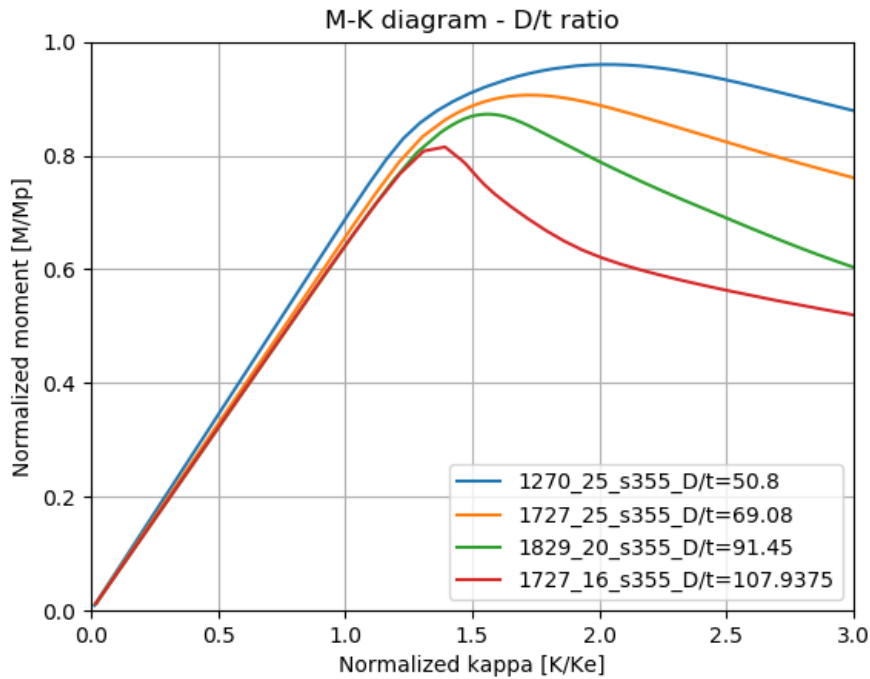


Figure 5.9: Normalized moment-curvature diagram for D/t ratios: 50, 70, 90 and 110

In the normalized moment-curvature diagrams of figure 5.9, a clear pattern is visible. An increasing D/t ratio comes with a decreasing normalized maximum moment and curvature. This pattern is also good visible in the figures 5.10 and 5.11 that show the development of the normalized maximum moment and corresponding critical curvature. For this study the curvature is normalized by the elastic curvature because of the varying D/t ratio.

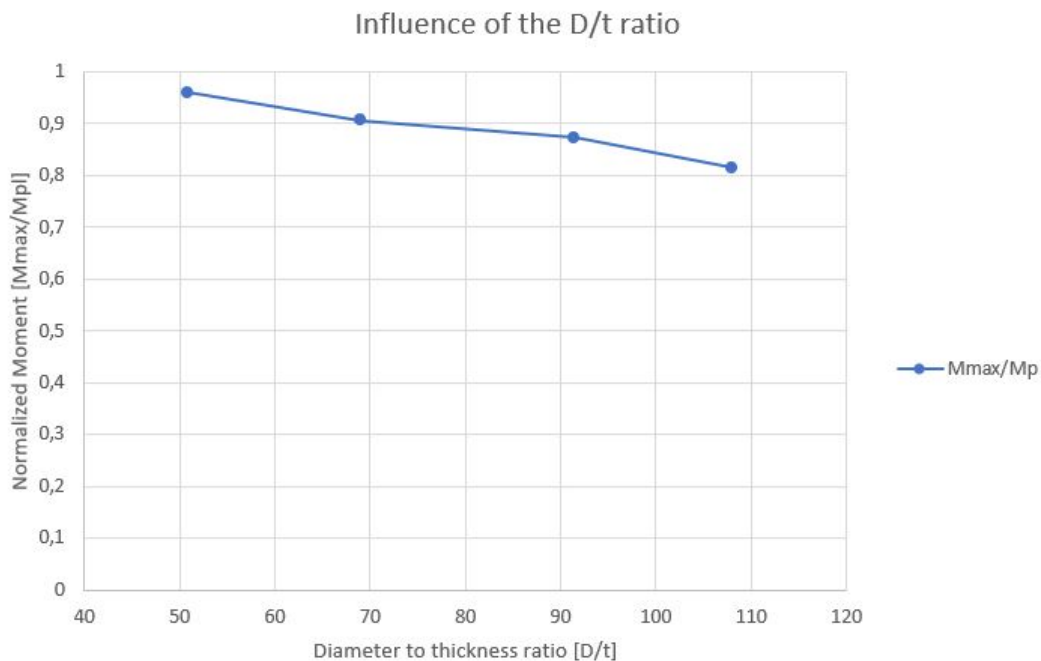


Figure 5.10: Influence of the D/t ratio on the Normalized moment for D/t ratios: 50, 70, 90 and 110

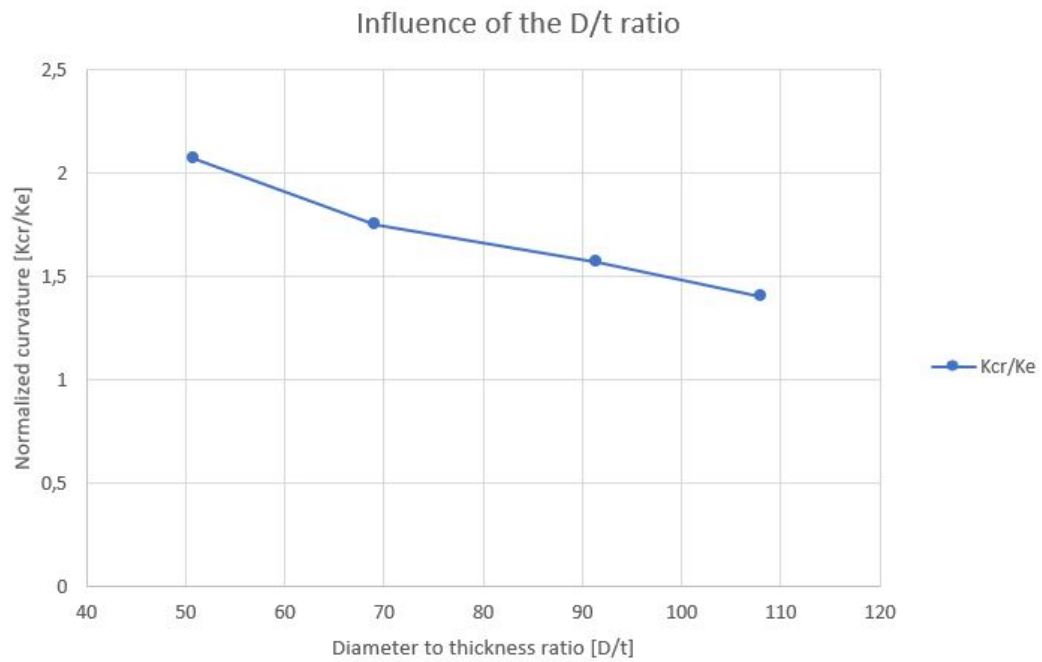


Figure 5.11: Influence the D/t on the Normalized curvature for D/t ratios: 50, 70, 90 and 110

5.4.1. Influence of the D/t ratio in the model study

The influence of the D/t ratio shown in paragraph 5.4, is also investigated for all other tests. Per D/t ratio, 72 FEM model tests are performed divided over 8 boundary conditions. Table 5.3 shows the averaged values of the normalized moment and curvature per boundary condition per D/t ratio.

Average per parameter					
BC		D/t			
		50	70	90	110
BC1F	Mmax/Mp	0,94	0,91	0,88	0,84
	Kcr/Ke	1,77	1,75	1,72	1,50
BC1R	Mmax/Mp	0,94	0,91	0,86	0,86
	Kcr/Ke	1,83	1,74	1,66	1,65
BC2F	Mmax/Mp	0,96	0,92	0,88	0,84
	Kcr/Ke	1,89	1,79	1,76	1,51
BC2R	Mmax/Mp	0,95	0,89	0,86	0,85
	Kcr/Ke	1,84	1,64	1,66	1,62
BC3R	Mmax/Mp	0,95	0,91	0,87	0,85
	Kcr/Ke	1,87	1,71	1,71	1,57
BC4F	Mmax/Mp	0,87	0,79	0,75	0,70
	Kcr/Ke	1,37	1,24	1,30	1,15
BC4R	Mmax/Mp	0,95	0,91	0,87	0,85
	Kcr/Ke	1,83	1,72	1,68	1,56
BC_UCF	Mmax/Mp	0,95	0,92	0,87	0,86
	Kcr/Ke	1,82	1,78	1,68	1,64

Table 5.3: Average normalized maximum moment and critical curvature per boundary condition per D/t ratio.

From table 5.3 can be concluded that BC4F gives divergent test results. Where all other boundary conditions are in line with each other, BC4F scores approximately 10–20% lower for as well the normalized maximum moment as the critical curvature. For an increasing D/t ratio from 50 to 110, the normalized moment approximately decreases 10% and the curvature 20%. The trends of the normalized maximum moment and critical curvature are displayed in corresponding figures 5.12 and 5.13. Because real tube dimensions are used, the D/t ratios are not exact 50, 70, 90 and 110 but values close to the target values what causes a small spread.

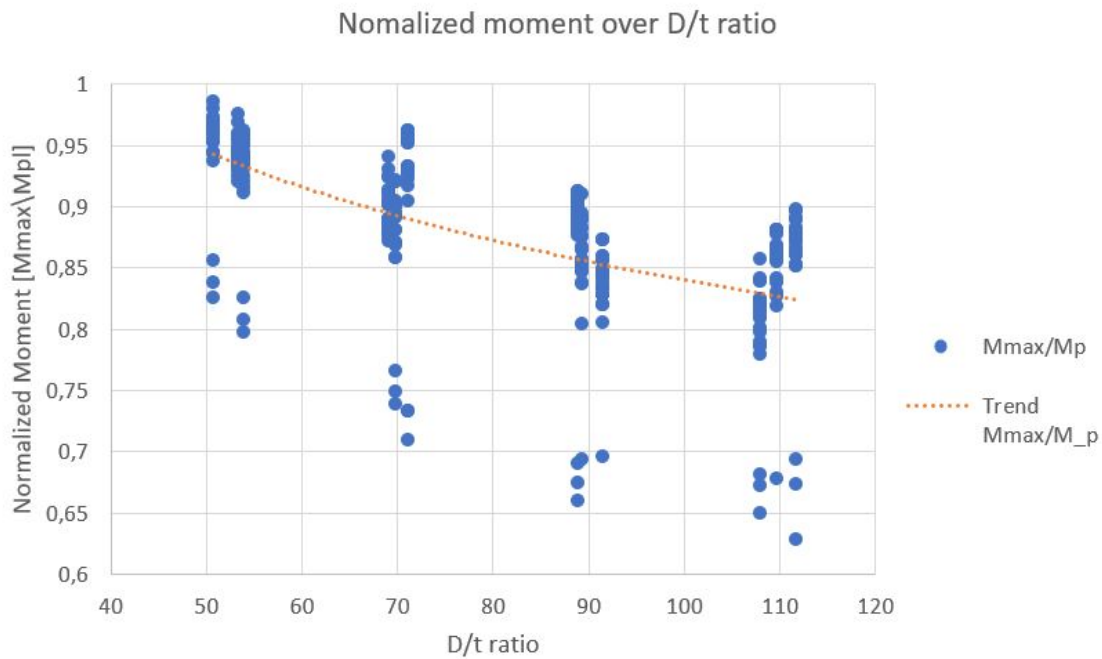


Figure 5.12: Trend of the influence of the D/t ratio on the Normalized moment for D/t ratios: 50, 70, 90 and 110

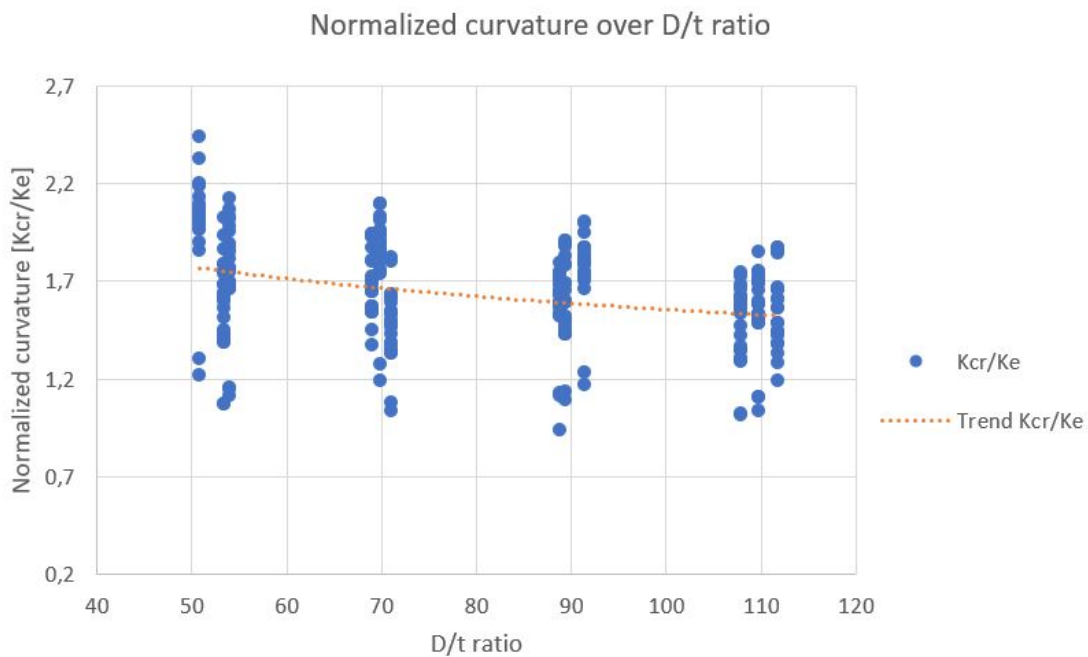


Figure 5.13: Trend of the influence of the D/t ratio on the Normalized curvature for D/t ratios: 50, 70, 90 and 110

Looking to the trend of the normalized maximum moment shown in figure 5.12, the bundle of BC4F test results are clearly diverging from the mean. This phenomenon is less but also visible for the normalized critical curvature as shown in figure 5.13.

5.5. Yield stress

In this parametric study most of the studies are to geometrical parameters as imperfections, D/t ratio and the influence length. Together with the residual stress this parameter tells something over the material properties. Where residual stresses are an accidental thing, the yield stress is something where the material is meant for. The steel quality, represented by the yield stress tells us something about the behaviour of the material. For this study, three different steel qualities are used listening to the names S355, S420 and S460. The influence of the steel quality on the buckling resistance is also tested for this parameter. Figure 5.14 shows the results of the FEM model tests of one single tube tested in the three different steel qualities.

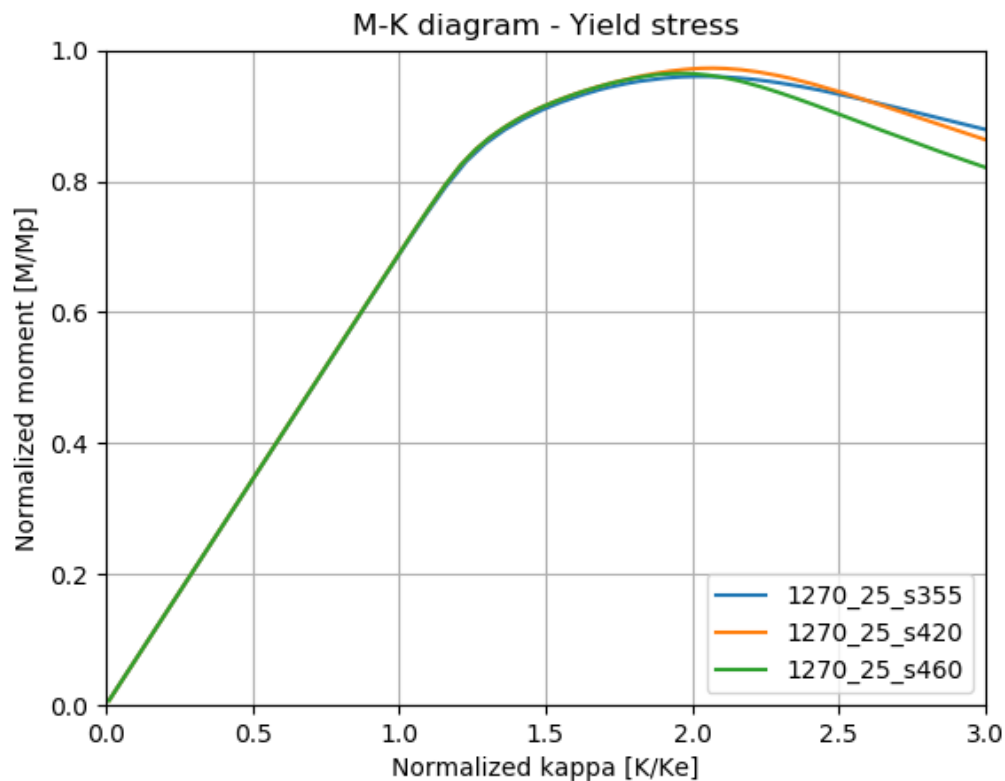


Figure 5.14: Normalized moment-curvature diagram for yield stresses: 355, 420 and 460 N/mm^2 . Tested tube: $D=1270mm$, $t=25mm$

For the three tested tubes represented in figure 5.14, the variations in normalized maximum moment and the corresponding critical curvature over an increasing yield stress are presented in the figures 5.15 and 5.16. Hardly any changes are observed in the normalized maximum moment over an increasing yield stress. A very small decrease of the normalized critical curvature by an higher steel quality can be seen.

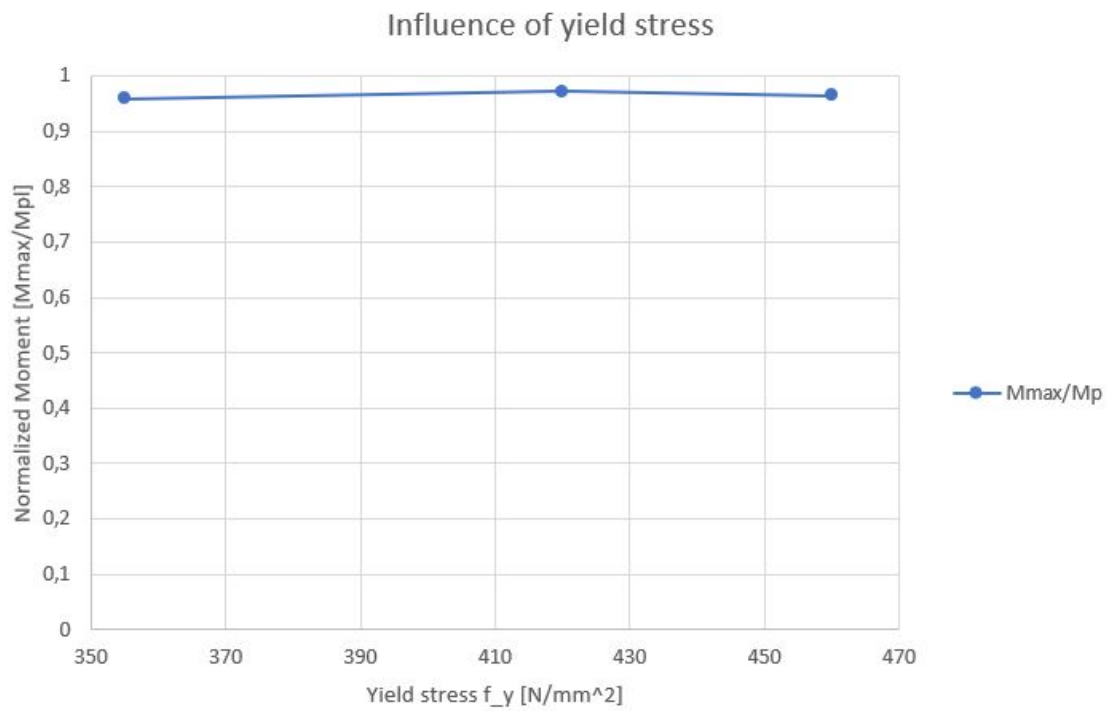


Figure 5.15: Influence of the yield stress on the Normalized moment for yield stresses: 355, 420 and 460 N/mm^2

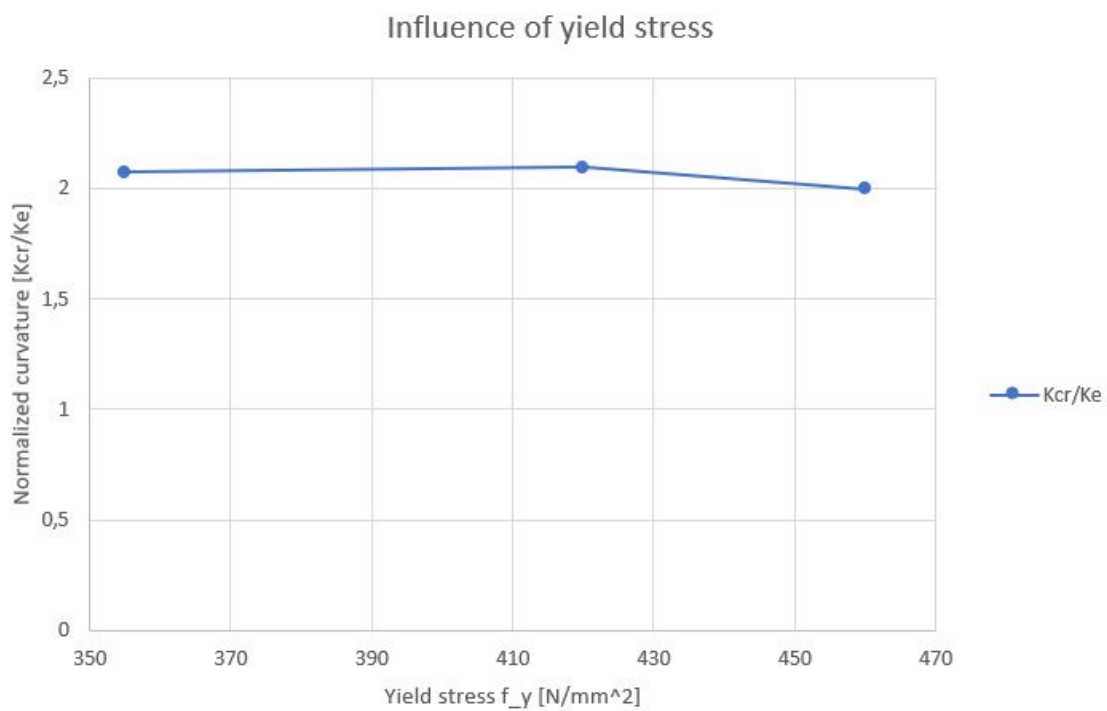


Figure 5.16: Influence of the yield stress on the Normalized curvature for yield stresses: 355, 420 and 460 N/mm^2 .

5.5.1. Influence of yield stress in the model study

However hardly any difference in normalized moment and curvature could be observed in the selected test results of paragraph 5.5, the effect of the yield stress on the total test range is studied for completeness. For the yield stress, also a conclusion per boundary condition can be derived from the results of the FEM model tests. Per boundary condition 12 models with the same steel quality are performed, these models together form an average normalized maximum moment and critical curvature to compare with the other boundary conditions. In table 5.4 the influences of the different yield stresses are presented per boundary condition. Also when looking to the yield stress, Boundary condition BC4F represents the set of divergent measurement results. The trend of the normalized maximum moment as well as for the normalized critical curvature is shown in the figures 5.17 and 5.18.

Average per parameter				
BC		f _y		
		S355	S420	S460
BC1F	M _{max} /M _p	0,90	0,89	0,88
	K _{cr} /K _e	1,78	1,67	1,61
BC1R	M _{max} /M _p	0,91	0,89	0,88
	K _{cr} /K _e	1,83	1,70	1,65
BC2F	M _{max} /M _p	0,92	0,90	0,89
	K _{cr} /K _e	1,84	1,68	1,66
BC2R	M _{max} /M _p	0,90	0,89	0,87
	K _{cr} /K _e	1,80	1,66	1,62
BC3R	M _{max} /M _p	0,91	0,89	0,88
	K _{cr} /K _e	1,81	1,67	1,65
BC4F	M _{max} /M _p	0,80	0,77	0,76
	K _{cr} /K _e	1,35	1,24	1,21
BC4R	M _{max} /M _p	0,91	0,89	0,88
	K _{cr} /K _e	1,80	1,66	1,62
BC_UCF	M _{max} /M _p	0,93	0,90	0,89
	K _{cr} /K _e	1,73	1,59	1,66

Table 5.4: Average normalized maximum moment and critical curvature per boundary condition per yield stress.

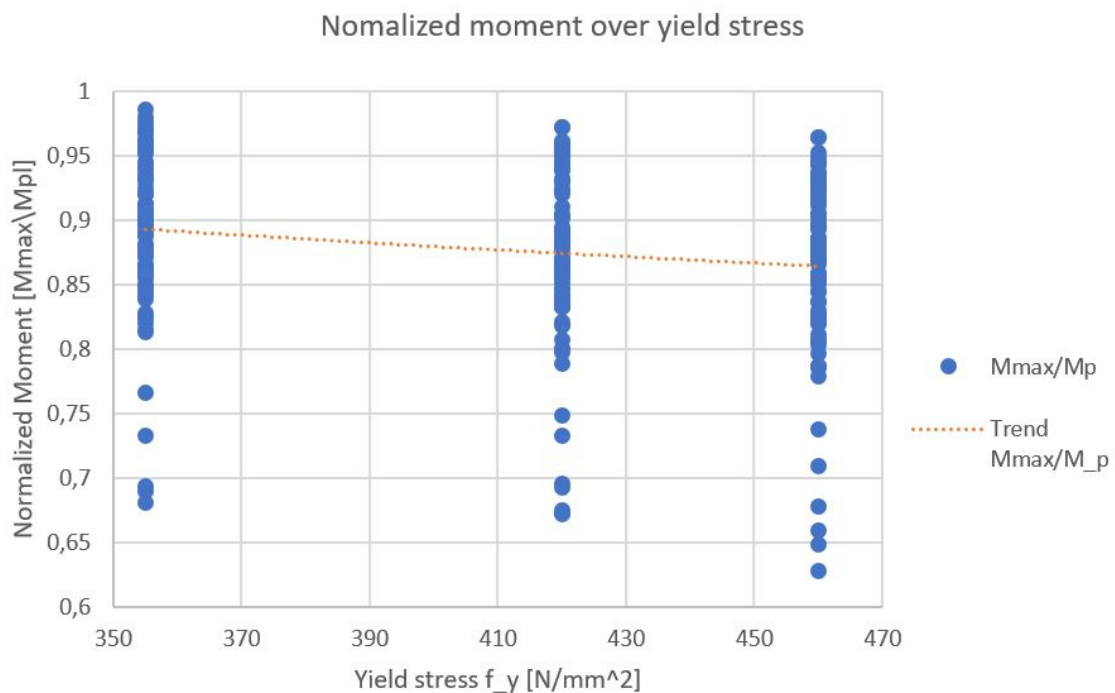


Figure 5.17: Trend of the influence of the yield stress on the Normalized moment for yield stresses: 355, 420 and 460 N/mm².

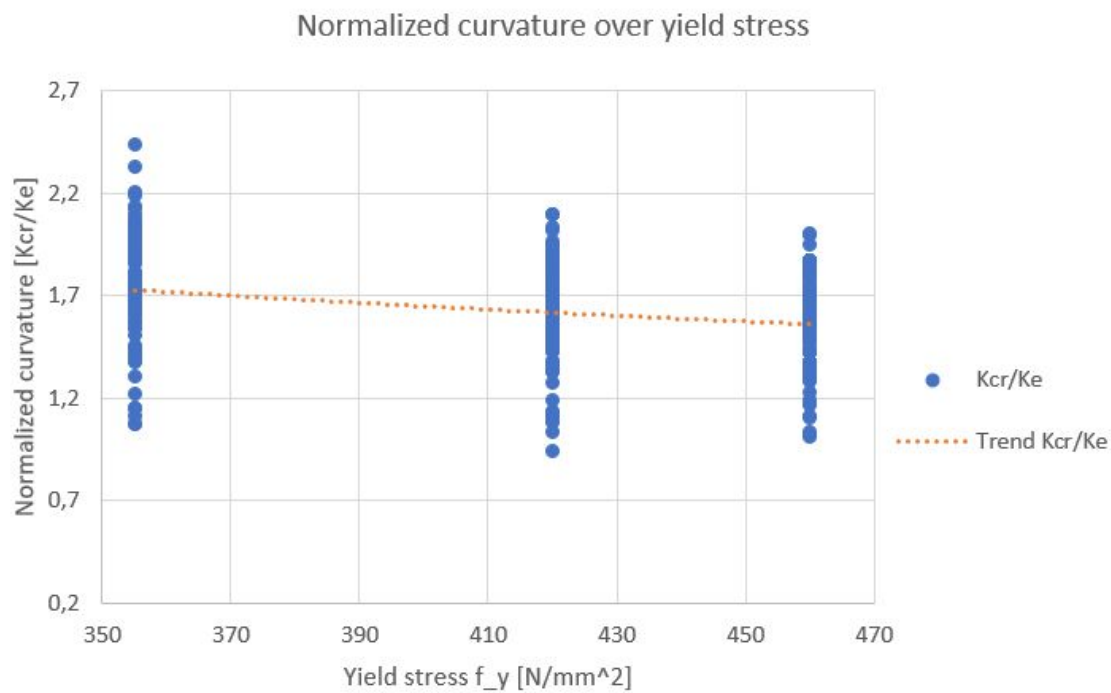


Figure 5.18: Trend of the influence of the yield stress on the Normalized curvature for yield stresses: 355, 420 and 460 N/mm^2 .

5.6. Influence length

In paragraph 3.2.1, the influence length is explained as the length over which the stiffness of a restrained cross-section influences the ovalization of a tubular pile. Since the model used for the FEM tests has a fixed system length of 6,6m and the calculated influence lengths are in a range of 2 to 10m, the direct relation to the moment and curvature of all the tubes is not representative in this case. An even moment distribution over the whole tested area, cause that tubes can buckle outside of the influence length for the same moment. A relative influence length to the system length is used to display the effects of the different influence length to the moment capacity and curvature behaviour of the tubes. The trends of the normalized maximum moment and the normalized critical curvature from the figures 5.19 and 5.20 show increasing maximum moments and increasing critical curvatures for a increasing relative influence lengths.

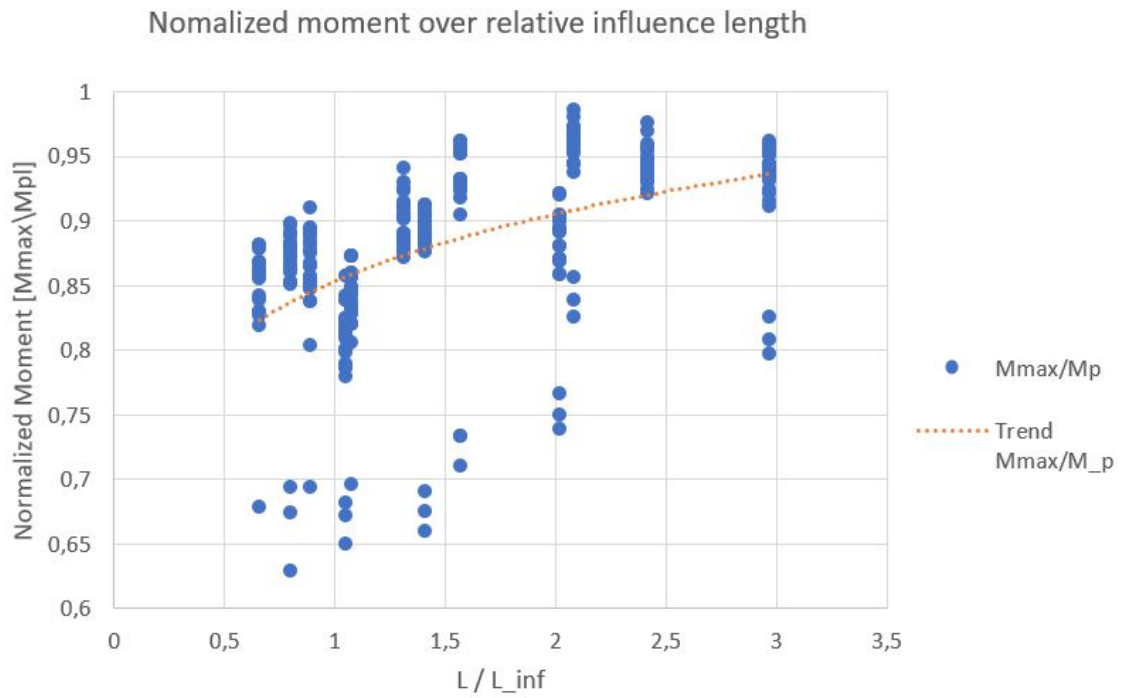


Figure 5.19: Trend of the influence of the relative influence length on the Normalized moment.

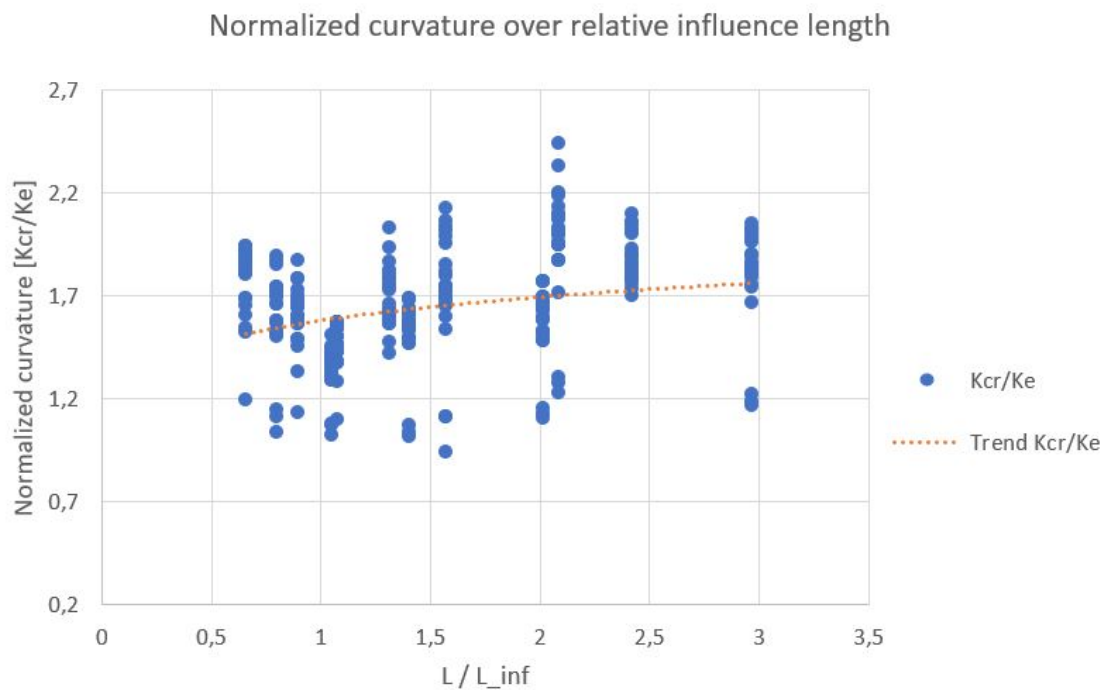


Figure 5.20: Trend of the influence of the relative influence length on the Normalized curvature.

The behaviour observed from the graphs is the opposite from what the theory behind it tells. Possible reasons why the theory is not valid for this study are, the use of an even moment over the entire tested area and/or dominant other parameters. The influence length is therefore excluded from the influence

study. In the graphs lower results are observed for an influence length equal to or half the system length ($L/L_{inf} = 1 \text{ and } 2$). No clear reason for this behaviour could be derived from these model data. In section 5.6.1, the relation of the influence length to the buckling location is studied.

5.6.1. Buckling location

From the study to the influence length in section 5.6 is concluded that the stiffening effect over a certain length caused by a restraint cross-section is not visible in the moment-curvature behaviour of the model data. Because of an even moment over the total test length, no difference in moment capacity is expected for influence lengths within the system length. The failure could take place outside the effected area of a restraint cross-section for the same moment. To check this theory the buckling locations of tubes with a restraint boundary condition are compared with the relative influence lengths as shown in figure 5.21

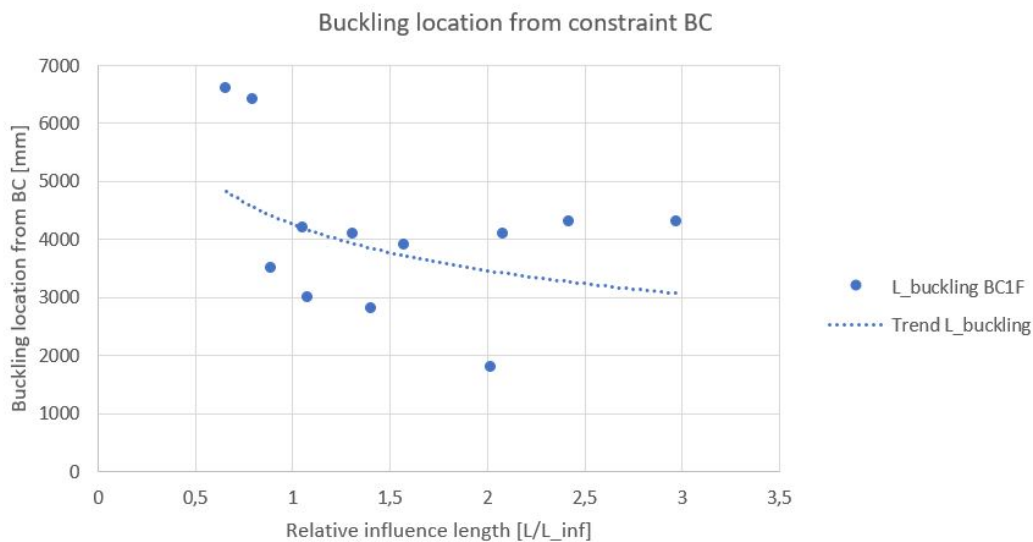


Figure 5.21: The buckling location with respect to the restraint boundary condition for all 12 tube geometries in the range

The wide scatter of results in the figure do not show a very clear dependency of the two parameters. However, the plotted trend shows a decreasing distance between the restrain boundary conditions and the failure location by a decreasing influence length. From the trend could be concluded that the buckling location is affected by the influence length. Further research is needed so more data can be collected to investigate the relationship.

5.7. Boundary conditions

The main focus of this thesis is to investigate the influence of different types of boundary conditions on the local buckling failure mechanism. In the previous paragraphs of this chapter, different parameters are discussed with their influence on the resistance capacity per boundary condition. In this chapter, the overall influence of the boundary conditions is discussed in combination with the type of (buckling) failure.

5.7.1. Overall trend over the boundary conditions

Looking to the results of all the 288 FEM model tests that are performed, not that much deviations can be observed between the different boundary conditions except for BC4F. This boundary condition shows in most cases the same trends for the tested parameters, but is not able to generate the same amount of resistance. This lack of resistance is also good visible in the overall plot of all the boundary conditions of figure 5.22 and in table 5.5 with all the influences per boundary per parameter. BC4F has a average normalized maximum moment that is approximately 14% lower than the one of the other boundary conditions. Because of the abrupt failure behaviour, BC4F has a average normalized critical curvature that is approximately 36% lower than the one of the other parameters. For the other boundary conditions, minimal differences of 1-2% are observed.

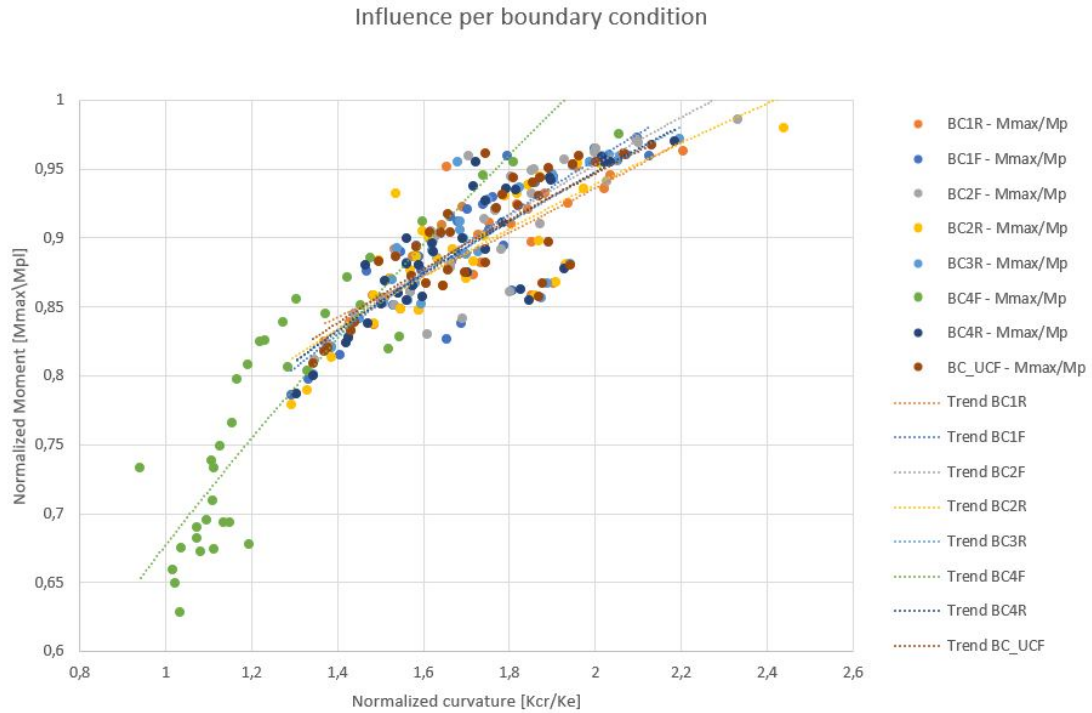


Figure 5.22: Total trend of the influence of boundary conditions on the moment-curvature behaviour.

Average per parameter		D/t				$\delta_{w/t}$			f _y			Overall Average
BC		50	70	90	110	0,16	0,2	0,25	S355	S420	S460	
BC1F	Mmax/Mp	0,94	0,91	0,88	0,84	0,90	0,90	0,88	0,90	0,89	0,88	0,89
	Kcr/Ke	1,77	1,75	1,72	1,50	1,77	1,66	1,62	1,78	1,67	1,61	1,69
BC1R	Mmax/Mp	0,94	0,91	0,86	0,86	0,90	0,90	0,88	0,91	0,89	0,88	0,89
	Kcr/Ke	1,83	1,74	1,66	1,65	1,82	1,70	1,66	1,83	1,70	1,65	1,72
BC2F	Mmax/Mp	0,96	0,92	0,88	0,84	0,91	0,91	0,89	0,92	0,90	0,89	0,90
	Kcr/Ke	1,89	1,79	1,76	1,51	1,83	1,68	1,67	1,84	1,68	1,66	1,73
BC2R	Mmax/Mp	0,95	0,89	0,86	0,85	0,89	0,90	0,87	0,90	0,89	0,87	0,89
	Kcr/Ke	1,84	1,64	1,66	1,62	1,80	1,67	1,62	1,80	1,66	1,62	1,69
BC3R	Mmax/Mp	0,95	0,91	0,87	0,85	0,90	0,90	0,88	0,91	0,89	0,88	0,89
	Kcr/Ke	1,87	1,71	1,71	1,57	1,81	1,66	1,66	1,81	1,67	1,65	1,71
BC4F	Mmax/Mp	0,87	0,79	0,75	0,70	0,82	0,78	0,73	0,80	0,77	0,76	0,78
	Kcr/Ke	1,37	1,24	1,30	1,15	1,39	1,25	1,15	1,35	1,24	1,21	1,27
BC4R	Mmax/Mp	0,95	0,91	0,87	0,85	0,89	0,90	0,88	0,91	0,89	0,88	0,89
	Kcr/Ke	1,83	1,72	1,68	1,56	1,78	1,66	1,64	1,80	1,66	1,62	1,70
BC_UCF	Mmax/Mp	0,95	0,92	0,87	0,86	0,91	0,91	0,89	0,93	0,90	0,89	0,90
	Kcr/Ke	1,82	1,78	1,68	1,64	1,71	1,73	1,66	1,73	1,59	1,66	1,70

Table 5.5: Overview of the influence of different parameters on the moment-curvature behaviour for the tested boundary conditions

5.7.2. Failure behaviour per boundary condition

To complete this chapter a visual overview of all boundary conditions is given in table 5.6. In the table, the normalized moment-curvature diagram of a boundary condition is placed next to the corresponding failure type and location of the tube.

Boundary condition visual scheme						
BC	Schematisation	Normalized M-K diagram	Failure location	Failure type	Average M_{max}/M_{pl}	Average K_{cr}/K_e
1F					0,89	1,69
1R					0,89	1,72
2F					0,9	1,73
2R					0,89	1,69
3R					0,89	1,71
4F					0,78	1,27
4R					0,89	1,70
UCF					0,9	1,70

Table 5.6: Visual overview of the boundary conditions and their failure behaviour, M-K diagrams and failure modes from tube: $D=2235\text{mm}$, $t=20\text{mm}$, $f_y = 355\text{N/mm}^2$

from the table can be observed that except of Boundary condition BC4F, all boundary conditions were able to force the buckling failure location away from the tube end. Studying the differences in failure behaviour, a more rapid decrease of moment capacity is observed for the boundary conditions that allow ovalization. Also a small difference can be observed between the boundary conditions with the rotational free and restrained tube ends. The tubes with a rotational restrained end show a more smooth behaviour after failure. The normalized moment-curvature diagrams used in table 5.6, are displayed for all tested tubular piles in appendix E. Figure 5.23 Shows the normalized moment-curvature diagrams of all boundary conditions of the tube used in the table.

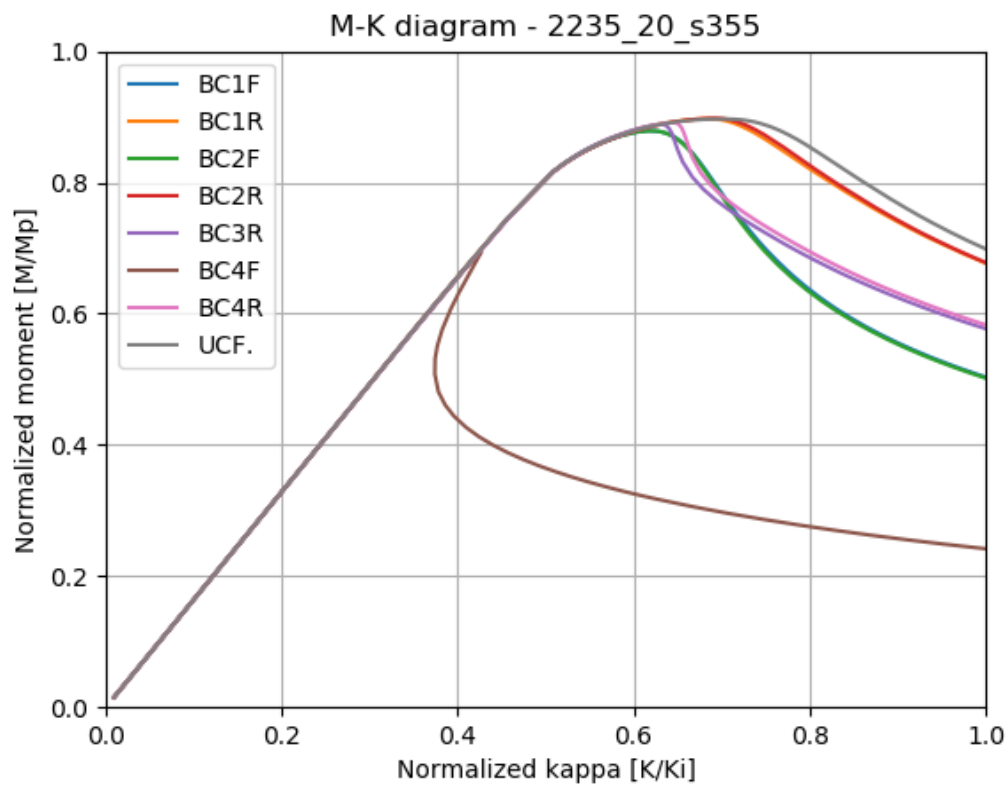


Figure 5.23: Illustrative graph of a normalized moment curvature diagrams for all boundary conditions of tube: $D=2235\text{mm}$, $t=20\text{mm}$, $f_y = 355\text{N/mm}^2$

From the graph, three couples of curves are observed that show a nearly identical behaviour. The couples are BC1F - BC2F, BC1R - BC2R and BC3R - BC4R. The difference within each of these couples is the possibility to displace in axial direction at the boundary. Since the model is based on pure bending without normal forces, the axial constraint has no influence on the moment-curvature behaviour for this specific model. In failure location and shape there are differences between the couples BC1F - BC2F, BC1R - BC2R and BC3R - BC4R as displayed in table 5.6.

6

Conclusions and recommendations

After completing this thesis, an answer on the main research question is formulated with the help of the conclusions of the executed studies. These studies on his own are answering the sub-questions. Parts of the subject that are of interest, but are not within the scope of this thesis are added to the recommendations for further research.

6.1. Conclusions

Boundary condition study

- In chapter 2, the theoretical approach of defining boundary conditions as used in the design code is studied. The radial, meridional and rotational direction of the local shell end is free or restrained for displacement, which generates nine theoretical conditions with simple visualisations (table 2.2b). From the nine boundary conditions, BC3R, BC4F, BC4R and BC-UCF are not yet included in the design code.
- By coupling the theoretical boundary conditions to practical applications, is concluded that BC2R, BC3R, and BC4R are not very common in the field of civil engineering.
- BC4F and BC-UCF are the two relevant missing boundary conditions in the current design code. With examples of several practical applications sub-question 2 is answered.

Residual stress

- Residual stress is a material imperfection common for steel tubular piles. The stresses are generated by several processes during production or assembling of tubular piles as welding, irregular cooling or cold deforming.
- From comparison with real tests of S. van Es [13], the residual stresses obtained from Vasilikis et al. [4], that represent only the cold spiral bending process, are validated. The same behaviour (but a smaller displacement) is observed in the FEM ring model as well as in the real experiments.
- The validated residual stresses are added to ABAQUS FEM models with the boundary conditions BC1 (no ovalization) and BC4 (ovalisation). The results of these tests show a similar behaviour for the tubes with BC1F, BC1R and BC4R. For this three tubes the normalized maximum moment shows a small increase of 1-3% and the normalized critical curvature shows an increase of approximately 20% in comparison with the tube without residual stresses. For the tube with boundary condition BC4F the normalized maximum moment decreases about 6-8% by a curvature that remains the same. This conclusion answers sub-question 3.

Geometrical imperfections

- All tubes in the tested range had an imperfection over thickness ratio of 0.16, 0.20 or 0.25. The overall trend shows a decreasing normalized maximum moment and corresponding critical curvature for an increasing imperfection/thickness ratio. BC4F shows a relative larger decrease over the increasing imperfection/thickness ratio than the other boundary conditions.
- BC4F deviates from the other boundary conditions with a 10-20% lower average normalized moment and a 30-40% lower average critical curvature. The other boundary conditions only deviate 1-3% from each other.
- In comparison with situations of the design code, BC1 (no ovalization) and BC4 (ovalization) conditions show almost in all cases higher normalized moments. For these analyses dimple imperfection heights corresponding to the limit values of the three quality classes in the design code are used in the FEM models. Only for BC4F the FEM model results show a lower moment resistance than the design code in the lowest quality class.
- Differences in trend between the FEM model results and the results of the design code calculations are observed. Over the tested dimple imperfection range the FEM model conditions BC1F, BC1R and BC4R show a decrease in normalized moment of approximately 10-12%. BC4F shows a decrease of 25% over the same imperfection range. The calculations from the design code only show a reduction in moment capacity of 5%. These differences in behaviour of the FEM model tests and the prescribed design code calculations answer sub-question 1.
- The imperfection heights corresponding to the quality classes excellent, good and normal are 2.56mm, 4.27mm and 6.43mm. These initial imperfections could be added to the models by eigenmodes and a scaling factor. This answers sub-question 4.

Parameters from the tested range

- In the tested range, tubes with diameter over thickness ratios of approximately 50, 70, 90 and 110 are used. For these mainly class 4 tubes an average decrease in normalized moment capacity of 10-11% is observed with an corresponding average decrease in normalized curvature of 12-20% for a increasing D/t ratio from 50 to 110. This result is known from other studies and confirmed here.
- For the yield stress these differences are much smaller. A decrease in maximum moment of 2-3% and an decrease of 8-11% of the normalized critical curvature is observed over an increasing yield stress from 355 to 460 N/mm^2 .

Influence length and buckling location

- From the analyses to the effect of the influence length on the moment curvature behaviour of the steel tubular piles is observed that the model used in this study is inappropriate to derive clear conclusions for this parameter. For most of the tubes in the test range the influence length is smaller than the system length over which the moment is even, the tube could buckle outside the influence length for the same moment. The normalized moment-curvature results from the FEM model tests show increasing values for an increasing relative influence length (system length / influence length) what counter acts the theory behind it.
- The buckling location does not show a clear dependency with the influence length for the tested tubes of BC1F. The trend shows a decreasing distance from the boundary condition for a increasing relative influence length (system length / influence length).

Influence of boundary conditions

- All material and geometrical parameters discussed in the previous chapters and paragraphs are tested for the eight boundary conditions BC1F, BC1R, BC2F, BC2R, BC3R, BC4F, BC4R and BC-UCF. A very consistent result is observed over all conditions except for boundary condition BC4F, this condition has an overall maximum normalized moment of approximately 14% lower than the other boundary conditions. The normalized critical curvature corresponding to the maximum moments is approximately 26% lower in comparison to the other boundary conditions.
- In the post-buckling trajectory, conditions with a rotational free boundary experience a more rapid decrease of the moment resistance capacity after the maximum moment occurs. For boundary conditions that are free to ovalize at the tube end, the decrease of moment capacity after failure is even more rapid.

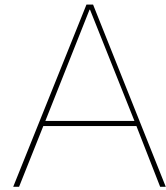
6.2. Recommendations

The following recommendations are made for future research to local buckling of steel tubular piles.

- Perform model studies to the influence of all boundary conditions in situation with shear and normal forces included. The combination of these researches gave a more overall view of the influence of the different boundary conditions.
- Extend the amount and the description of boundary conditions in the design code when the behaviour the conditions is better known. Add simple visualizations to clarify the differences between the conditions and corresponds more to the practical applications.
- Further research to the behaviour of BC4F is intended. This boundary condition deviates from all the other boundaries and shows local buckling failure for moments close to the calculated moments from the design code. Real tests to the currently used practical application as shown in chapter 2 should determine the accuracy of the situation.
- A verification to the parameters that determine the strength reduction caused by imperfections should be preformed. Looking to the comparison made between the design code and the FEM model results a larger relative decrease in capacity is observed in the FEM model results compared to the numbers calculated following the design code.
- perform a study to the influence of the tube length for the different boundary conditions. In this study, the effect of boundary conditions on the influence length and corresponding buckling location also need to be investigated more in detail.
- Tubular piles are very often used in combination with sheet piles in a combi-wall structures. The effect of the added stiffness as well as the lateral support by the sheet piles could influence the buckling behaviour of the tubular pile. The sheet pile also can be a loading condition. The combined behaviour of this system should be investigated more in detail.

Bibliography

- [1] Normcommissie 351 001. Eurocode 3: Design of steel structures - Part 1- 6: General - Strength and Stability of Shell Structures, 2018.
- [2] Normcommissie 351001. Eurocode 3: Design of steel structures - Part 1- 1: General rules and rules for buildings, 2018.
- [3] Normcommissie 351001. Eurocode 3: Design of steel structures - Part 4- 3: Pipelines, 2018.
- [4] Arnold M. Gresnigt Delft Daniel Vasilikis, Spyros A. Karamanos Sjors H. J. van Es. Ultimate Bending Capacity of Spiral-Welded Steel Tubes - Part II : Ultimate Bending Capacity of Spiral-Welded Steel Tubes – Part II : Predictions. Technical report, 2016.
- [5] Det Norske Veritas AS. Buckling Strength Analysis of Bars and Frames , and Spherical Shells, 2004.
- [6] DNV. RP-C202: Buckling Strength of Shells, 2013.
- [7] Projects Europe. Company Profile. *Filtration Industry Analyst*, 1997(5):5–6, 1997.
- [8] A. M. Gresnigt. Plastic Design of Buried Steel Pipelines in Settlement Areas. *Heron*, 31(4):3–113, 1986.
- [9] N Kostis. *Local buckling of sand-filled steel tubes for combined walls*. PhD thesis, 2016.
- [10] Junzhi Liu. *Numerical Simulations of Spirally Welded Steel Tubes Under 4-Point Bending*. PhD thesis, 2015.
- [11] J. Michael Rotter and Adam J. Sadowski. Full Plastic Resistance of Tubes Under Bending and Axial Force: Exact Treatment and Approximations. *Structures*, 10(November):30–38, 2016.
- [12] C A E User. Abaqus/CAE User's Manual Abaqus 6.11 Abaqus/CAE User's Manual.
- [13] S van Es. *On the aerodynamics of a vertical axis wind turbine wake An experimental and numerical study*. Number 2. Tu-delft, 2017.
- [14] J Winkel. *Large diameter dolphin piles*. PhD thesis, 2016.



Literature study

A.1. Buckling of steel tubular piles

Steel tubular piles that nowadays commonly are used in the field of civil engineering are local buckling sensitive elements. The current design code the NEN-EN 1993-1-6 [1] describes the failure mechanism of buckling as: “the ultimate limit state where the structure suddenly loses its stability under membrane compression and/or shear. It leads either to large displacements or to the structure being unable to carry the applied loads” (NEN-EN 1993-1-6, 2007, p.8) [1]. This description belongs to the phenomenon of global buckling. Local buckling is a type of buckling where the shell is locally deformed as result of membrane compression. For perfect round, homogeneous and undamaged tubular piles without residual stresses, it is less likely that buckling occurs. Nevertheless bifurcation buckling has no stable equilibrium and therefore it can always occur. In practice, there are always imperfections operating as a trigger point for local buckling.

The geometry of the tubular pile cross-section influences the sensitivity to local buckling. The general design code NEN-EN 1993-1-1 [2] for steel structures describes four cross-section classes. The four classifications describe a degree of limitation on resistance and rotational capacity due to the buckling resistance. The four classes are:

- Class 1: Plastic cross-sections where a plastic hinge can be formed so that the rotational capacity is enough for a plastic calculation without resistance losses.
- Class 2: Compact cross-sections where the plastic moment can be reached, however the rotational capacity is limited by local buckling.
- Class 3: Semi-compact cross-sections where the elastic moment can be reached, local buckling obstructs the development of the plastic moment.
- Class 4: Slender cross-sections where local buckling will take place before reaching the yield stress in one or more parts of the cross-section.

The diameter to thickness ratio (D/t) is a parameter used to determine the classification of the pile cross-section. The influence of the yield stress of an element compared to a yield stress of $f_{y,ref} = 235N/mm^2$ is included in the classification criteria as:

$$\varepsilon^2 = \frac{f_{y,ref}}{f_y} \tag{A.1}$$

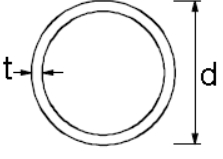
Ronde buizen						
						
Klasse	Doorsnede in druk en/of buiging					
1	$d/t \leq 50\varepsilon^2$					
2	$d/t \leq 70\varepsilon^2$					
3	$d/t \leq 90\varepsilon^2$					
	OPMERKING Voor $d/t > 90\varepsilon^2$ zie EN 1993-1-6.					
$\varepsilon = \sqrt{235 / f_y}$	f_y	235	275	355	420	460
	ε	1,00	0,92	0,81	0,75	0,71
	ε^2	1,00	0,85	0,66	0,56	0,51

Table A.1: Cross-section classification [2]

In table A.1 below the criteria for the classification of tubular piles are listed.

Tubular piles with a high diameter to thickness ratio, the so-called slender cross sections have an upper stress limit lower than the yield stress due to local buckling. This type of tubular piles is commonly used in civil structures and is therefore the main research objective. The NEN-EN 1993-1-6 [1] describes more in detail the application of these steel shell structures.

A.1.1. Types of analysis

To analyze the behavior of shell structures, the following three gradations of theories can be used:

- First-order plate / shell theory (thin plate / shell theory)
- Second-order plate / shell theory (Thick plate / shell theory)
- Three-dimensional continuum theory

The theories make use of specific assumptions that simplify the analysis by reducing the dimensions. The first-order plate/shell theory is based on the three kinematic assumptions of the Kirchhoff-Love theory. These assumptions are:

1. Normal straight lines to the shell reference surface remain straight after deformation.
2. Normal straight lines to the shell reference surface remain normal after deformation.
3. The transverse shear strains are negligible.

The second-order plate / shell theory neglect assumption 2 and therefore accounts for transverse shear deformation, corresponding to the Mindlin-Reissner theory. By neglecting all the above assumptions, a higher-order theory like the three-dimensional continuum theory is obtained.

A.1.2. Class 4 cross-sections

The NEN-EN 1993-1-6 [1] describes four different limit states for tubular piles cross-section class 4, that make use of different types of analyses. The four limit states and their analysis that are distinguished are:

- LS1: Plastic limit
 - Membrane theory
 - Linear elastic analysis (LA)
 - Materially nonlinear analysis (MNA)
 - Geometrically and materially nonlinear analysis (GMNA)
- LS2: Cyclic plasticity
 - Elastic analysis (LA or GNA)
 - Geometrically and materially nonlinear analysis (MNA or GMNA □ plastic strain range)
- LS3: Buckling
 - Membrane theory for asymmetric conditions
 - Linear elastic analysis (LA)
 - Linear elastic bifurcation analysis (LBA)
 - Materially nonlinear analysis (MNA)
 - Geometrically and materially nonlinear imperfection analysis
- LS4: Fatigue
 - Elastic analysis (LA or GNA)

The interest of this research is especially LS3, the buckling limit state. This limit state is taking into account all relevant load combinations that cause compressive membrane and/or shear membrane stresses. An other important aspect in the buckling limit state is the quality of the construction. The NEN-EN 1993-1-6 [1] expresses this quality in different types of tolerances.

A.2. Geometrical tolerances

Quality tolerances are included in the testing procedure of the buckling limit state. The different quality classes A, B and C are chosen to represent a certain tolerance level from normal to excellent. The lowest quality class measured for one of the imperfections types is normative for the whole analysis. The tolerances described in the NEN-EN 1993-1-6 [1] are in accordance with the tolerances they have been specified in the execution standard EN 1090. The tolerances that have been assessed in the buckling limit state are:

- Out of roundness tolerance
- Accidental eccentricity tolerance
- Dimple tolerances
- Interface flatness tolerance

A.2.1. Out of roundness

The out of roundness (ovalisation) of tubular piles influences the resistance of piles against local buckling. Ovalisation causes irregularities in the diameter of the pile, which are characterized by the ovalisation parameter a as shown in figure A.1. The ovalisation parameter is used to determining the radius of curvature r_o of the ovalised cross-section.

$$r_o = \frac{r}{1 - \frac{3a}{r}} \quad (\text{A.2})$$

with:

$$r = D/2, \quad D = D_e - t$$

$$a = (D_{max} - D_{min})/4$$

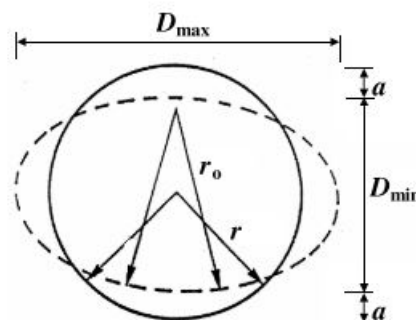


Figure A.1: Radius r_o in an ovalised cross section [3]

The NEN-EN 1993-4-3 [3] describes the mechanisms curvature, direct earth pressure and indirect earth pressure that cause ovalisation of tubular piles. Elastic ovalisation models by Reissner and Weinitschke 1963 and plastic ovalisation models by Gresnigt 1986 are used to determine the ovalisation parameter a .

In practice, even unloaded steel tubular piles are not perfectly round. Depending on the fabrication quality, the piles are indicated with a quality class as listed in table A.2. The NEN-EN 1993-1-6 [1]

prescribes imperfection reduction factors corresponding to the quality class of the steel tubular piles. For out-of-roundness, the parameter U_r is determined following figure A.2 and equation A.3.

$$U_r = \frac{d_{max} - d_{min}}{d_{nom}} \tag{A.3}$$

With:

d_{max} = Maximum measured internal diameter

d_{min} = Minimum measured internal diameter

d_{nom} = Nominal internal diameter

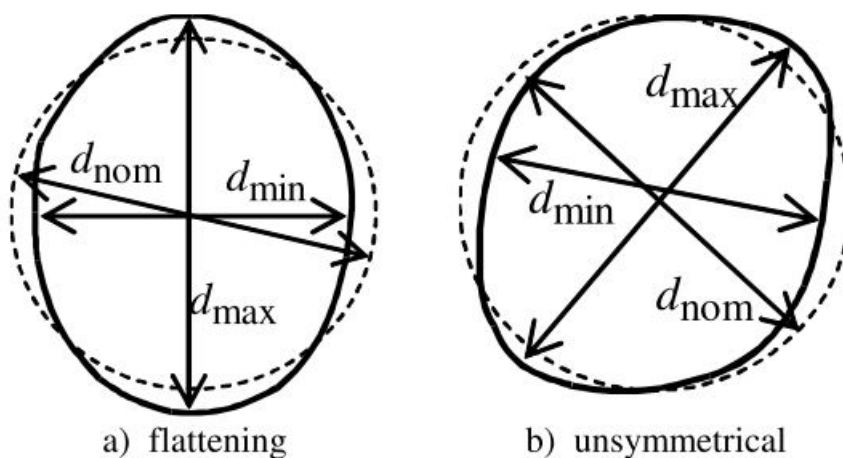


Figure A.2: Ovalisation dimensions [1]

To meet a certain quality class, the out of roundness parameter needs to meet the condition of equation A.4.

$$U_r \leq U_{r,max} \tag{A.4}$$

The parameter $u_{r,max}$ depends on the diameter as well as the quality class.

	Diameter range	$d [m] \leq 0,50m$	$0,50m < d [m] < 1,25m$	$1,25m \leq d [m]$
Fabrication tolerance quality class	Description	Recommended value of $U_{r,max}$		
Class A	Excellent	0,014	$0,007 + 0,0093(1,25-d)$	0,007
Class B	High	0,020	$0,010 + 0,0133(1,25-d)$	0,010
Class C	Normal	0,030	$0,015 + 0,0200(1,25-d)$	0,015

Table A.2: Recommended values for out-of-roundness tolerance parameter $U_{r,max}$ [1]

A.2.2. Accidental eccentricity

Steel tubular piles can consist of two or more separate pieces of tube connected by joints perpendicular to the membrane compressive forces. The connection between the two pieces can consist of two the same or two deviating thicknesses. Eccentricity in the joints can cause additional bending effects due to an eccentric stress path. The accidental eccentricity e_a consists of the total eccentricity e_{tot} minus the intended eccentricity e_{int} , see figure A.3 and equation A.5.

$$e_a = e_{tot} - e_{int} \quad (\text{A.5})$$

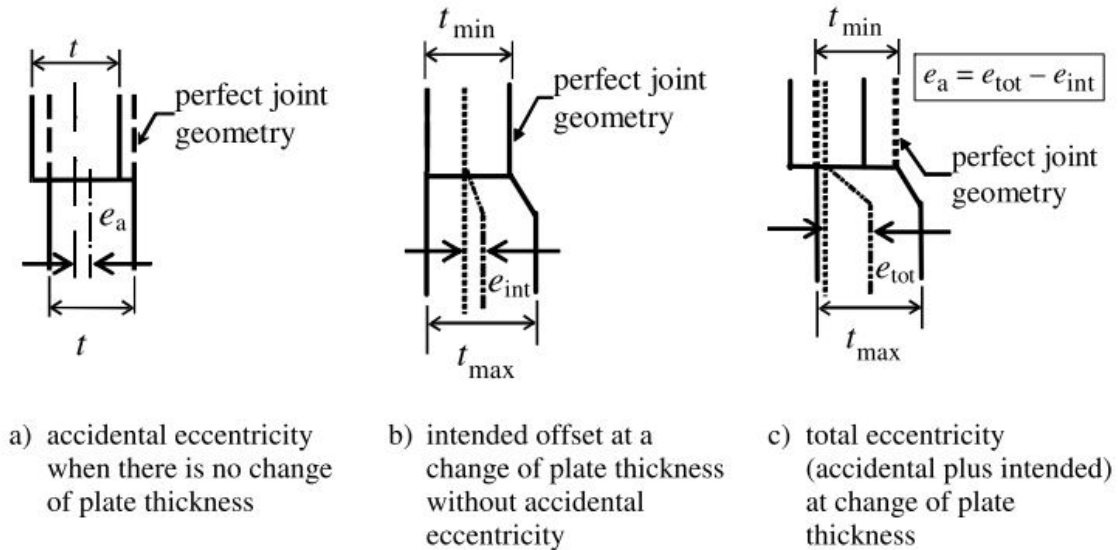


Figure A.3: Accidental eccentricity

The same as for out of roundness, accidental eccentricity has specified maximum eccentricities for each quality class. the maximum eccentricities $e_{a,max}$ per quality class are given in table A.3

Fabrication tolerance quality class	Description	Recommended values for maximum permitted accidental eccentricity $e_{a,max}$
Class A	Excellent	2 mm
Class B	High	3 mm
Class C	Normal	4 mm

Table A.3: Recommended values for maximum permitted accidental eccentricities [1]

Also the accidental eccentricity parameter U_e represents a condition that has a specified $U_{e,max}$ per quality class.

$$U_e = \frac{e_a}{t_{av}} \quad \text{or} \quad U_e = \frac{e_a}{t} \quad (\text{A.6})$$

with:

t_{av} = mean thickness of the thinner and thicker plates at the joint

Fabrication tolerance quality class	Description	Recommended value of $U_{e,max}$
Class A	Excellent	0,14
Class B	High	0,20
Class C	Normal	0,30

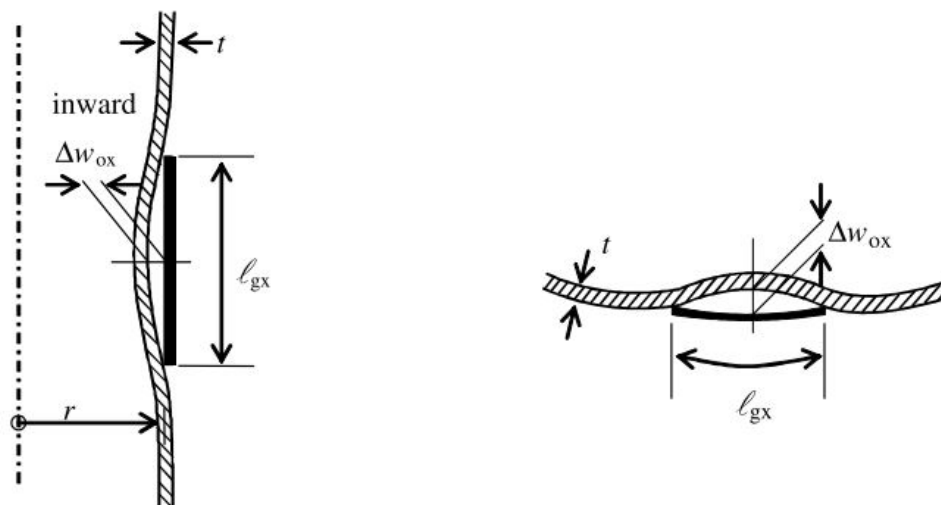
Table A.4: Recommended values for accidental eccentricity tolerances [1]

A.2.3. Dimples

Dimples are unevenness on the shell surface that reduce the radius of the shell locally. Dimples are measured with a gauge of specific length corresponding to a radius (see figure A.4), thickness and length ratio. The gauge length is specified in circumferential and meridional direction. The parameter δ_{w0} indicates the dimple depth. The parameters U_{0x} , $U_{0\theta}$ and U_{0w} are derived by dividing the dimple depth by the specific gauge length for that direction. Each quality class has a recommended value of $U_{0,max}$, see table A.5.

Fabrication tolerance quality class	Description	Recommended value of $U_{0,max}$
Class A	Excellent	0,006
Class B	High	0,010
Class C	Normal	0,016

Table A.5: Recommended values for dimple tolerance parameter $U_{0,max}$ [1]



a) Measurement on a meridian (see 8.4.4(2)a) b) First measurement on a circumferential circle

Figure A.4: Dimple measurements [1]

A.2.4. Interface flatness

The interface flatness refers to a tolerance of the interface between the shell and a boundary in circumferential direction. according the NEN-EN 1993-1-6 [1] the interface should not have a slope larger than $\beta_{\theta} = 0.001$ radials.

A.3. Boundary conditions

The use of steel tubular piles in different types of civil constructions comes with all kind of boundary conditions. Boundary conditions have influence on the failure mechanism of local buckling by limiting certain displacements at a support end. The NEN-EN 1993-1-6 [1] for shells describes three types of boundary conditions: clamped, pinned and free edge conditions that have their origin from the EN 1993 for silos and tanks. Table A.6 shows an overview of the available boundary conditions in the current design code for shell structures.

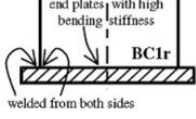

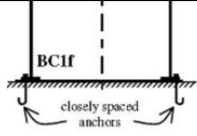


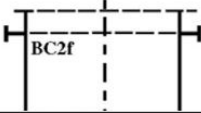

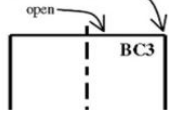
Boundary condition	Simple term	Description	Normal displacements	Meridional displacements	Meridional rotation	Current visualisation	Mechanical model
BC1r	Clamped	Radially restrained Meridionally restrained Rotation restrained	$w = 0$	$u = 0$	$\phi = 0$		
BC1f	Fixed-support	Radially restrained Meridionally restrained Rotation free	$w = 0$	$u = 0$	$\phi \neq 0$		
BC2r	Fixed-sliding	Radially restrained Meridionally free Rotation restrained	$w = 0$	$u \neq 0$	$\phi = 0$	-	
BC2f	Pinned	Radially restrained Meridionally free Rotation free	$w = 0$	$u \neq 0$	$\phi \neq 0$		
BC3	Free	Radially free Meridionally free Rotation free	$w \neq 0$	$u \neq 0$	$\phi \neq 0$		-

Table A.6: Boundary conditions for shells [1]

In the table above is shown that the displacements and rotations in normal, meridional direction are zero or non-zero. The two situations that are suggested for each direction are fully fixed and free. For civil engineering applications the current list of boundary conditions is in many cases not sufficient. In reality, boundary conditions can have a certain level of stiffness $0 < k < k_{max}$ that do not match the correctly to the conditions from the table above but have a springy boundary condition, see table A.7.




Boundary condition	Simple term	Description	Normal displacement	Meridional displacements	Meridional rotation	Current visualisation	Mechanical model
BC1k	Clamped-rotational spring	Radially restrained Meridionally restrained Rotation springy	$w = 0$	$u = 0$	$0 \leq k \leq k_{max}$	-	
BC2k	pinned rotational spring	Radially restrained Meridionally free Rotation springy	$w = 0$	$u \neq 0$	$0 \leq k \leq k_{max}$	-	
BC3k	Translation spring	Radially springy Meridionally free Rotation free	$0 \leq k \leq k_{max}$	$u \neq 0$	$\phi \neq 0$	-	

Table A.7: Springy boundary conditions for shells

A.4. Residual stress

Residual stresses present in steel spirally welded tubular piles can have several reasons. Sources of influence could be:

- Production process
- Uncoiling of the plate material
- Uneven heating and cooling
- Spiral bending
- Welding
 - Spiral welding
 - Girth welding

Most of these possible sources of residual stresses are hardly predictable. The bending process to make a spiral welded tube from a flat steel plate is a source that is modeled in ABAQUS by Vasilikis and Karamanos (2014) [4]. This research work resulted in a normalized residual stress distribution over the thickness (15 integration points) of the tube. These normalized distributions (see table A.8) can be used to generate the residual stresses for each steel spiral welded tube by multiplying them with the yield stress.

Integration points	Normalized Thickness	NormalizedAxial Stress	NormalizedHoop Stress
1	0	-0.018	0.598
2	0.071	-0.096	0.354
3	0.143	-0.171	0.114
4	0.214	-0.248	-0.139
5	0.286	-0.312	-0.392
6	0.357	-0.342	-0.641
7	0.429	-0.262	-0.862
8	0.5	0.01	-0.017
9	0.571	0.284	0.875
10	0.643	0.343	0.646
11	0.714	0.307	0.398
12	0.786	0.241	0.146
13	0.857	0.165	-0.106
14	0.929	0.089	-0.345
15	1	0.01	-0.59

Table A.8: Residual stress distribution (from inner surface to outer surface) [10]

A.5. Design codes

Several design codes describe a manner of assessing the failure mechanism of local buckling on tubular piles. For this literature study the current European design code NEN-EN and the offshore code DNV are studied to get insight in the assessment methods. From the European Standards the codes NEN-EN 1993-1-6 [1] and NEN-EN 1993-4-3 [3] are studied and from the DNV the DNV-RP-C202 [6] in combination with classification notes - No. 30.1 [5].

A.5.1. NEN-EN 1993-1-6

In the NEN-EN 1993-1-6 [1] the buckling limit state describes a stress based analysis, used to assess the strength of the shell membranes under compression. The buckling strength verification consists of three separate checks of the meridional, circumferential and the buckling shear membrane stresses, see equations A.7 to A.9. A unity check of the combined effects as represented in equation A.10 also need to be fulfilled. A calculation example of the buckling limit state is shown in appendix A. As described in subsection A.2 the NEN-EN 1993-1-6 includes imperfections in the calculation by adding partial factors indicated by a quality class.

$$\sigma_{x,Ed} \leq \sigma_{x,Rd} \quad (\text{A.7})$$

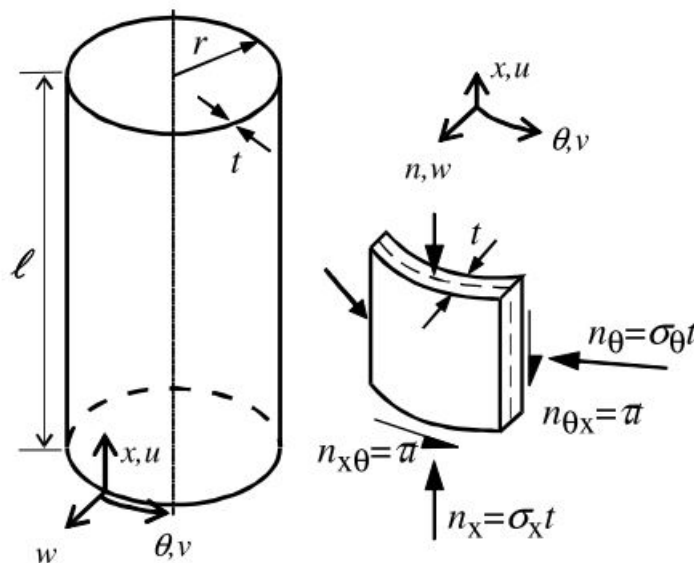


Figure A.5: Cylinder geometry, membrane stresses [1]

$$\sigma_{\theta,Ed} \leq \sigma_{\theta,Rd} \quad (\text{A.8})$$

$$\tau_{x\theta,Ed} \leq \tau_{x\theta,Rd} \quad (\text{A.9})$$

$$\left(\frac{\sigma_{x,Ed}}{\sigma_{x,Rd}}\right)^{k_x} - k_i \left(\frac{\sigma_{x,Ed}}{\sigma_{x,Rd}}\right) \left(\frac{\sigma_{\theta,Ed}}{\sigma_{\theta,Rd}}\right) + \left(\frac{\sigma_{\theta,Ed}}{\sigma_{\theta,Rd}}\right)^{k_\theta} + \left(\frac{\tau_{x\theta,Ed}}{\tau_{x\theta,Rd}}\right)^{k_\theta} \leq 1 \quad (\text{A.10})$$

A.5.2. NEN-EN 1993-4-3

The NEN-EN 1993-4-3 [3] describes a strain based method that assess the compressive strains in the deformation limit state (local buckling). A critical strain value ϵ_{cr} (Gresnigt) is calculated with the use of the radius of curvature r_0 of the ovalized cross-section. The method is derived for buried pipelines under possible internal or external pressure. Internal pressure can function as a support against ovalisation called the re-rounding effect, external pressure works negative on the local buckling capacity of a pipe. Equations A.11, A.12 shows the calculation of the critical value of the compressive strain.

$$\epsilon_{cr} = 0.25 * \frac{t}{r_0} - 0.0025 + 3000 * \frac{pr_0^2 |p|}{Et p} \quad \text{for } \frac{r_0}{t} \leq 60 \quad (\text{A.11})$$

$$\epsilon_{cr} = 0.10 * \frac{t}{r_0} + 3000 * \frac{pr_0^2 |p|}{Et p} \quad \text{for } \frac{r_0}{t} \geq 60 \quad (\text{A.12})$$

A.5.3. DNV-RP-C202 (classification Notes – No. 30.1)

The calculation method described in the DNV-RP-C202 is quite similar as the method described in the NEN-EN 1993-1-6, and concerns a stress based method as well. The DNV-RP-C202 suggests

the possibility to include stiffeners in two directions into the shell stability calculation, see figure A.6 imperfections are not directly included as explicit parameters in the calculation, but the calculations are based on an assumed level of imperfections. An example calculation of the buckling stability as described in the DNV-RP-C202 [6] can be found in Appendix A.

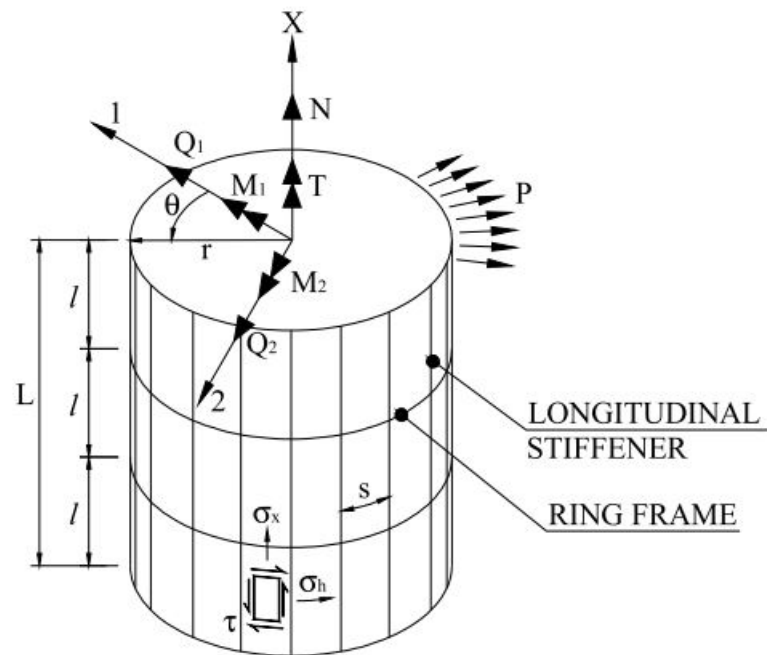


Figure A.6: Stiffened cylindrical shell [6]

A.6. Thesis scope

Within the seen literature this thesis is supported on available reports that are closely related to this study. The figure below (figure A.7) shows the connections and defines the scope of this thesis.

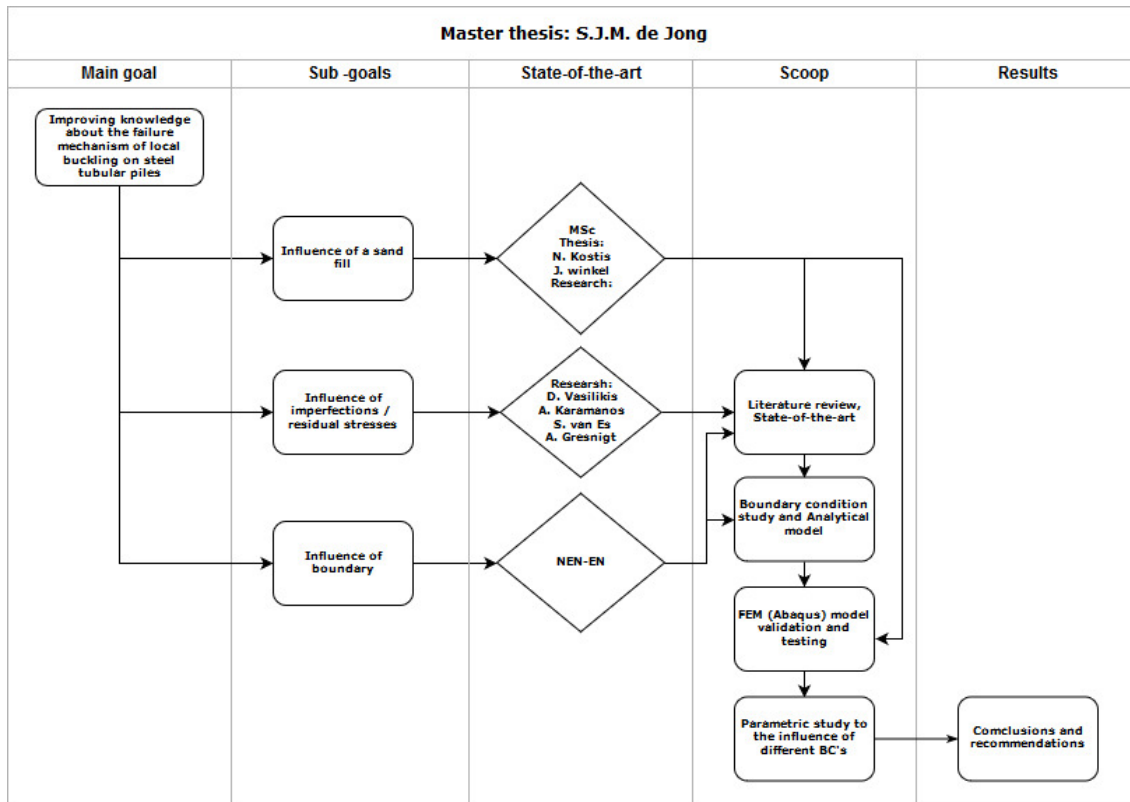


Figure A.7: Scoop and related literature

B

Design code calculations

B.1. NEN-EN 1993-1-6

Pile parameters:

$$\gamma_{m1} := 1.1$$

$$t := 18\text{mm}$$

$$L_{\text{Beam}} := 30000\text{mm} \quad \eta := 1$$

$$f_{yk} := 430 \frac{\text{N}}{\text{mm}^2}$$

$$r := 900\text{mm}$$

$$E := 210000 \frac{\text{N}}{\text{mm}^2} \quad \beta := 0.6$$

$$C_{xb} := 6 \quad \text{From table D1 EN1993-1-6}$$

$$Q := 16 \quad \text{From Table D2 EN 1993-1-6}$$

$$C_{\theta} := 0.6 \quad \text{From table D3 EN 1993-1-6}$$

$$C_{\theta_s} := 1.5 \quad \text{From table D4 EN 1993-1-6}$$

$$\alpha_{\theta} := 0.5 \quad \text{From table D5 EN 1993-1-6}$$

$$\alpha_{\tau} := 0.5 \quad \text{From table D6 EN 1993-1-6}$$

Load Parameters:

$$F_{xE_d} := 3750\text{kN}$$

$$\sigma_{FxE_d} := \frac{F_{xE_d}}{2 \cdot \pi \cdot r \cdot t} = 36.841 \cdot \frac{\text{N}}{\text{mm}^2}$$

$$M_{xE_d} := 10670\text{kN} \cdot \text{m}$$

$$\sigma_{MxE_d} := \frac{M_{xE_d}}{\pi \cdot r^2 \cdot t} = 232.947 \cdot \frac{\text{N}}{\text{mm}^2}$$

$$P_{\theta E_d} := 0 \cdot \frac{\text{N}}{\text{mm}^2}$$

$$\sigma_{P_{\theta E_d}} := P_{\theta E_d} \cdot \frac{r}{t} = 0 \cdot \frac{\text{N}}{\text{mm}^2}$$

$$M_{\tau E_d} := 1\text{kN} \cdot \text{m}$$

$$\sigma_{M_{\tau E_d}} := \frac{M_{\tau E_d}}{2 \cdot \pi \cdot r^2 \cdot t} = 0.011 \cdot \frac{\text{N}}{\text{mm}^2}$$

$$V_{\tau E_d} := 4025\text{kN}$$

$$\sigma_{V_{\tau E_d}} := \frac{V_{\tau E_d}}{\pi \cdot r \cdot t} = 79.086 \cdot \frac{\text{N}}{\text{mm}^2}$$

$$\sigma_{xE_d} := \sigma_{FxE_d} + \sigma_{MxE_d} = 269.788 \cdot \frac{\text{N}}{\text{mm}^2}$$

$$\sigma_{\theta E_d} := \sigma_{P_{\theta E_d}} = 0 \cdot \frac{\text{N}}{\text{mm}^2}$$

$$\tau_{x\theta E_d} := \sigma_{M_{\tau E_d}} + \sigma_{V_{\tau E_d}} = 79.097 \cdot \frac{\text{N}}{\text{mm}^2}$$

Dimensionless length parameter:

$$\omega := \frac{L_{\text{Beam}}}{\sqrt{r \cdot t}} = 235.702$$

The elastic critical meridional buckling stress:

$$C_{\text{xN}} := \max \left[1 + \frac{0.2}{C_{\text{xb}}} \cdot \left(1 - 2 \cdot \omega \cdot \frac{t}{r} \right), 0.6 \right] = 0.719$$

$$C_{\text{xs}} := \text{if} \left[\omega \leq 1.7, \left(1.36 - \frac{1.83}{\omega} + \frac{2.07}{\omega^2} \right), 0 \right] = 0$$

$$C_{\text{xm}} := \text{if} \left(1.7 \leq \omega \leq 0.5 \cdot \frac{r}{t}, 1, 0 \right) = 0$$

$$C_{\text{xI}} := \text{if} \left(\omega > 0.5 \cdot \frac{r}{t}, C_{\text{xN}}, 0 \right) = 0.719$$

$$C_{\text{x}} := \max(C_{\text{xs}}, C_{\text{xm}}, C_{\text{xI}}) = 0.719$$

$$\sigma_{\text{xRcr}} := 0.605 \cdot E \cdot C_{\text{x}} \cdot \frac{t}{r} = 1.827 \times 10^3 \cdot \frac{\text{N}}{\text{mm}^2}$$

The elastic critical circumferential buckling stress:

$$\sigma_{\text{Rcr.s}} := \text{if} \left[20 > \frac{\omega}{C_{\theta}}, 0.92 \cdot E \cdot \left(\frac{C_{\theta s}}{\omega} \right) \left(\frac{t}{r} \right), 0 \right] = 0$$

$$\sigma_{\text{Rcr.m}} := \text{if} \left[20 \leq \frac{\omega}{C_{\theta}} \leq 1.63 \cdot \frac{r}{t}, 0.92 \cdot E \cdot \left(\frac{C_{\theta}}{\omega} \right) \left(\frac{t}{r} \right), 0 \right] = 0$$

$$\sigma_{\text{Rcr.l}} := \text{if} \left[\frac{\omega}{C_{\theta}} > 1.63 \cdot \frac{r}{t}, E \cdot \left(\frac{t}{r} \right)^2 \cdot \left[0.275 + 2.03 \cdot \left(\frac{C_{\theta}}{\omega} \cdot \frac{r}{t} \right)^4 \right], 0 \right] = 23.145 \cdot \frac{\text{N}}{\text{mm}^2}$$

$$\sigma_{\text{Rcr}} := \max(\sigma_{\text{Rcr.s}}, \sigma_{\text{Rcr.m}}, \sigma_{\text{Rcr.l}}) = 23.145 \cdot \frac{\text{N}}{\text{mm}^2}$$

The elastic critical shear buckling stress:

$$C_{\tau s} := \text{if} \left(\omega \leq 10, \sqrt{1 + \frac{42}{\omega^3}}, 0 \right) = 0$$

$$C_{\tau m} := \text{if} \left(10 \leq \omega \leq 8.7 \cdot \frac{r}{t}, 1, 0 \right) = 1$$

$$C_{\tau l} := \text{if} \left(\omega > 8.7 \cdot \frac{r}{t}, \frac{1}{3} \cdot \sqrt{\omega \cdot \frac{t}{r}}, 0 \right) = 0$$

$$C_{\tau} := \max(C_{\tau s}, C_{\tau m}, C_{\tau l}) = 1$$

$$\tau_{x\theta R,cr} := 0.75 \cdot E \cdot C_{\tau} \cdot \sqrt{\frac{1}{\omega} \cdot \frac{t}{r}} = 205.177 \cdot \frac{\text{N}}{\text{mm}^2}$$

The characteristic imperfection amplitude:

$$\Delta_{wk} := \frac{1}{Q} \cdot \sqrt{\frac{r}{t}} \cdot t = 7.955 \times 10^{-3} \text{ m}$$

Meridional elastic imperfection reduction factor:

$$\alpha_x := \frac{0.62}{1 + 1.91 \left(\frac{\Delta_{wk}}{t} \right)^{1.44}} = 0.39$$

The circumferential squash limit slenderness:

$$\lambda_{0x} := 0.2$$

$$\lambda_{0\theta} := 0.4$$

$$\lambda_{0\tau} := 0.4$$

The plastic limit relative slenderness:

$$\lambda_{px} := \sqrt{\frac{\alpha_x}{1 - \beta}} = 0.988$$

$$\lambda_{p\theta} := \sqrt{\frac{\alpha_{\theta}}{1 - \beta}} = 1.118$$

$$\lambda_{p\tau} := \sqrt{\frac{\alpha_{\tau}}{1 - \beta}} = 1.118$$

The relative shell slenderness for different stress components:

$$\lambda_x := \sqrt{\frac{f_{yk}}{\sigma_{xRcr}}} = 0.485 \quad \lambda_\theta := \sqrt{\frac{f_{yk}}{\sigma_{\theta Rcr}}} = 4.31 \quad \lambda_\tau := \sqrt{\frac{\left(\frac{f_{yk}}{\sqrt{3}}\right)}{\tau_{x\theta Rcr}}} = 1.1$$

The buckling reduction factors:

$$\chi_{x1} := \text{if}(\lambda_x \leq \lambda_{0x}, 1, 0) = 0$$

$$\chi_{x2} := \text{if}\left[\lambda_{0x} < \lambda_x < \lambda_{px}, 1 - \beta \cdot \left(\frac{\lambda_x - \lambda_{0x}}{\lambda_{px} - \lambda_{0x}}\right)^\eta, 0\right] = 0.783$$

$$\chi_{x3} := \text{if}\left(\lambda_{px} \leq \lambda_x, \frac{\alpha_x}{2}, 0\right) = 0$$

$$\chi_x := \max(\chi_{x1}, \chi_{x2}, \chi_{x3}) = 0.783$$

$$\chi_{\theta 1} := \text{if}(\lambda_\theta \leq \lambda_{0\theta}, 1, 0) = 0$$

$$\chi_{\theta 2} := \text{if}\left[\lambda_{0\theta} < \lambda_\theta < \lambda_{p\theta}, 1 - \beta \cdot \left(\frac{\lambda_\theta - \lambda_{0\theta}}{\lambda_{p\theta} - \lambda_{0\theta}}\right)^\eta, 0\right] = 0$$

$$\chi_{\theta 3} := \text{if}\left(\lambda_{p\theta} \leq \lambda_\theta, \frac{\alpha_\theta}{2}, 0\right) = 0.027$$

$$\chi_\theta := \max(\chi_{\theta 1}, \chi_{\theta 2}, \chi_{\theta 3}) = 0.027$$

$$\chi_{\tau 1} := \text{if}(\lambda_\tau \leq \lambda_{0\tau}, 1, 0) = 0$$

$$\chi_{\tau 2} := \text{if}\left[\lambda_{0\tau} < \lambda_\tau < \lambda_{p\tau}, 1 - \beta \cdot \left(\frac{\lambda_\tau - \lambda_{0\tau}}{\lambda_{p\tau} - \lambda_{0\tau}}\right)^\eta, 0\right] = 0.415$$

$$\chi_{\tau 3} := \text{if}\left(\lambda_{p\tau} \leq \lambda_\tau, \frac{\alpha_\tau}{2}, 0\right) = 0$$

$$\chi_\tau := \max(\chi_{\tau 1}, \chi_{\tau 2}, \chi_{\tau 3}) = 0.415$$

The resistance limitations:

$$\sigma_{xRk} := \chi_x f_{yk} = 336.595 \cdot \frac{\text{N}}{\text{mm}^2} \quad \sigma_{\theta Rk} := \chi_{\theta} f_{yk} = 11.572 \cdot \frac{\text{N}}{\text{mm}^2}$$

$$\sigma_{xRd} := \frac{\sigma_{xRk}}{\gamma_{m1}} = 305.996 \cdot \frac{\text{N}}{\text{mm}^2} \quad \sigma_{\theta Rd} := \frac{\sigma_{\theta Rk}}{\gamma_{m1}} = 10.52 \cdot \frac{\text{N}}{\text{mm}^2}$$

$$\tau_{x\theta Rk} := \chi_{\tau} \frac{f_{yk}}{\sqrt{3}} = 103.047 \cdot \frac{\text{N}}{\text{mm}^2}$$

$$\tau_{x\theta Rd} := \frac{\tau_{x\theta Rk}}{\gamma_{m1}} = 93.679 \cdot \frac{\text{N}}{\text{mm}^2}$$

The stress limitations (UC's):

$$UC_x := \frac{\sigma_{xE d}}{\sigma_{xRd}} = 0.882$$

$$UC_{\theta} := \frac{\sigma_{\theta E d}}{\sigma_{\theta R d}} = 0$$

$$UC_{\tau} := \frac{\tau_{x\theta E d}}{\tau_{x\theta R d}} = 0.844$$

The combination of stresses:

$$k_x := 1.0 + \chi_x^2 = 1.613$$

$$k_{x1} := 1.25 + 0.75 \cdot \chi_x = 1.837$$

$$k_{\theta} := 1.0 + \chi_{\theta}^2 = 1.001$$

$$k_{\theta 1} := 1.25 + 0.75 \cdot \chi_{\theta} = 1.27$$

$$k_{\tau} := 1.5 + 0.5 \cdot \chi_{\tau}^2 = 1.586$$

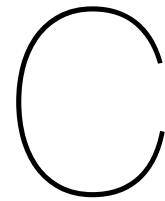
$$k_{\tau 1} := 1.75 + 0.25 \cdot \chi_{\tau} = 1.854$$

$$k_i := (\chi_x \chi_{\theta})^2 = 4.438 \times 10^{-4}$$

$$k_{i1} := (\chi_x \chi_{\theta})^2 = 4.438 \times 10^{-4}$$

$$UC_{\text{combi}} := \left(\frac{\sigma_{xE d}}{\sigma_{xRd}} \right)^{k_x} - k_i \left(\frac{\sigma_{xE d}}{\sigma_{xRd}} \right) \left(\frac{\sigma_{\theta E d}}{\sigma_{\theta R d}} \right) + \left(\frac{\sigma_{\theta E d}}{\sigma_{\theta R d}} \right)^{k_{\theta}} + \left(\frac{\tau_{x\theta E d}}{\tau_{x\theta R d}} \right)^{k_{\tau}} = 1.581$$

$$UC_{\text{combi}_2} := \left(\frac{\sigma_{xE d}}{\sigma_{xRd}} \right)^{k_x} + \left(\frac{\sigma_{\theta E d}}{\sigma_{\theta R d}} \right)^{k_{\theta}} + \left(\frac{\tau_{x\theta E d}}{\tau_{x\theta R d}} \right)^{k_{\tau}} = 1.581$$



ABAQUS modeling and post-processing

C.1. Modeling resources

To create a steel tubular pile in ABAQUS with the correct properties and configurations of a model, many tutorials and manuals are available. Depending on the type of analyses and data that are desirable, settings can be different. Many research analyses to the local buckling failure mechanism are performed with ABAQUS over the past years. Some of these researches describe exactly the steps to generate a working shell model for a parametric study. The model for this study is based on the following resources:

1. To create the base model with buckling eigenmodes, the steps of appendix C from the thesis report of N. kostis [9] are followed.
2. Appendix B from the thesis report of J. Liu [10] describes in detail how to implement residual stresses in the ABAQUS FEM model, and show the possibility to run multiple models in a row using batch files.
3. A detailed description of keyword editing is given in Appendix D of the thesis report of J. Winkel [14].
4. All general information can also be found in the ABAQUS manual [12].

C.2. Post-processing python script

```

1 import pylab as plt
2 import numpy as np
3
4 name = __file__.split('/')[0]
5 name = name[:-3]
6 print(name)
7
8 filenames = [name + "_BC1F.dat",
9             name + "_BC1R.dat",
10            name + "_BC2F.dat",
11            name + "_BC2R.dat",
12            name + "_BC3R.dat",
13            name + "_BC4F.dat",
14            name + "_BC4R.dat",
15            name + "_BC_UCF.dat"]
16
17 for filename in filenames:
18     # Displacement / Force from Abaqus .DAT file
19     f = open(filename, "r")
20     lines = f.readlines()
21     f.close()
22     printing = False
23
24     displa = []
25     forces = []
26     i = 0
27
28     for line in lines:
29         if "ESTIMATE OF THE SCRATCH DISK SPACE IS NOT
30         POSSIBLE." in line:
31             # hier is het beschouwd gedeelte!!!!
32             printing = True
33             if "MINIMUM" in line and printing:
34                 if line.split()[0] == "MINIMUM" and i % 2 == 0
35                 :
36                     displa.append(float(line.split()[1]))
37                 if line.split()[0] == "MINIMUM" and i % 2 == 1
38                 :
39                     forces.append(float(line.split()[1]))
40                 i += 1
41
42     fname = filename.replace('_', ' ')
43     print(filename)
44
45     if "s355" in fname or "s420" in fname or "s460" in

```

Figure C.1: Post-processing script part 1

```
42 fname:
43     sigma = fname.split()[2][1:]
44     sigma = float(sigma)
45     print(float(sigma))
46
47     # Pile diameter
48     D = fname.split()[0]
49     D = float(D)
50     print('D =', D)
51
52     # Pile thickness
53     t = fname.split()[1]
54     t = float(t)
55     print('t =', t)
56
57     # Central diameter
58     D_m = D - t
59     print('D_m =', D_m)
60
61     # Plastic moment
62     M_p = (1 / 6) * ((D ** 3) - ((D - (2 * t)) ** 3)) *
sigma
63     M_p = float(M_p)
64     print('M_p =', M_p)
65
66     # Curvature-like
67     kappa_i = t / (D_m ** 2)
68     kappa_i = float(kappa_i)
69     print('kappa_i =', kappa_i)
70
71     # Beam lengths:
72     L_1 = 3333
73     print('L_1 =', L_1)
74     L_2 = 6666
75     print('L_2 =', L_2)
76
77     forces = np.array(forces)
78     displa = np.array(displa)
79
80     moment = (forces * L_1)
81
82     kappa = (displa / L_1) / L_2
83
84     kappa_norm = kappa / kappa_i
85
```

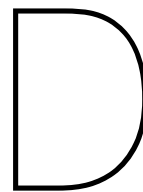
Figure C.2: Post-processing script part 2

```

86     print('kappa_norm =', kappa_norm)
87
88     moment_norm = moment / M_p
89
90     print('moment_norm =', moment_norm)
91
92     M_max = moment_norm.max()
93     print('M_max', M_max)
94
95     K_max = kappa_norm[moment_norm.argmax()]
96     print('K_max', K_max)
97
98     plt.plot(kappa_norm, moment_norm, label=filename.
split("_")[-1][:4])
99     plt.legend(loc="upper left")
100    plt.title('M-K diagram - ' + filename.split(".")[0][:
12])
101    plt.xlabel('Normalized kappa [K/Ki]')
102    plt.ylabel('Normalized moment [M/Mp]')
103    plt.xlim(0,1)
104    plt.ylim(0,1)
105    plt.grid(True)
106
107    M_max = moment_norm.max()
108    K_max = kappa_norm[moment_norm.argmax()]
109
110    f = open('MAX.txt', 'a')
111    line = f'{M_max}, {K_max}\n'
112    f.write(line)
113
114    f = open(filename.split(".")[0] + '_output.txt', 'w')
115    for i in range(len(kappa)):
116        line = f'{round(kappa_norm[i],16)}, {round(
moment_norm[i],3)}\n'
117        f.write(line)
118    f.close()
119
120    plt.savefig(filename.split(".")[0][:12] + '_fig.png')
121    plt.show()
122    plt.close()
123
124

```

Figure C.3: Post-processing script part 3



Eigenmode analyses

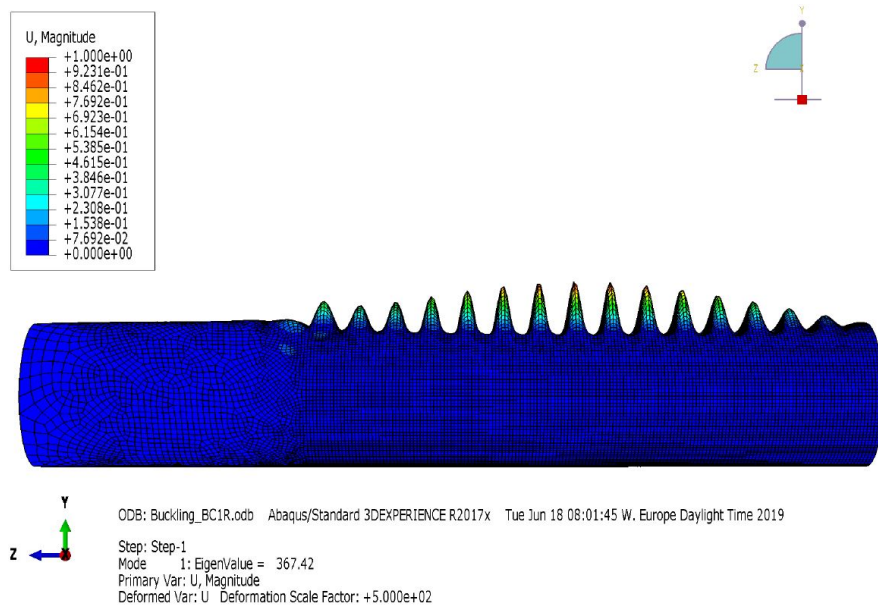


Figure D.1: Eigenmode 1

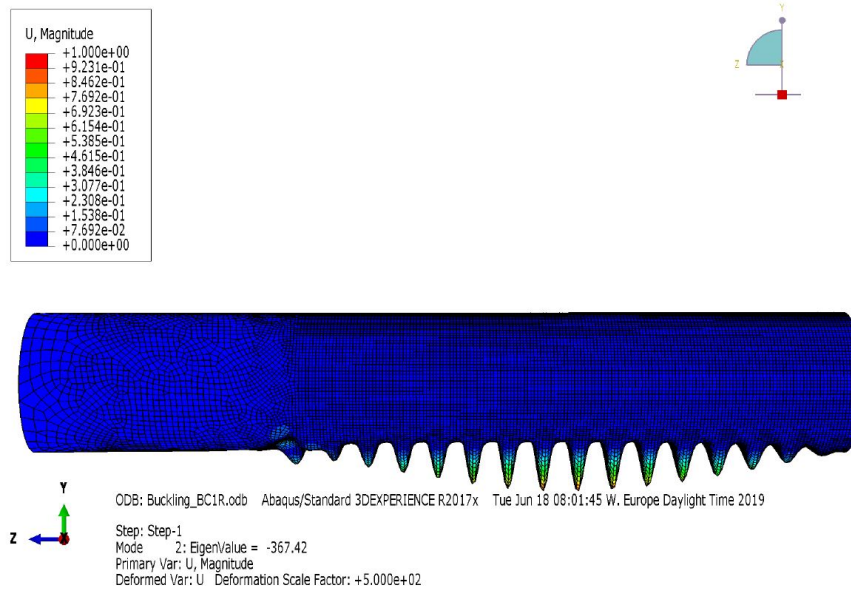


Figure D.2: Eigenmode 2

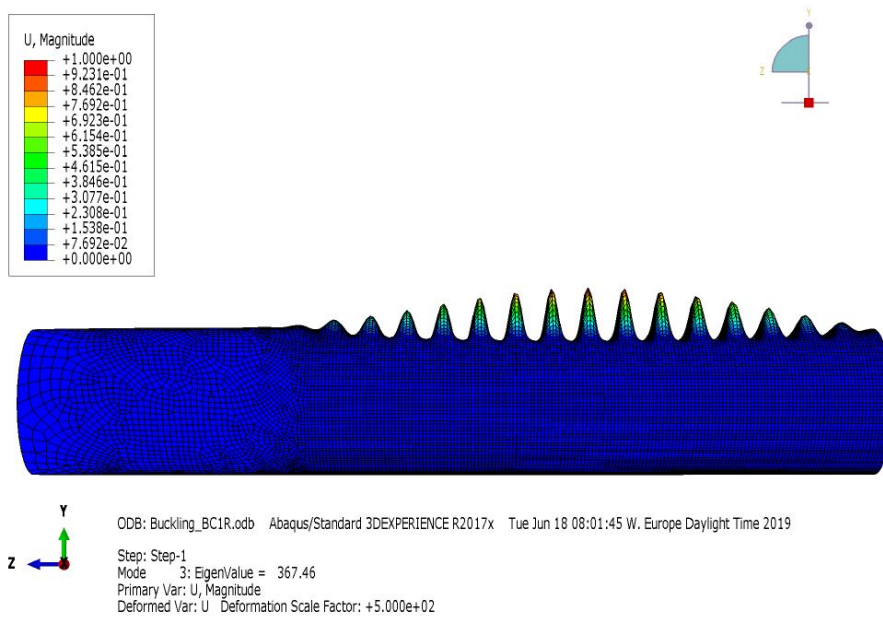


Figure D.3: Eigenmode 3

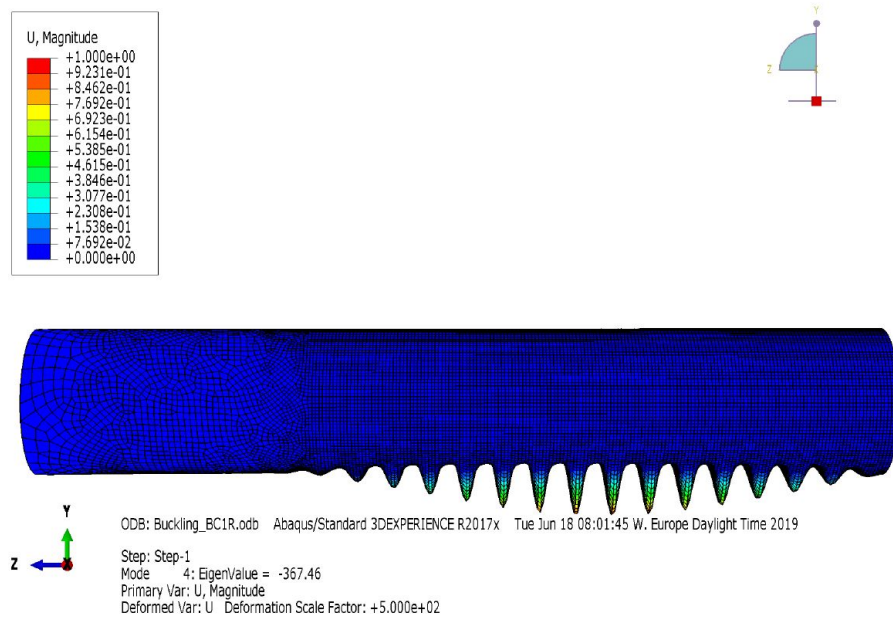


Figure D.4: Eigenmode 4

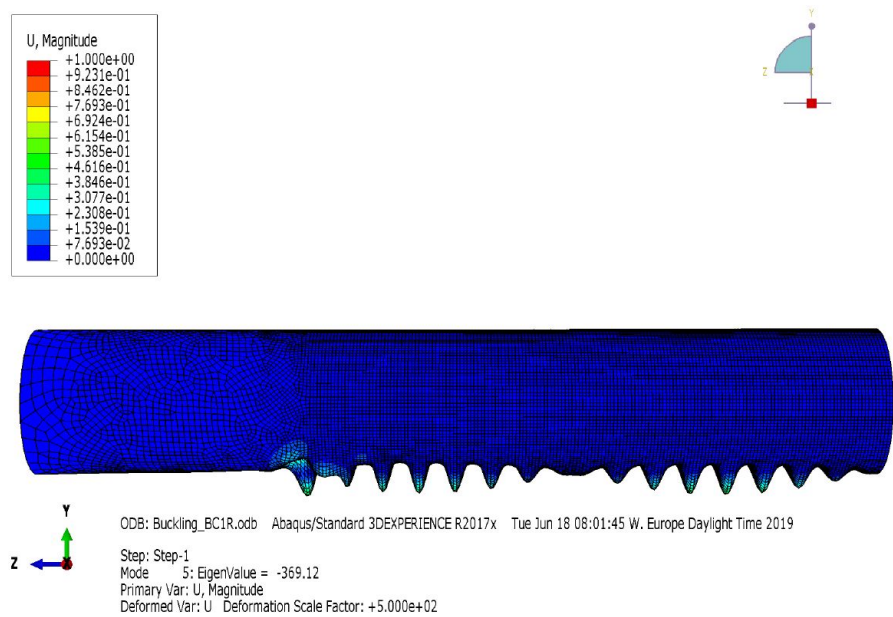


Figure D.5: Eigenmode 5

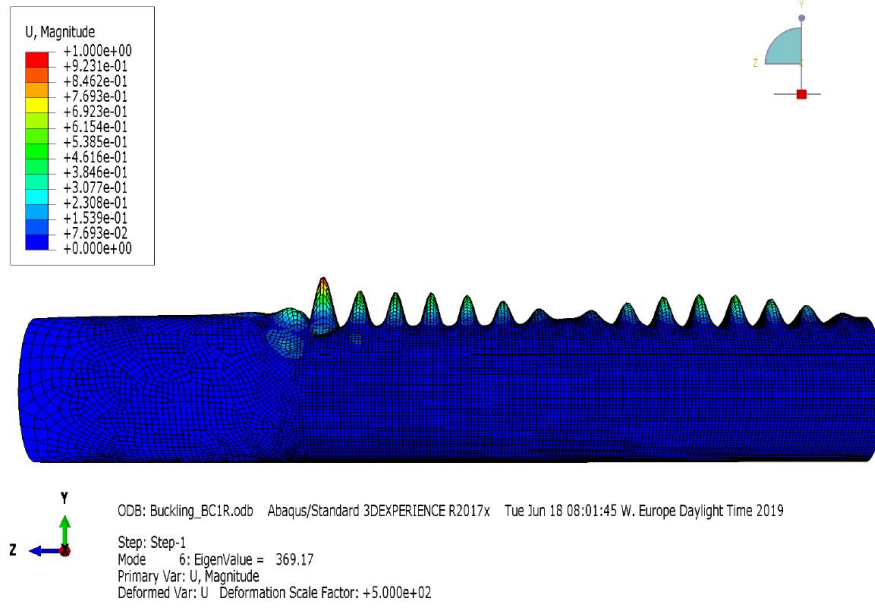


Figure D.6: Eigenmode 6

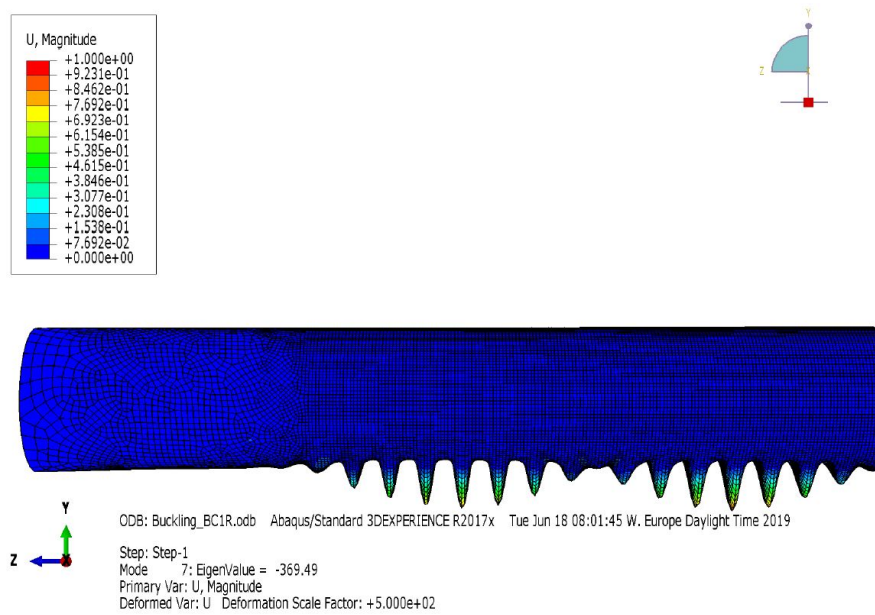


Figure D.7: Eigenmode 7

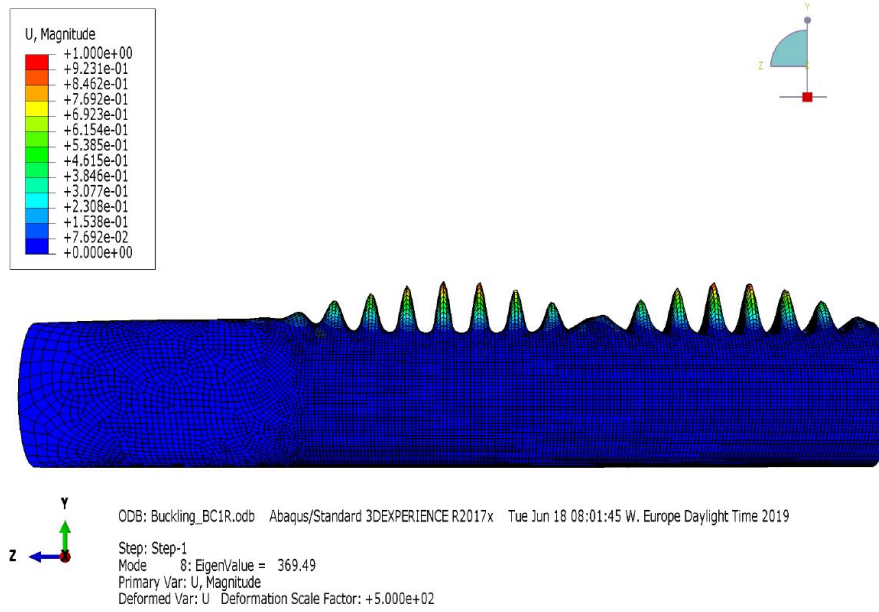


Figure D.8: Eigenmode 8

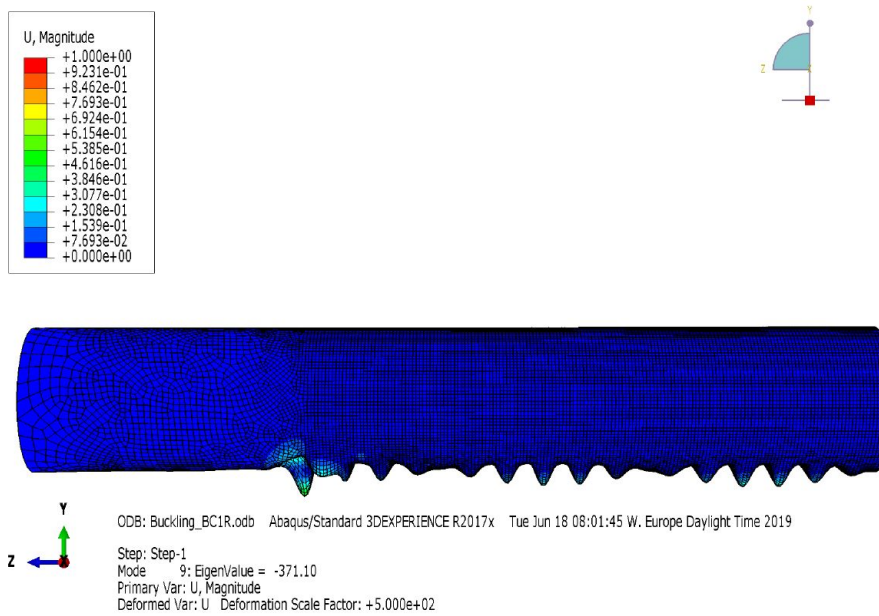


Figure D.9: Eigenmode 9

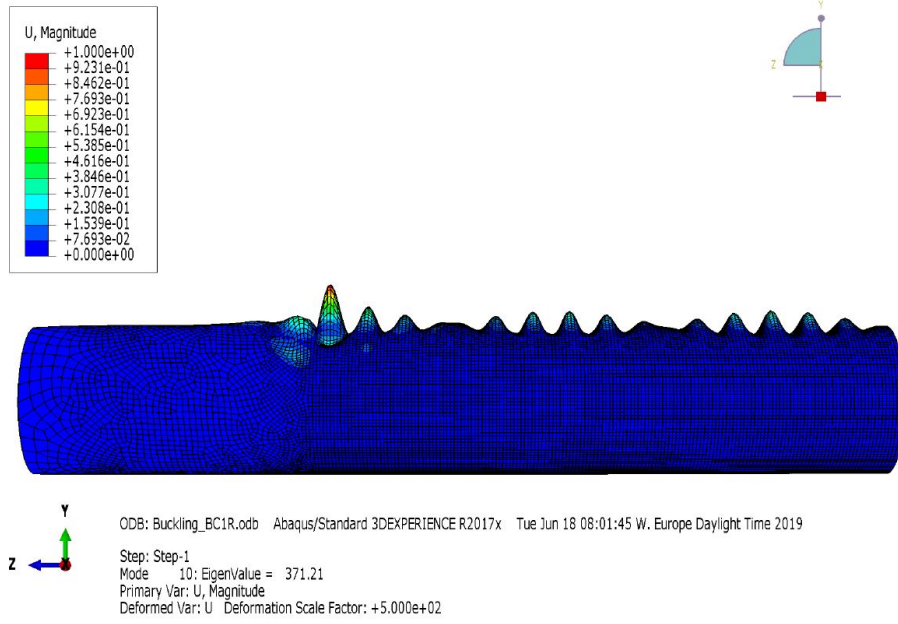


Figure D.10: Eigenmode 10

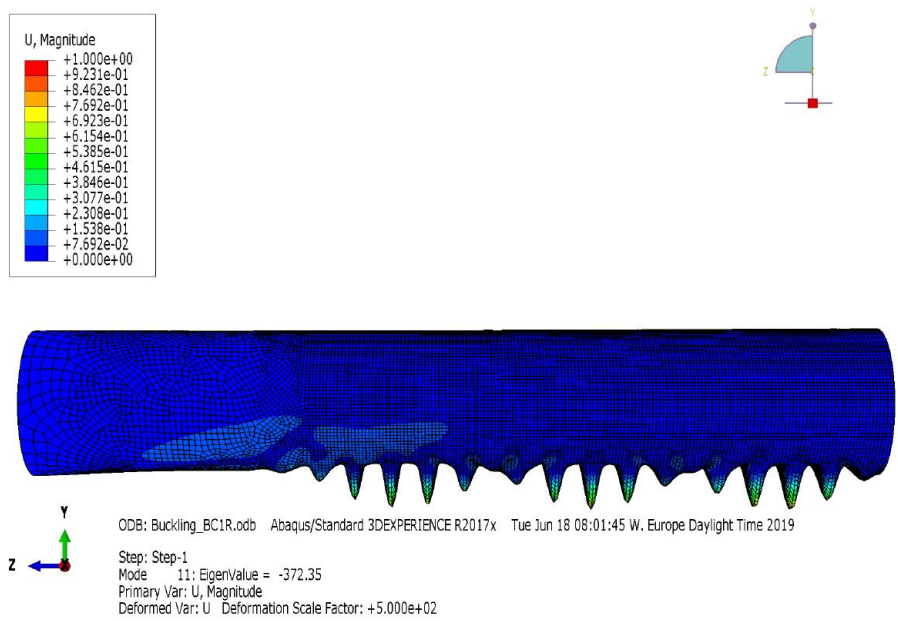


Figure D.11: Eigenmode 11

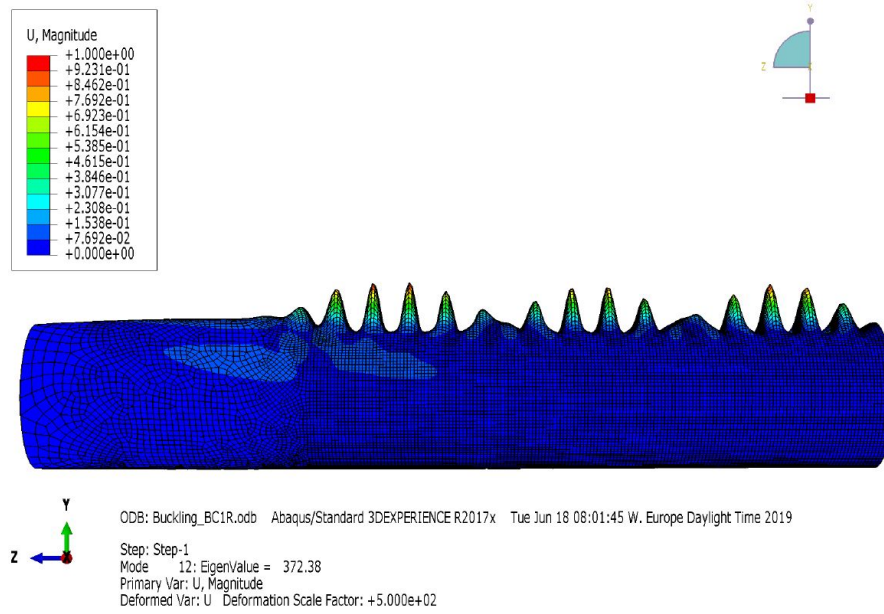
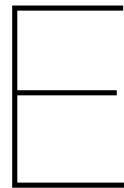


Figure D.12: Eigenmode 12



Moment curvature diagrams from FEM models

